



Effective Algorithms for the Study of Miscible Gas Injection Processes

Jessen, Kristian

Publication date:
2000

Document Version
Publisher's PDF, also known as Version of record

[Link back to DTU Orbit](#)

Citation (APA):
Jessen, K. (2000). *Effective Algorithms for the Study of Miscible Gas Injection Processes*.

General rights

Copyright and moral rights for the publications made accessible in the public portal are retained by the authors and/or other copyright owners and it is a condition of accessing publications that users recognise and abide by the legal requirements associated with these rights.

- Users may download and print one copy of any publication from the public portal for the purpose of private study or research.
- You may not further distribute the material or use it for any profit-making activity or commercial gain
- You may freely distribute the URL identifying the publication in the public portal

If you believe that this document breaches copyright please contact us providing details, and we will remove access to the work immediately and investigate your claim.

**Effective Algorithms for the Study of
Miscible Gas Injection Processes**

by

Kristian Jessen

March 2000

IVC-SEP

Department of Chemical Engineering

Technical University of Denmark

Building 229, DK-2800 Lyngby,

Denmark

Copyright © 2000: Kristian Jessen

Printed by Tekst og Tryk A/S, Vedbæk, Denmark

ISBN 87-90142-53-5

Preface

This thesis is submitted as partial fulfillment of the requirements for obtaining the Ph.D. degree at the Technical University of Denmark. The work was carried out at IVC-SEP, Department of Chemical Engineering, from February 1997 to February 2000 under the supervision of Professor Erling H. Stenby and Associate Professor Michael L. Michelsen.

During my study various people have contributed to a joyful and highly inspiring time by invaluable discussions on research related as well as non-research related topics. First of all I am grateful to Professor Erling H. Stenby for his supervision throughout the project.

I would also like to express my gratitude to Associate Professor Michael L. Michelsen for many invaluable discussions on the computational aspects of my research project.

Further I would like to thank Professor Franklin M. Orr Jr. for offering me the opportunity of working with him and his research group at the Department of Petroleum Engineering, Stanford University, California, for a six-month period.

Finally, I wish to thank my colleagues at IVC-SEP for an enjoyable time.

Copenhagen, March 2000

Kristian Jessen

Summary

In recent decades, an increasing effort has been spent on studies and development of improved oil recovery processes. Gas injection can be a very efficient method for improving the oil production, particularly in the case where miscibility develops during the displacement process. The minimum pressure at which a gas should be injected into the reservoir in order to obtain a multicontact miscible displacement (the MMP, minimum miscibility pressure) has consequently obtained a very important status in IOR/EOR studies. Another area to which increasing attention is paid is the ongoing development of a new generation of reservoir simulators. The new simulators, based on streamline technology, decompose the three-dimensional (3-D) structure of a reservoir into a sequence of one-dimensional (1-D) problems. Efficient methods for generating solutions to the 1-D gas injection problem are hence needed.

A new algorithm has been developed for calculation of minimum miscibility pressures for the displacement of oil by multicomponent gas injection. The algorithm is based on the key tie line identification approach initially addressed by Wang and Orr⁵². In this work a new global approach is introduced. A number of deficiencies of the sequential approach have been eliminated, resulting in a robust and highly efficient algorithm. The time consumption for calculation of the MMP in multicomponent displacement processes has been reduced significantly, so that the calculation can now be performed within a few seconds on a PC for a 15-component gas mixture. The algorithm is therefore particularly suitable for gas enrichment studies or other case studies where a large number of MMP calculations are required. Predicted results from the key tie line identification approach are shown to be in excellent agreement with slimtube data and with results from multicell/slimtube simulators presented in the literature.

The solution to mass conservation equations governing one-dimensional (1-D) dispersion-free flow in which components are partitioned between two equilibrium phases is controlled by the geometry of key tie lines. It has previously been proven that for systems with an arbitrary number of components, the key tie lines can be approximated quite accurately by a sequence of intersecting tie lines. This experience was utilized in the development of the new MMP algorithm.

Tools developed during the implementation of the global approach to calculation of the MMP have been combined with tools from the analytical theory of 1-D gas injection processes. As a result, a new approach to generating approximate 1-D analytical solutions to problems with constant initial and injection compositions (Riemann problems) has been developed. For fully self-sharpening systems, in which all key tie lines are connected by shocks, the obtained analytical solutions are rigorously accurate, while for systems where some key tie lines are connected by spreading waves, the analytical solutions are approximations, but accurate ones. Detailed comparison between analytical solutions with both coarse and fine grid compositional simulations indicates that even for systems with continuous variation between key tie lines, approximate analytical solutions predict composition profiles far more accurately than coarse grid numerical simulations. Because of the generality of the new approach, approximate analytical solutions can be obtained for any system whose phase behavior can be modeled by an equation of state. The construction of approximate analytical solutions is shown to be orders of magnitude faster than the equivalent coarse grid compositional simulation. Hence, the new approach is valuable in areas where fast compositional solutions to Riemann problems are required. The new approach to construction of approximate analytical solutions to the 1-D gas injection problem is initially described for a simplified version of the conservation equations. In the simplified version, described in Chapter 4, components are assumed to take up a constant volume throughout the displacement. This assumption is relaxed in Chapter 5 where a general approach to constructing approximate analytical solutions is presented.

A large number of finite difference (FD) simulations were performed as part of developing the algorithms for constructing approximate analytical solutions. The well-documented existence of a system dependent sensitivity to numerical dispersion in FD simulations was observed. An approach to a qualitative estimation of the sensitivity for a given system is suggested. The approach, presented in Chapter 6, is based on the key tie line orientation of the approximate analytical solutions. A qualitative estimate can hence be obtained directly from the new MMP algorithm without increase in the required CPU time.

Resumé

Gennem det sidste årti er en væsentlig forskningsmæssig indsats blevet rettet mod indblik i og udvikling af metoder til forbedring af olieindvinding fra eksisterende oliefelter. Injektion af gas kan bidrage til en væsentlig forbedring af indvindingsgraden. Specielt hvis der under fortrængningsprocessen optår blandbarhed mellem den injicerede gas og olien. Det laveste tryk, ved hvilket der under fortrængningsprocessen opstår multikontakt blandbarhed (MMP), har som følge deraf en afgørende rolle i forbindelse med studier af metoder til forbedring af indvindingsgraden. Den igangværende udvikling af en ny type reservoirsimulatorer har ligeledes fået stor opmærksomhed. Den nye type reservoirsimulator, baseret på strømningslinjeteknologi, opsplitter den tredimensionale beskrivelse af et oliereservoir til en sekvens af endimensionalt (1-D) formulerede problemstillinger. Der er derfor opstået et behov for effektive metoder til løsning af flow problemer for 1-D gasinjektionsprocesser.

Der er blevet udviklet en ny algoritme til beregning af MMP for fortrængningsprocesser, hvor multikomponent gas injiceres i en olie. Algoritmen er baseret på nøglebindelinie konceptet introduceret af Wang og Orr⁵². En ny global formulering af problemstillingen er beskrevet og implementeret. Reformuleringen eliminerer en række begrænsende faktorer fra den oprindelige formulering. Dette resulterer i en robust og meget effektiv algoritme. Beregningstiden for bestemmelsen af MMP er reduceret signifikant, således at beregningen nu kan udføres med PC på få sekunder for systemer med 15 komponenter i injektionsgassen. Den nye algoritme er derfor velegnet til studier af forskellige injektionsgasser og blandinger heraf. Generelt er den nye algoritme velegnet til studier af injektionsprojekter, hvor mange MMP beregninger er en nødvendighed. Resultater opnået med den nye angrebsvinkel er i god overensstemmelse med slimtube data og med resultater beskrevet i litteraturen fra numeriske simulatorer.

Løsninger til bevarelsesligninger, der beskriver endimensionalt dispersionsfrit flow, hvor komponenter fordeler sig mellem to faser i ligevægt, er bestemt ved geometrien af nøgle bindelinier. Det er tidligere blevet demonstreret, at disse nøglebindelinier kan beskrives tilnærmelsesvist korrekt ved en serie af bindelinier, hvis forlængelse skærer hinanden parvist. Dette faktum blev benyttet i udviklingen af den nye MMP algoritme. En kombination af

værktøj, udviklet i forbindelse med implementeringen af MMP algoritmen, med værktøj fra den analytiske teori for 1-D gasinjektionsprocesser har ført til udviklingen af en ny metode til generering af approksimative analytiske løsninger til 1-D gasinjektionsprocesser. Løsningsmetoden kan anvendes til problemstillinger med konstante begyndelsebetingelser (Riemann problemer). For systemer, hvor den korrekte løsning udelukkende består af chokfronter, vil den udviklede løsningsmetode være uomtvistelig nøjagtig. For systemer, hvor nøglebindelinier er forbundet ved kontinuert variation, vil de genererede løsninger være approksimative men stadig meget nøjagtige. En detaljeret sammenligning af de approksimative analytiske løsninger med numeriske simuleringer demonstrerer, at de approksimative løsninger er mere nøjagtige end numeriske simuleringer, hvis antallet af gridblokke er lavt. På baggrund af den generelle formulering af den nye metode kan den anvendes til alle 1-D problemstillinger, hvor fasebetingelser for de involverede fluider kan beskrives med eksempelvis en tilstandsligning. Beregningstiden for den nye metode er størrelsesorden lavere end for tilsvarende numeriske simuleringer selv med få gridblokke. Metoden er derfor velegnet til problemstillinger, hvor løsning af mange Riemann problemer er påkrævet. Den nye løsningsmetode blev i første omgang udviklet for en simplificeret udgave af bevarelsesligningerne. I den simplificerede udgave, beskrevet i kapitel 4, antages komponenterne at have konstant molar volumen under hele fortrængningsprocessen. Den simplificerede metode er videreudviklet i kapitel 5, hvor en generel metode bliver præsenteret.

Et stort antal numeriske simuleringer, baseret på differensmetoden, blev udført som led i udviklingen af den nye løsningsmetode. Den vel dokumenterede eksistens af en systemafhængig følsomhed over for numerisk dispersion blev observeret. En generel metode til kvalitativ estimering af denne følsomhed er beskrevet i kapitel 6. Metoden benytter sig af den geometriske struktur af den tilsvarende approksimative analytiske løsning. Dette betyder, at et kvalitativt estimat for følsomheden af et givet system kan genereres sideløbende med en MMP beregning uden at påvirke den nødvendige beregningstid.

Table of Contents

Preface	i
Summary	i
Resumé.....	iii
Table of Contents	v
1. Introduction.....	1
2. Conservation Equations and Analytical Theory of the 1-D Gas Injection Process	3
2.1 General Formulation of the Conservation Equations	3
2.2 Conservation Equations with No Volume Change on Mixing (NVC)	7
2.3 Geometry of 1-D Analytical Solutions	9
2.4 Solution Construction Tools	13
2.4.1 Shocks due to Phase Appearance/Disappearance.....	13
2.4.2 Shocks in the two-phase region	15
2.4.3 Continuous Variation along Tie Lines and Constant States	16
2.4.4 Continuous Variation along Nontie Line Paths	18
2.5 Approximation of Key Tie Lines.....	20
2.6 Summary	21
3. Determination of the Minimum Miscibility Pressure	23
3.1 First contact miscibility	23
3.2 Multicontact Miscibility	24
3.3 Traditional Determination of the MMP	28
3.3.1 Empirical Correlations.....	30
3.3.2 Ternary Representation/Limiting Tie Line Approach	30
3.3.3 Single Cell Simulators	32
3.3.4 Slimtube and Multicell Simulations	34
3.3.5 Semi-analytical Calculation of the MMP	36
3.4 Global Approach for Calculation of the MMP	37
3.4.1 Mathematical Approach.....	37

3.4.2 Solution Strategy	39
3.4.3 Linear Solver for Newton-Raphson Iteration	41
3.4.4 Modification of Iterative Scheme in the Near-critical Region	43
3.4.5 Examples of MMP Calculation	45
3.4.6 Discussion of the Global Approach for Calculation of the MMP	51
3.5 Application of the New MMP Algorithm.....	52
3.5.1 Effect of Tuning and Lumping	54
3.5.2 Gas Enrichment Study	57
3.6 Summary	59
4. Approximate Semi-analytical Solutions to the 1-D Gas Injection Problem (NVC).....	61
4.1 Grouping of Analytical Solutions	61
4.2 Self-sharpening Systems.....	62
4.3 Solution Example for Fully Self-sharpening System	65
4.4 Systems with Nontie-line Rarefactions (Spreading Waves).....	68
4.5 Prediction of Spreading Waves in 1-D Solutions	69
4.5.1 The Fanning Rule (Envelope Rule)	70
4.5.2 Algorithm for Systems with Nontie-line Rarefactions	73
4.6 Solution Example with Nontie-line Rarefaction.....	74
4.7 Significance of Spreading Waves in the 1-D Solutions.....	76
4.8 Example of Curvature of Surface Traveled by a Spreading Wave.....	78
4.9 Analytical Solution below the Saturation Pressure of the Initial Oil.....	81
4.10 Recovery Curves from Analytical 1-D Solutions	82
4.11 Supplementary NVC Solutions.....	88
4.11.1 Displacement of Oil 3 by Gas 3 at 300 atm and 368.15 K.....	88
4.11.2 Displacement of Oil 3 by Gas 5 at 250 atm and 368.15 K.....	89
4.11.3 Displacement of Oil 3 by Pure CH ₄ at 300 atm and 368.15 K.....	90
4.11.4 Displacement of Oil 3 by 75% CO ₂ and 25% CH ₄ at 275 atm and 368.15 K.....	91
4.12 Summary	92
5. Approximate Analytical 1-D Solutions with Volume Change (VC).....	93
5.1 Shocks in the Two-phase Region	93
5.2 Shocks due to Phase Appearance and Disappearance	95

5.3 Algorithm for Construction of Fully Self-sharpening Solutions (VC)	96
5.4 Examples of Analytical Solutions with Volume Change on Mixing.....	98
5.5 Recovery Curves from Analytical Solutions with Volume Change on Mixing	103
5.5 Summary	105
6. On System-dependent Sensitivity of Numerical Dispersion in FD Simulations	107
6.1 Results from Commercial Simulator E300.....	114
6.2 Summary	115
7. Conclusions and Suggestions for Future Work	117
8. Nomenclature	121
9. Bibliography	123
10. Appendix.....	127
A.1 Critical Properties of Oil 3	127
A.2 Calculation Results from Displacement of Oil 3 by Gas 5	128
A.3 Finite Difference (FD) Simulation.....	129
A.4 Determination of Normal Vectors in Multidimensional Space	131
A.5 Details of 1-D Shock Solution Given in Figure 4.8.....	132
A.6 Details of 1-D Shock Solution Given in Figure 4.9	133
A.7 Details of 1-D Shock Solution Given in Figure 4.10.....	134
A.8 Details of 1-D shock solution given in Figure 4.11	135
A.9 Details of 1-D shock solution given in Figure 4.14.....	136
A.10 Details of 1-D Shock Solution Given in Figure 4.21	137
A.11 Details of 1-D Shock Solution Given in Figure 4.22.....	138
A.12 Details of 1-D Shock Solution Given in Figure 4.23.....	139
A.13 Details of 1-D Shock Solution Given in Figure 4.24.....	140
A.14 Displacement (VC) of Oil 4 by Gas 6 at 275 atm and 387.45 K	141
A.15 Displacement (VC) of Oil 4 by pure N ₂ at 275 atm and 387.45 K	142
A.16 Displacement (VC) of Oil 3 by Gas 3 at 300 atm and 368.15 K	143
A.17 Displacement (VC) of Oil 3 by CO ₂ /CH ₄ at 275 atm and 368.15 K	144
A.18 Input file for Eclipse (E300) Slimtube Simulation	145

1. Introduction

Miscible gas injection processes have become a widely used technique for enhanced/improved oil recovery (EOR/IOR) throughout the world. The understanding of the multiphase, multicomponent flow taking place in any miscible displacement process is essential for successful design of gas injection projects. Due to complex reservoir geometry and reservoir fluid properties, numerical simulations of the flow processes are usually conducted to obtain such understanding. In principle, compositional simulation could be used to study such problems. But in practice conventional finite difference simulation is so slow that three-dimensional (3-D) computations are feasible only when coarse grid blocks are used. Such simulations are not very useful, however, because they are severely affected by numerical dispersion.

Recent progress in the application of streamline methods offers a way to overcome the limitations of 3-D finite difference compositional simulations^{2,3,48,49}. In the streamline approach, a one-dimensional (1-D) solution is mapped onto streamlines which capture the effects of reservoir heterogeneity. Thiele *et al.*⁵⁰ described 2-D and 3-D streamline compositional simulations in which analytical and finite difference approaches were used to solve the 1-D flow problem. Thiele *et al.*⁵⁰ used a numerical solution to the 1-D problem to perform a compositional simulation for a heterogeneous 3-D reservoir described with 518000 grid blocks. At that time, analytical solutions for problems with an arbitrary number of components in the oil and injection gas were not available. Application of analytical solutions in simulations like that of Thiele *et al.*⁵⁰ could lead to substantial additional speed-ups in streamline calculations.

Gas injection can be a very efficient method for EOR/IOR, particularly if miscibility develops during the displacement process. Hence, the task of determining the minimum pressure at which a given gas should be injected into the reservoir in order to achieve multicontact miscibility (the MMP) has obtained a very important role in production case studies. Various approaches have been suggested in the literature for determining the MMP. Many attempts based on ternary representations have later been proven to apply only to the special cases of a vaporizing or a condensing mechanism controlling the development of miscibility. Zick⁵⁸ and

subsequently Stalkup⁴⁴ demonstrated that the mechanism controlling the development of miscibility could be (and often is) of a combined vaporizing and condensing nature. Furthermore, they showed that the MMP in general could be determined by 1-D compositional simulation.

A massive effort has been spend on the development of the analytical theory of 1-D gas injection problems. The development of this theory has offered a very helpful tool for understanding the nature of the mechanisms controlling the development of miscible displacements. The current work is devoted to the further development of the analytical theory and to the implementation of the theory into effective algorithms for the study of miscible gas injection problems.

The need for effective algorithms for 1-D gas injection problems is evident since time-consuming finite difference simulations are still used for streamline simulations and for determination of the minimum miscibility pressure.

Chapter 2 presents the conservation equations governing 1-D dispersion free two-phase flow and introduces the reader to the analytical theory forming the backbone of this study. In Chapter 3 a brief introduction is given to the mechanisms controlling the development of a miscible displacement along with an overview of different methods for calculation of the MMP previously presented in the literature. Subsequently, a new algorithm for effective calculation of the MMP, based on the analytical theory, is presented. In Chapter 4, the tools developed in Chapter 3 are combined with tools from the analytical theory to construct approximate analytical solutions to a simplified version of the conservation equations. This chapter also presents some new contributions to the analytical theory. In Chapter 5 the algorithms of Chapter 4 are extended to consider the general formulation of the conservation equations. Finally, Chapter 6 demonstrates how the effects of numerical dispersion in finite difference simulations can be linked to the geometry of the approximate analytical solutions.

2. Conservation Equations and Analytical Theory of the 1-D Gas Injection Process

This chapter introduces the flow equations and the analytical theory forming the basis of the work described in the later chapters. Two different formulations of the one-dimensional (1-D) two-phase flow problem are presented. Initially, the general form of the conservation equations is presented in which the components are allowed to change volume as they transfer between phases. Then a simplified version of the conservation equations is given. In the simplified version components do not change volumes as they transfer between the equilibrium phases. The mathematical problem of solving the conservation equations for the latter case is much simpler than for the general case and is used as a starting point for generating general approximate analytical solutions of the 1-D flow problem.

A sketch of the physical system considered in the modeling work is given in Figure 2.1.

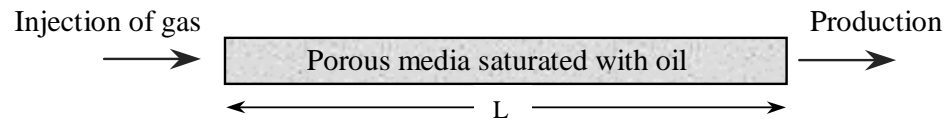


Figure 2.1: Sketch of the 1-D gas injection problem.

2.1 General Formulation of the Conservation Equations

The derivation of the conservation equations for the one-dimensional (1-D) flow problem is based on the following assumptions:

- The porous medium is homogeneous and incompressible
- Instantaneous thermodynamic equilibrium exists everywhere
- The gradient in pressure along the system is small compared to the total pressure
- Capillary forces and gravity are neglected
- The flow is isothermal and linear
- Mass transfer by dispersion/diffusion is neglected

Given these assumptions, the mass conservation equation for flow of two phases in a 1-D porous media is given by

$$\frac{\partial}{\partial t} \left(\sum_{j=1}^2 \rho_{mj} S_j \right) + \frac{\partial}{\partial x} \left(\frac{v}{\phi} \sum_{j=1}^2 \rho_{mj} f_j \right) = 0 \quad (2.1)$$

where t is the time, x is the distance, ρ_{mj} is the density of phase j , v is the linear flow velocity based on an empty tube and ϕ is the porosity. S_j and f_j are the saturation and the fractional flow of phase j respectively. In the absence of chemical reactions during the displacement process, Eq. 2.1 can be rewritten in terms of molar phase densities (ρ_j) and mole fractions for each of the nc components as

$$\frac{\partial}{\partial t} \left(\sum_{j=1}^2 x_{ij} \rho_j S_j \right) + \frac{\partial}{\partial x} \left(\frac{v}{\phi} \sum_{j=1}^2 x_{ij} \rho_j f_j \right) = 0, \quad i = 1, \dots, nc \quad (2.2)$$

where x_{ij} is the mole fraction of component i in phase j . By introducing the dimensionless variables

$$\tau = \frac{v_{inj} t}{L\phi} \quad z = \frac{x}{L} \quad (2.3)$$

where L is the system length and v_{inj} is the injection velocity (volumetric flow rate divided by cross sectional area), Eq. 2.2 can be written as

$$\frac{\partial C_i}{\partial \tau} + \frac{\partial F_i}{\partial z} = 0, \quad i = 1, \dots, nc \quad (2.4)$$

with

$$C_i(\underline{Z}) = \sum_{j=1}^2 x_{ij} \rho_j S_j \quad (2.5)$$

and

$$F_i(\underline{Z}, v_d) = v_d \sum_{j=1}^2 x_{ij} \rho_j f_j \quad (2.6)$$

\underline{Z} is the overall composition in mole fractions and v_d is the velocity scaled with respect to the injection velocity v_{inj} ($v_d = v/v_{inj}$). \underline{Z} contains only $nc-1$ elements due to the constraint on mole

fractions. To close the mathematical formulation of the flow problem, initial data must be specified. This work deals strictly with the case of constant initial data which is the overall composition of the injection gas and the overall composition of the initial oil connected by a discontinuity at $z = 0$.

$$\underline{Z}(z, \tau = 0) = \begin{cases} \underline{Z}_{inj} & \text{for } z < 0 \\ \underline{Z}_{oil} & \text{for } z > 0 \end{cases} \quad (2.7)$$

The mathematical formulation of the flow problem is given by a set of coupled first order partial differential equations (PDEs). Specification of constant initial data gives rise to a Riemann problem, which may be solved by the method of characteristics. Lax²⁷ demonstrated that the solution to Eq. 2.4 is self-similar. The self-similarity of the solution allows the flow problem to be reformulated into an eigenvalue problem by introducing the variable

$$\eta = \frac{z}{\tau} \quad (2.8)$$

By application of the chain rule the derivatives of Eq. 2.4 can be rewritten as

$$\frac{\partial C_i}{\partial \tau} = \left(\sum_{j=1}^{nc-1} \frac{\partial C_i}{\partial Z_j} \frac{dZ_j}{d\eta} \right) \frac{\partial \eta}{\partial \tau} \quad (2.9)$$

and

$$\frac{\partial F_i}{\partial z} = \left(\frac{\partial F_i}{\partial v_d} \frac{dv_d}{d\eta} + \sum_{j=1}^{nc-1} \frac{\partial F_i}{\partial Z_j} \frac{dZ_j}{d\eta} \right) \frac{\partial \eta}{\partial z} \quad (2.10)$$

Substitution of Eqs. 2.8-10 into Eq. 2.4 yields the eigenvalue problem

$$\frac{\partial F_i}{\partial v_d} \frac{dv_d}{d\eta} + \sum_{j=1}^{nc-1} \frac{\partial F_i}{\partial Z_j} \frac{dZ_j}{d\eta} - \eta \sum_{j=1}^{nc-1} \frac{\partial C_i}{\partial Z_j} \frac{dZ_j}{d\eta} = 0, \quad i = 1, \dots, nc \quad (2.11)$$

Eq. 2.11 can be written in the matrix-vector notation

$$(\underline{A} - \lambda \underline{B})\underline{X} = \underline{0} \quad (2.12)$$

where the elements of \underline{A} and \underline{B} are given by

$$A_{ij} = \begin{cases} \frac{\partial F_i}{\partial Z_j} & \text{for } i = 1, \dots, nc \\ & j = 1, \dots, nc-1 \\ \frac{\partial F_i}{\partial v_d} & \text{for } j = nc \end{cases} \quad B_{ij} = \begin{cases} \frac{\partial C_i}{\partial Z_j} & \text{for } i = 1, \dots, nc \\ & j = 1, \dots, nc-1 \\ 0 & \text{for } j = nc \end{cases} \quad (2.13)$$

The eigenvalues of Eq. 2.12 ($\lambda=\eta$) correspond to the characteristic wave velocity of a given overall composition whereas the associated eigenvectors

$$\underline{X} = \left[\frac{dZ_1}{d\eta}, \frac{dZ_2}{d\eta}, \dots, \frac{dZ_{nc-1}}{d\eta}, \frac{dv_d}{d\eta} \right]^T \quad (2.14)$$

are tangents to composition paths. The physical interpretation of the characteristic wave velocities is the speed at which a given overall composition propagates throughout the porous media. The eigenvalue problem can be used to generate analytical solutions to the 1-D flow problem (Eq. 2.2). Due to the non-linearity introduced by normal S-shaped fractional flow functions (f_j), the set of partial differential equations is not strictly hyperbolic. In terms of the corresponding eigenvalue problem, this means that the eigenvalues are not strictly ordered and hence that the composition path may change from a tie line path to a nontie line path at points of equal eigenvalues. This fact plays an important role in the construction of 1-D solutions described in subsequent sections.

The fractional flow function used in this work is based on the Darcy law for multiphase flow with no gravity or capillary forces acting on the fluids. On these assumptions the fractional flow of phase j can be written in terms of the phase relative permeability (k_{rj}) and the phase viscosity (μ_j) as

$$f_j = \frac{k_{rj} / \mu_j}{\sum_{i=1}^2 k_{ri} / \mu_i} \quad (2.15)$$

The phase relative permeability (k_{rj}) is described by Corey type expressions. For the liquid and the vapor phase, respectively, these are

$$k_{rl} = k_{rle} \left(\frac{1-S-S_{or}}{1-S_{or}} \right)^{nl} \quad (2.16)$$

and

$$k_{rv} = k_{rve} \left(\frac{S}{1-S_{or}} \right)^{nv} \quad (2.17)$$

S_{or} is the residual oil saturation, k_{rle} and k_{rve} are the effective relative permeabilities of liquid and vapor respectively and nl , nv are system specific constants. Before turning attention to the

tools available for construction of 1-D solutions, a simplified version of the flow problem is considered.

2.2 Conservation Equations with No Volume Change on Mixing (NVC)

Various authors have studied simplified versions of the conservation equations presented in the previous section. In the work of Johns²⁴ and Wang⁵⁴ components are assumed to mix ideally. Thus, components do not change molar volume/density in the transition between liquid phase and vapor phase. The assumption about no volume change is reasonable when pressures are high. For systems at lower pressures where the solubility of light components in undisplaced oil is high but the gas density is low, effects of volume change can be significant and the general formulation of the conservation equations should be used.

The assumption leads to a major simplification of the mathematics involved in solving the resultant conservation equations, since overall convective velocity will be constant in the NVC formulation of the displacement process. Further, the overall molar compositions (C_j) and the overall molar fluxes (F_j) entering into Eq. 2.4 can be substituted by an overall volume fraction and an overall fractional flow term. Consequently, the conservation equations are written in the form

$$\frac{\partial G_i}{\partial \tau} + \frac{\partial Q_i}{\partial z} = 0 \quad , \quad i = 1, \dots, nc - 1 \quad (2.18)$$

where

$$G_i = \sum_{j=1}^2 c_{ij} S_j \quad (2.19)$$

and

$$Q_i(\underline{G}) = \sum_{j=1}^2 c_{ij} f_j \quad (2.20)$$

Due to the restrictions on the overall volume fractions (G_i) and the overall fractional flows (Q_i)

$$\sum_{i=1}^{nc} G_i = \sum_{i=1}^{nc} Q_i = 1 \quad (2.21)$$

only $nc-1$ of the conservation equations (Eq. 2.18) are independent. The component volume fractions are defined by

$$c_{ij} = \frac{x_{ij} \rho_j^{ideal}}{\rho_{ci}} \quad (2.22)$$

where ρ_{ci} is the molar density of the pure component i taken at the pressure and temperature of the displacement process. ρ_j^{ideal} is the molar density of phase j based on the assumption about ideal mixing. That is

$$\rho_j^{ideal} = \left(\sum_{i=1}^{nc} \frac{x_{ij}}{\rho_{ci}} \right)^{-1} \quad (2.23)$$

By applying the concept of self-similarity (Lax²⁷), the conservation equations are rewritten in terms of the ratio of independent variables:

$$\frac{\partial G_i}{\partial \eta} \frac{\partial \eta}{\partial \tau} + \frac{\partial Q_i}{\partial \eta} \frac{\partial \eta}{\partial z} = 0, \quad i = 1, \dots, nc - 1 \quad (2.24)$$

where η is defined by Eq. 2.8. Inserting the derivatives of the new independent variable η into Eq. 2.24 brings the conservation equations on the form

$$\frac{\partial Q_i}{\partial \eta} - \eta \frac{\partial G_i}{\partial \eta} = 0, \quad i = 1, \dots, nc - 1 \quad (2.25)$$

The derivative of the overall fractional flow (Q_i) can be expressed in terms of the overall volume fractions by applying the chain rule:

$$\sum_{j=1}^{nc-1} \frac{\partial Q_i}{\partial G_j} \frac{\partial G_j}{\partial \eta} - \eta \frac{\partial G_i}{\partial \eta} = 0, \quad i = 1, \dots, nc - 1 \quad (2.26)$$

This is the eigenvalue problem associated with the NVC conservation equations. In matrix-vector notation the eigenvalue problem is given by

$$(\underline{A} - \eta \underline{I}) \underline{Y} = 0 \quad (2.27)$$

where \underline{I} is the unity matrix and the elements of \underline{A} and \underline{Y} are given by

$$A_{ij} = \frac{\partial Q_i}{\partial G_j}, \quad Y_i = \frac{\partial G_i}{\partial \eta}, \quad i, j = 1, \dots, nc - 1 \quad (2.28)$$

In equivalence with the general eigenvalue problem including volume change (VC), the eigenvalues of Eq. 2.27 correspond to characteristic wave velocities of a given overall volume fraction and the eigenvectors are tangents to the associated composition paths. The initial data of the NVC formulation is specified by

$$\underline{G}(z, \tau = 0) = \begin{cases} \underline{G}_{inj} & \text{for } z < 0 \\ \underline{G}_{oil} & \text{for } z > 0 \end{cases} \quad (2.29)$$

2.3 Geometry of 1-D Analytical Solutions

The analytical solutions to Eq. 2.4 (or Eq. 2.18) are constructed by solving the eigenvalue problem associated with the mass conservation equations. In the compositional space, the corresponding problem is to identify the correct (unique) route, which connects the initial oil composition and the injection gas composition. The composition route describing the analytical solution geometrically is subject to the following requirements:

1. The composition route must have characteristic wave velocities in the two-phase region which increase monotonically from upstream to downstream locations. This condition is known as the velocity rule. If the velocity rule should be violated by a continuous variation (known as a rarefaction), a shock must be introduced to ensure that the solution remains single-valued. In other words, the velocity rule emphasizes that a state property can only assume one value at a given point in the solution. Violation of the velocity rule and the appearance of shocks are well known issues from the Buckley-Leveret (1941) theory. Shocks must be introduced in the 1-D dispersion-free solution to resolve possible multivaluedness arising from neglecting terms which account for physical dispersion/diffusion (i.e. secondorder derivatives with respect to the space variable). A shock must satisfy the integral form of the mass conservation equations (Eq. 2.4):

$$\Lambda = \frac{F_i^u - F_i^d}{C_i^u - C_i^d}, \quad i = 1, \dots, n_c \quad (2.30)$$

where Λ is the shock velocity. Hence, a shock is a weak solution to the conservation equations. Upstream and downstream parts of the shock are denoted u and d respectively. Eq. 2.30 is a Rankine-Hugoniot condition^{6,27}.

2. Any shock present in a solution must satisfy an entropy condition. Lax^{27,28} introduced the term entropy condition in the study of gas dynamics where the actual entropy of the system was used as a measurement to rule out non-physical shock solutions. For the more complex systems studied in this work the entropy condition is of a mathematical nature and requires any shock to be stable in the presence of a small amount of dispersion. The entropy condition thus dictates that a composition just upstream of the shock must move faster than a composition just downstream of the shock. This feature will allow the shock to regenerate upon small perturbations.
3. In addition, solutions must satisfy a continuity condition with respect to initial and injection data. In other words, small perturbations to the initial or the injection compositions must result in small changes in the solution.

A substantial body of mathematical theory now exists for construction of analytical solutions to the dispersion-free 1-D multicomponent flow problem^{7,8,21,22,23,36}. This theory, based on the method of characteristics (MOC), illustrates that the behavior of the solution is controlled by the geometry of key tie lines in the compositional space. Larson and Hirasaki²⁹ demonstrated that shocks from the single-phase region into the two-phase region must occur along the extension of tie lines. Hence, two tie lines, the tie line extending through the initial oil and the tie line extending through the injection gas, are key tie lines in the analytical solutions. These key tie lines are referred to as the initial tie line and the injection tie line respectively. Monroe et al.³⁶ showed that for gas injection problems with four components, the 1-D solution is bound to intersect a third key tie line. This third tie line is known as a crossover tie line. Johns²⁴, Dindoruk⁷ and Orr et al.³⁸ generalized the work of Monroe et al. to systems with nc components. They established that for a system with nc components the 1-D solutions is controlled by the geometry of $nc-1$ key tie lines: The initial tie line, the injection tie line and $nc-3$ crossover tie lines. The $nc-1$ key tie lines belong to $nc-2$ families of tie lines, each of which generates a ruled surface. Thus, the crossover tie lines are lines of intersection between the ruled surfaces. Wang⁵⁴ demonstrated that ruled surfaces are also developable surfaces. The existence of key tie lines and ruled surfaces is illustrated for a four-component system in Figure 2.2. Only the part of the ruled surfaces spanned by the key tie lines is included in the

sketch. G denotes the injection gas composition and O the initial oil composition. The solution path enters the two-phase region from O along the initial tie line and from G along the injection tie line.

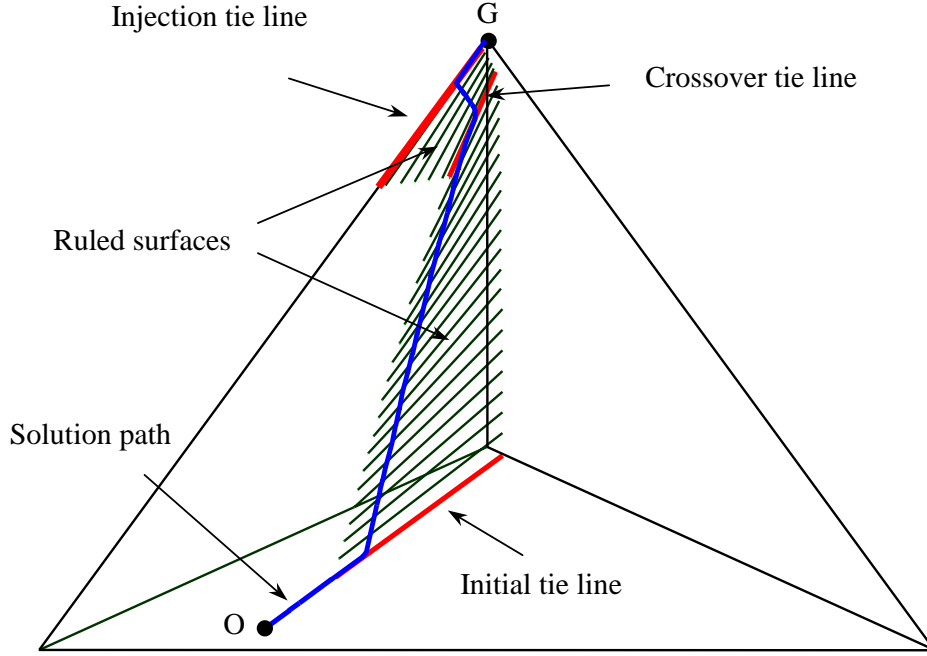


Figure 2.2: Illustration of key tie lines and ruled surfaces for a quaternary system.

Based on the study of surfactant/oil/water (ternary) systems Helfferich¹⁴ demonstrated that the two eigenvectors, associated with the conservation equations, at a given point in the two-phase region may point in two different directions. One of the directions was shown to coincide with the tie line through the given point whereas the other pointed in a nontie line direction. This discovery gave rise to the formalism of tie line paths and nontie line paths in the analytical theory of 1-D displacements. Helfferich¹⁵ and Dumoré⁹ also illustrated that the tie line eigenvalue was linked to the fractional flow function by

$$\lambda_{tie\ line} = \frac{df}{dS} \quad (2.31)$$

The subscripts of f and S have been removed in Eq. 2.31 and unless otherwise mentioned, f denotes the fractional flow of vapor and S the volume fraction of vapor. Variation along a tie line is referred to as a tie line path whereas variation in a nontie line direction is referred to as

a nontie line path. For an nc component system each point in the two-phase region is intersected by $nc-2$ nontie line paths corresponding to the nontie line eigenvectors. By recalling that the conservation equations are given by a set of non-strictly hyperbolic PDEs, the corresponding eigenvalue problem will degenerate when two eigenvalues coincide. In the analytical theory of 1-D gas injection processes only equal eigenvalue points of mixed type ($\lambda_{\text{tie line}} = \lambda_{\text{nontie line}}$) are of importance, because solution paths may switch from a tie line path to a nontie line path at these points. A sketch of some nontie line paths is given for a simple ternary system in Figure 2.3. An equal eigenvalue point is an apex on the given nontie line path.

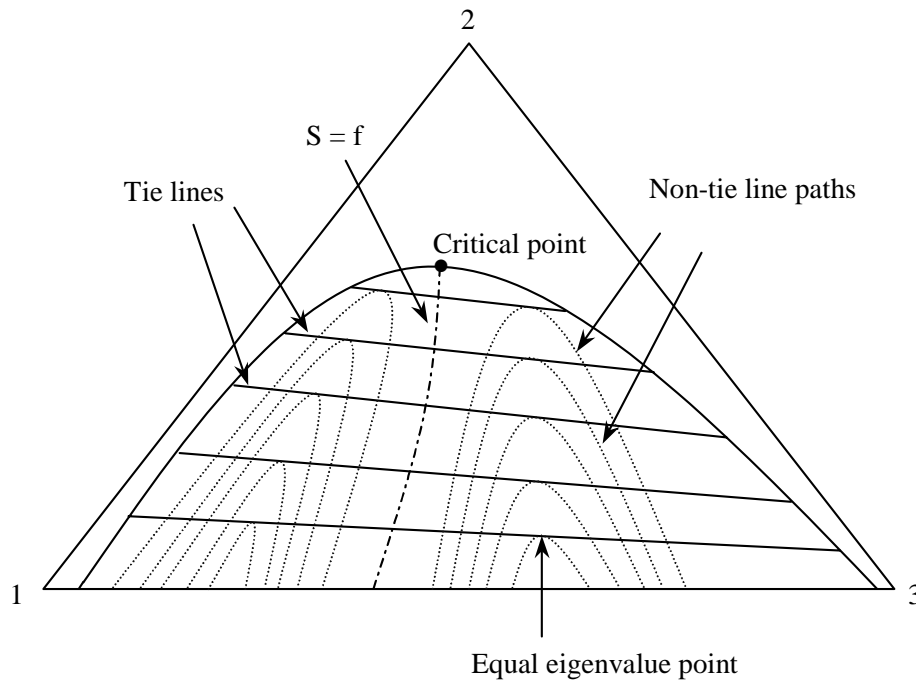


Figure 2.3: Tie line paths, nontie line paths and equal eigenvalue points.

A nontie line path can be traced by integration of nontie line eigenvalues in the corresponding eigenvector directions. The surface of tie lines traveled by a nontie line path is a ruled surface. For systems with more than three components these surfaces are not planar but developable surfaces as pointed out by Wang⁵⁴.

2.4 Solution Construction Tools

The solution to a given 1-D displacement process is made up by a sequence of different segments. Possible segments are

- Shocks along key tie lines when entering and leaving the two-phase region
- Shocks connecting key tie lines (nontie line shock)
- Continuous variation along key tie lines (tie line paths)
- Constant states (on key tie lines)
- Continuous variation connecting key tie lines (nontie line paths)

In the following attention is focused on the geometrical construction of shocks and their relation to the fractional flow curve. Three different types of shocks can occur in the 1-D solution, Johns²⁴.

1. The genuine shock where both the up- and downstream compositions of the shock have eigenvalues (composition velocities) different from the shock velocity.
2. The semi-shock (tangent shock) where either the up- or downstream composition of the shock has an eigenvalue equal to the shock velocity.
3. The contact discontinuity (indifferent shock) where both the up- and down-stream compositions of the shock have eigenvalues identical to the shock velocity.

2.4.1 Shocks due to Phase Appearance/Disappearance

If the leading and the trailing shocks (entering the two-phase region from the initial and the injection compositions respectively) are considered first, these occur along single key tie lines. The properties of the initial and the injection tie line are found by performing negative flash calculations⁵⁶. A typical plot of an s-shaped fractional flow curve is illustrated in Figure 2.4. The shock balance for a shock entering the two-phase region is written as

$$\Lambda = \frac{Q_i^{II} - Q_i^I}{G_i^{II} - G_i^I}, \quad i = 1, \dots, nc \quad (2.32)$$

The superscripts *I* and *II* refer to the single- and two-phase regions respectively. In Eq. 2.32

the shock balance is written in terms of the NVC formulation for simplicity. By inserting the definitions of Q_i and G_i into Eq. 2.32 it is easily seen that

$$\Lambda = \frac{f - \theta}{S - \theta} \quad (2.33)$$

where θ is the superficial vapor saturation corresponding to the single-phase composition (gas or oil).

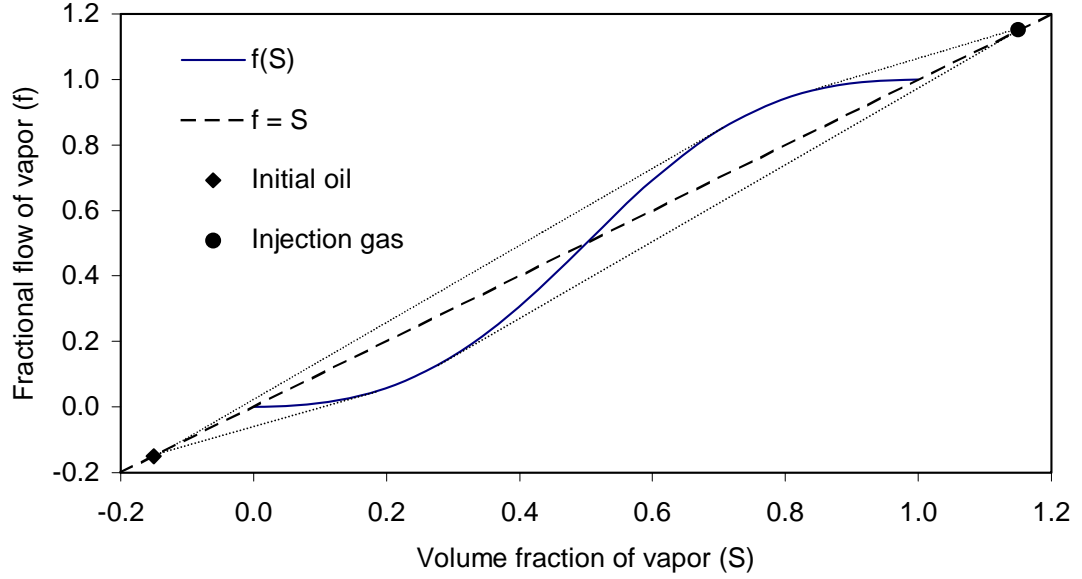


Figure 2.4: Semi-shock construction along initial or injection tie line.

For semi-shocks the tie line eigenvalue must be equal to the shock velocity on the up- or downstream side of the shock. For shocks entering the two-phase region the shock velocity Λ can hence easily be determined by locating the line from θ which is tangent to the fractional flow curve (ff-curve). The vapor saturation corresponding to the point of tangency on the ff-curve can be found by solving

$$\Lambda = \frac{df}{dS} = \frac{f - \theta}{S - \theta} \quad (2.34)$$

where f is given as an explicit function in S (Eq.2.15). This type of tangent constructions is also known from the Buckley-Leveret⁴ theory. For s-shaped ff-curves two tangent constructions are possible as illustrated in Figure 2.4. Helfferich¹⁵ demonstrated that the solutions to gas injection problems are bound to be in the $f > S$ part of the compositional space and therefore one of the tangent constructions can easily be ruled out. Dindoruk⁷ stresses that

not all shocks, due to phase appearance or disappearance, are tangent shocks. Depending on the compatibility with the rest of the solution they can be genuine shocks. In the latter case the landing point in the two-phase region is known and the shock velocity can be calculated directly from Eq. 2.33.

2.4.2 Shocks in the two-phase region

A significant contribution to the analytical theory was made by the work of Orr et al.³⁸, who demonstrated that if two key tie lines are connected by a shock they must intersect. Dindoruk⁷ later used the VC formulation of the conservation equations to derive the general proof. In the NVC formulation a nontie line shock must fulfill

$$\Lambda = \frac{Q_i^u - Q_i^x}{G_i^u - G_i^x} = \frac{Q_i^d - Q_i^x}{G_i^d - G_i^x}, \quad i = 1, \dots, n_c \quad (2.35)$$

The superscript x denotes the composition point at which the key tie lines intersect upon extension. By comparison of Eq. 2.35 and Eq. 2.32 it is seen that an expression similar to Eq. 2.33 can be derived. Hence, Eq. 2.35 can be rewritten as

$$\Lambda = \frac{f^u - \theta^u}{S^u - \theta^u} = \frac{f^d - \theta^d}{S^d - \theta^d}, \quad i = 1, \dots, nc \quad (2.36)$$

To illustrate the construction of a nontie line tangent shock, it is convenient to use a plot of the Q vs. G plot for the adjacent key tie lines. Such a plot is given in Figure 2.5.

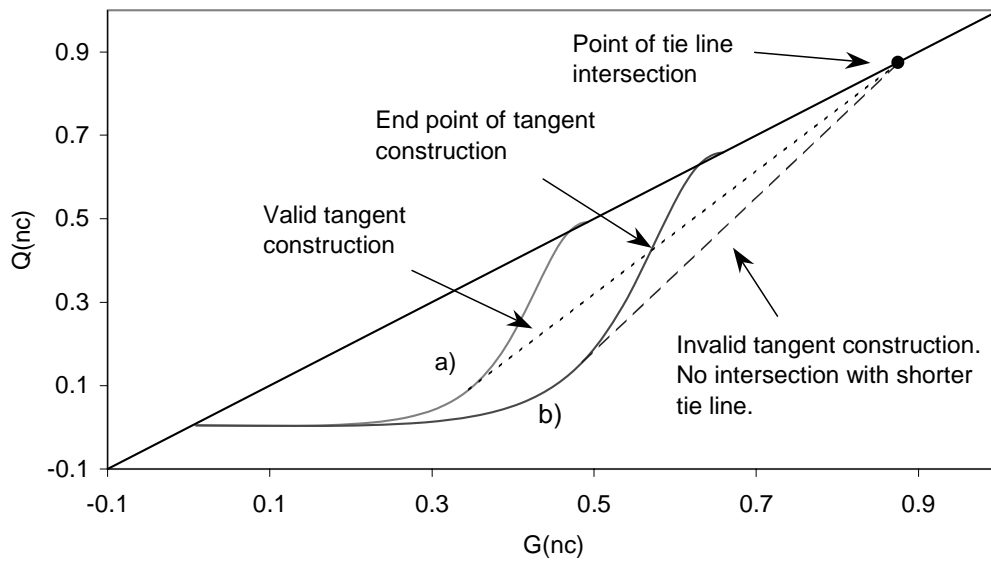


Figure 2.5: Nontie line tangent shock construction.

The Q vs. G curves for two neighboring key tie lines a) and b) are shown in Figure 2.5. Component nc is used as a reference component but in general any component present on both tie lines can be used. By discarding the solutions in the $f < S$ region of the compositional space, only two tangent constructions are possible, but only one of the tangent constructions will, as illustrated in the figure, give the correct shock solution. From a computational point of view, Eq. 2.36 can be solved for one of the key tie lines (b) to determine a shock velocity. Subsequently, the left-hand side of Eq. 2.36 is fixed and solved for S on the adjacent tie line (a). If a solution exists, tie line (b) holds the tangent part of the shock and the construction is completed. Otherwise the procedure is reversed (tangent construction to tie line (a)) and a solution will be found. Two neighboring key tie lines may also be connected by a genuine shock. In such a case a composition point on one of the tie lines is known in advance and Eq. 2.35 is used directly to calculate the shock velocity and the landing point composition on the neighboring key tie line.

2.4.3 Continuous Variation along Tie Lines and Constant States

To illustrate the existence and the nature of continuous variation along key tie lines as well as constant states three neighboring key tie lines are considered. A sketch of the tie lines is given in Figure 2.6.

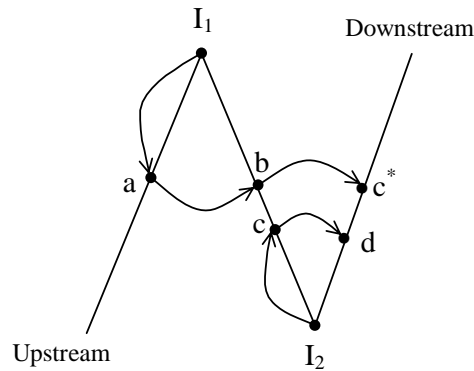


Figure 2.6: Illustration of continuous variation along a key tie line and constant states.

It is assumed that the tie lines are connected by shocks and hence must intersect at I_1 and I_2 upon extension. Starting at the upstream intersection point I_1 a tangent construction is made,

which results in the jump point a , the landing point b and the shock velocity Λ_{ab} . The shock velocity is equal to the tie line eigenvalue at point a ($df/dS_a = \lambda_a$). Next, two different cases can arise. In the first case, a tangent construction from the intersection point I_2 is made giving the jump point c , the landing point d and the shock velocity Λ_{cd} . For this construction the shock velocity equals the tie line eigenvalue at point c ($df/dS_c = \lambda_c$). In order for the two segments to be compatible they must comply with the velocity rule. That is, characteristic wave velocities must increase in the downstream direction. Thus, for the segments to be compatible

$$\Lambda_{cd} \geq \lambda_b \geq \Lambda_{ab} \quad (2.37)$$

On the assumption that Eq. 2.37 is not violated in this scenario, the saturation profile corresponding to the shock segments is sketched (full line) in Figure 2.7.

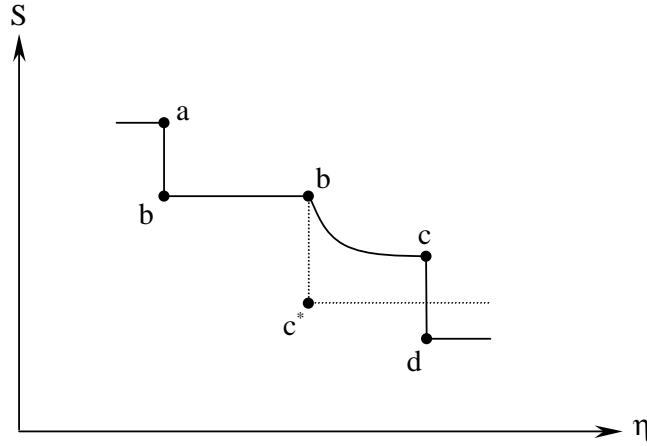


Figure 2.7: Sketch of some possible combinations of constant states and continuous variation on key tie lines.

The saturations at points a and b are connected by a shock (vertical line). As the tie line eigenvalue at point b exceeds the speed of the shock, a constant state (constant saturation) follows the tangent shock allowing the saturation at the landing point to speed up and match the tie line eigenvalue. The compositions corresponding to points b and c are then connected by continuous variation along the tie line (curved segment in Figure 2.7) until the tangent point of the second shock construction is reached.

By, on the other hand, assuming that Eq. 2.37 is violated by the two tangent constructions a different scenario will arise. In the illustrated case the tangent construction from I_2 must be replaced by a genuine shock. As stated previously, one point is known in advance when the shock balance for a genuine shock is solved. In Figure 2.6 that is the composition at point b . The shock velocity of the genuine shock Λ_{bc*} must be larger than Λ_{ab} and hence a constant state enters the solution. The saturation profile corresponding to the second scenario is illustrated in Figure 2.7 by the dotted line from point b and on.

2.4.4 Continuous Variation along Nontie Line Paths

As pointed out previously a solution path can switch from a tie line path to a nontie line path due to the non-strictly hyperbolic nature of the conservation equations. Thus, two adjacent key tie lines can be connected by continuous variation along a nontie line path (rarefaction) as opposed to the shock constructions described in the preceding sections. The nontie line path travels a sequence (family) of tie lines which form a ruled surface. In general the ruled surface of a given nontie line path can be linked to an envelope curve as illustrated by Figure 2.8 in a 2-D projection.

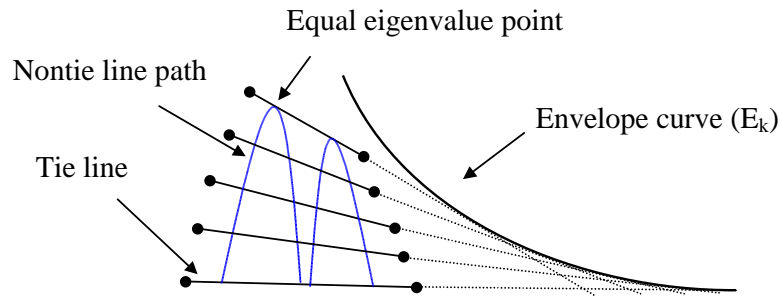


Figure 2.8: 2-D projection of ruled surface of tie lines and corresponding envelope curve.

The tie lines on a ruled surface are all tangents to the envelope curve upon extension as depicted in Figure 2.8. The switch between tie line and nontie line paths can only take place at equal eigenvalue points and hence a method for locating the equal eigenvalue points is required. Two methods for location of the equal eigenvalue points are available. One approach is to locate the equal eigenvalue points by combining an iterative scheme with a direct calculation of the eigenvalues along a given key tie line. Dindoruk⁷ suggests a far

simpler and more elegant approach where the variation of nontie line eigenvalues along a key tie line is linked to the corresponding envelope curves. Each key tie line connects $nc-2$ ruled surfaces corresponding to the directions of the nontie line eigenvectors (e_k) and can thus be linked to $nc-2$ envelope curves (E_k). Dindoruk⁷ demonstrates that the superficial vapor saturation θ_k at which a key tie line extension is tangent to the envelope curve E_k can be calculated as

$$\theta_k = \frac{\lambda_k S - f}{\lambda_k - 1} \quad (2.38)$$

λ_k is the k 'th nontie line eigenvalue at an arbitrary point on the key tie line corresponding to the vapor saturation S and a fractional flow of vapor $f(S)$. In this approach the eigenvalues only have to be calculated once to determine the $nc-2$ θ_k 's. The variation of the nontie line eigenvalues along a key tie line can subsequently be calculated by isolation of λ_k in Eq. 2.38. The equal eigenvalue points are calculated, in a tangent construction manner, by solving Eq. 2.39:

$$\lambda_k = \frac{df}{dS} = \frac{f - \theta_k}{S - \theta_k} \quad (2.39)$$

for the vapor saturation. A plot of the typical variation in eigenvalues along a key tie line along with the equal eigenvalue points is given for a quaternary system in Figure 2.9.

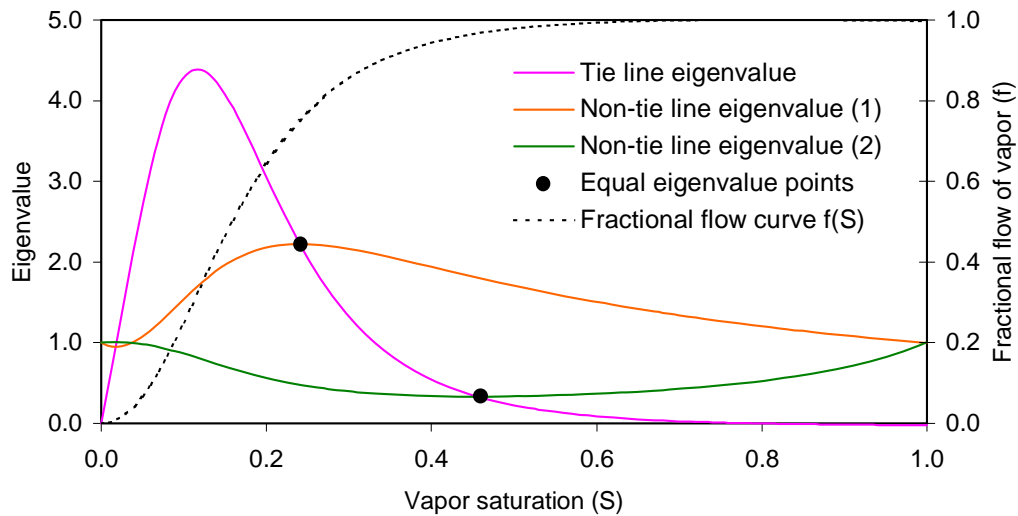


Figure 2.9: Equal eigenvalue points and variation of eigenvalues along a key tie line.

2.5 Approximation of Key Tie Lines

The tools for constructing solutions to the 1-D gas injection problem, presented in the previous sections, all assumed that the location of all key tie lines was known in advance. However, that is not the case in general. The analytical solutions previously presented in the literature have been restricted to considering only quaternary systems when more than one component is present in the injected gas. For systems with more than four components the presented solutions have been restricted to considering injection of pure component gases and fully self-sharpening systems. For a fully self-sharpening system the solution path is made up exclusively of shocks and hence the key tie lines must intersect pairwise³⁸ as illustrated in Figure 2.10.

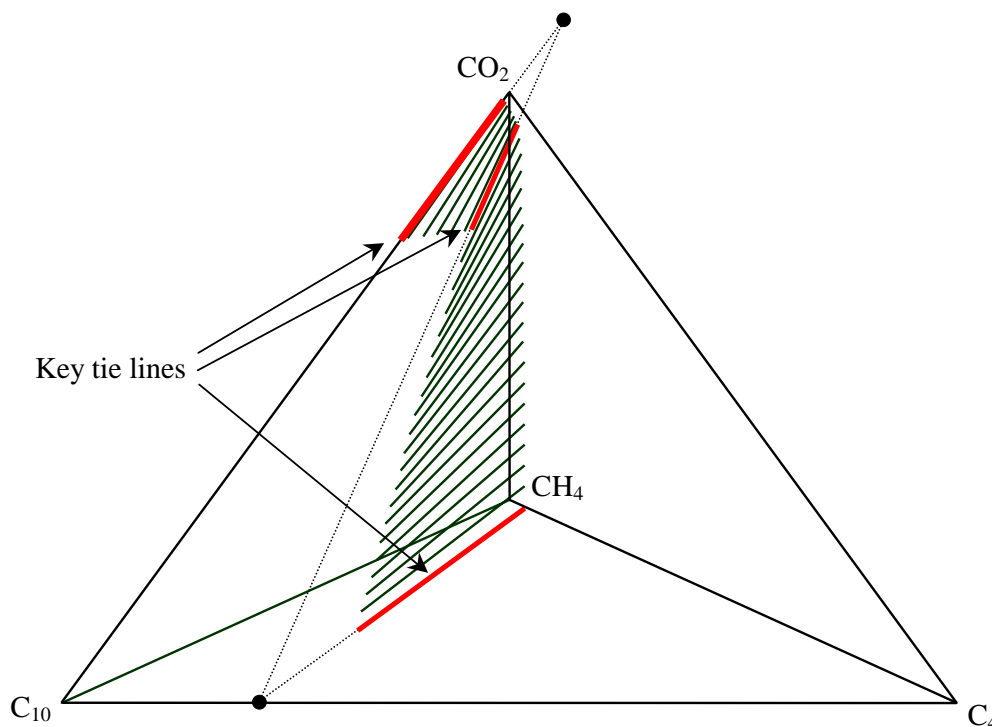


Figure: 2.10 Illustration of intersecting key tie lines.

The combination of using a pure component injection gas and a self-sharpening system allows the key tie lines to be located in a sequential manner. The approach to location of the tie lines is discussed in sections 3.3.6 and 3.4.

If two key tie lines are connected by continuous variation along a nontie line path (spreading wave), there is no proof whether or not these tie lines will intersect upon extension. Wang and Orr^{52,53} demonstrated by calculations the modesty of the error introduced by assuming that tie lines connected by a spreading wave intersect. The tie line intersection approach can thus be used to approximate key tie lines. The intersection approach forms the backbone of this work in the sense that it is used for predicting the minimum miscibility pressure in Chapter 3 and for generating approximate 1-D solutions in Chapters 4 and 5.

2.6 Summary

In this chapter a mathematical formulation of the one-dimensional dispersion free two-phase flow problem has been presented. The presentation includes two versions of the mass conservation equations: A general version and a simplified version. In the simplified version components are assumed to mix ideally as they transfer between equilibrium phases. The conservation equations are given by a set of first order non-strictly hyperbolic PDEs which along with the specification of constant initial data give rise to a Riemann problem. It is illustrated how the PDEs can be transformed into an eigenvalue problem which can be solved analytically due to the self-similarity of the solution.

The uniqueness requirement, the velocity rule and the entropy condition are outlined. It is emphasized that the solution to the 1-D flow problem is controlled by the geometry of *nc-I* key tie lines in the compositional space. Two of these are the initial and the injection tie lines. The remainder of the key tie lines is known as crossover tie lines.

The reader is introduced to the tools available for constructing analytical solutions to the 1-D flow problem. In this connection it has been demonstrated how shock balances can be solved on the basis that two key tie lines connected by a shock must intersect. The appearance of spreading waves (continuous variation along nontie line paths) due to the non-strictly hyperbolic nature of the conservation equations has been discussed.

The need for a general approach to approximation of the key tie lines has been discussed. An approach, known as the tie line intersection approach, has been sketched and will be developed further in the following chapters for the purpose of calculating the minimum miscibility pressure and for generation of approximate 1-D solutions to the simplified and the general 1-D flow problem.

3. Determination of the Minimum Miscibility Pressure

In this section the problem is addressed how to determine the minimum miscibility pressure (MMP). Initially, the reader is introduced to the main mechanisms controlling the development of a miscible displacement. Then a brief presentation of the methods, previously presented in the literature, for prediction of the MMP is given. Finally, a new approach to calculation of the MMP is presented.

3.1 First contact miscibility

At a given temperature and pressure, an injection gas is first contact miscible with an oil if any mixture of the two fluids forms a single phase. The lowest pressure at which two fluids are first contact miscible is known as the first contact miscibility pressure (FCMP). The definition of the FCMP is sketched in Figure 3.1.

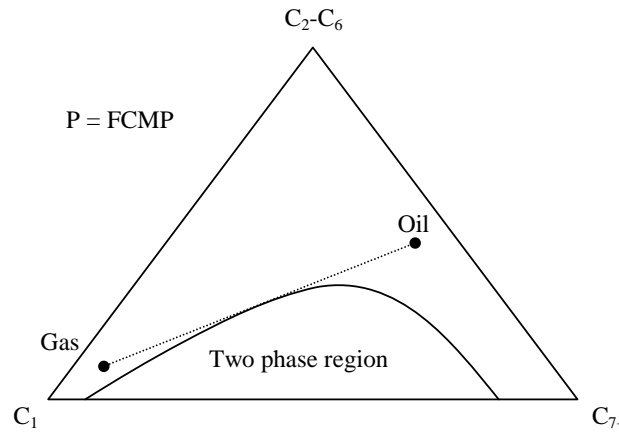


Figure 3.1: Definition of the first contact miscibility pressure (FCMP).

In the pseudoternary representation of Figure 3.1 the dilution line connecting the oil and the gas compositions must be tangent to the phase boundary at the FCMP. For a multicomponent fluid description, the FCMP can be determined by plotting the saturation pressure of all possible mixtures of the oil and the gas vs. the mixing ratio α . The maximum on the P_{sat} vs. α curve is then the FCMP. Reservoir engineers refer to the P_{sat} vs. α curve as a swelling test.

3.2 Multicontact Miscibility

When the vapor and the liquid phases move through the porous media, the fluids come into contact with multiple different compositions. As a consequence, the component present in the system partition between the equilibrium phases and miscibility may develop along the displacement by three different mechanisms. These are

- The vaporizing gas drive
- The condensing gas drive
- The combined vaporizing/condensing gas drive

When the development of miscibility is controlled by a vaporizing gas drive (VGD), intermediate components (C_2 - C_6) from the oil phase are gradually vaporized by the passing vapor, forming a denser vapor phase. At some point during the displacement an enriched vapor phase becomes locally miscible with the liquid phase. The characteristic features of the vaporizing gas drive are sketched in Figures 3.2 and 3.3

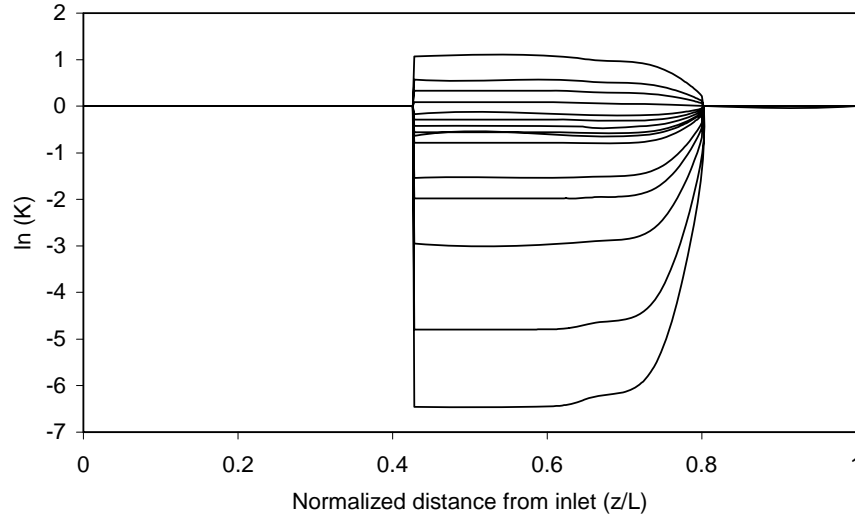


Figure 3.2: Developed multicontact miscible displacement. Vaporizing drive. The figure illustrates the development of K-factors (vapor to liquid phase ratio of components present in the mixture) along the displacement direction.

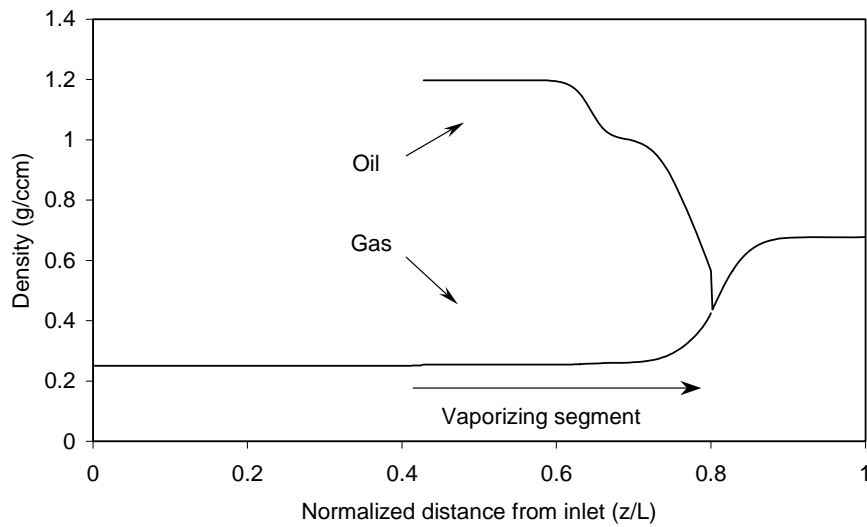


Figure 3.3: Developed multicontact miscible displacement. Vaporizing drive. The figure illustrates the development of phase densities along the displacement direction.

Figure 3.3 illustrates how the density of the vapor phase starts to increase in the vaporizing segment of the displacement. The density of the liquid phase decreases over the same segment and coincides with the vapor phase at the single phased displacement front. In the illustrated case the miscible front is also the leading front of the displacement. Development of multicontact miscibility by a vaporizing mechanism will, due to the nature of the VGD, normally be possible if light gases are injected. Examples of light injection gases are pure N_2 and pure methane.

On the other hand, if gas mixtures with a high content of intermediate and heavier components (enriched gas) are injected into the porous media, a different mechanism may control the development of miscibility. When an enriched gas comes into contact with the oil in place, intermediate and heavier components may condense into the oil forming a lighter oil phase. Eventually, the enriched oil phase can become locally miscible with the gas phase. If multicontact miscibility develops by this phenomenon, the mechanism controlling the development of miscibility is known as a condensing gas drive (CGD). The characteristic features of a CGD are given in Figures 3.4 and 3.5.

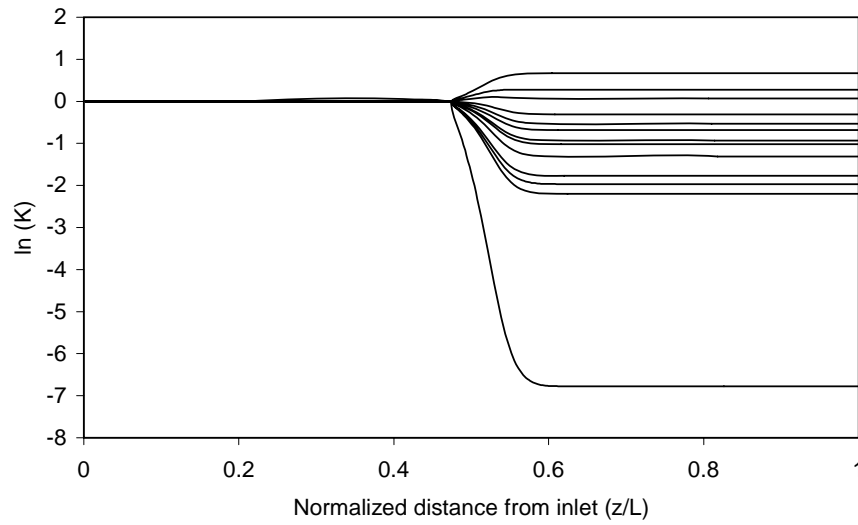


Figure 3.4: Sketch of a developed multicontact miscible displacement. Condensing drive. The figure illustrates the variation in K-factors along the displacement direction.

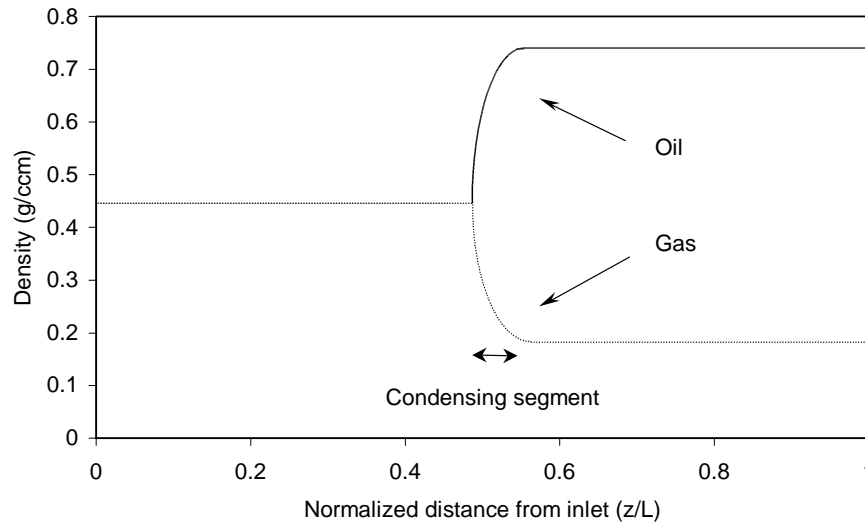


Figure 3.5: Sketch of a developed multicontact miscible displacement. Condensing drive. The figure illustrates the development of phase densities along the displacement direction.

In Figure 3.5 the density of the gas phase decreases across the condensing segment as the intermediate components are migrating into the oil phase. The original injection gas becomes locally miscible with the lighter oil phase at the back of a two-phase region. In this case the

miscible front differs from the leading front, which is located at the end of the condensing segment.

The existence of a combined vaporizing and condensing gas drive was discovered by Zick⁵⁸ and subsequently by Stalkup⁴⁴. They pointed out the possible coexistence of a vaporizing and a condensing segment along the displacement direction. The typical features of the combined mechanism are illustrated in Figures 3.6 and 3.7.

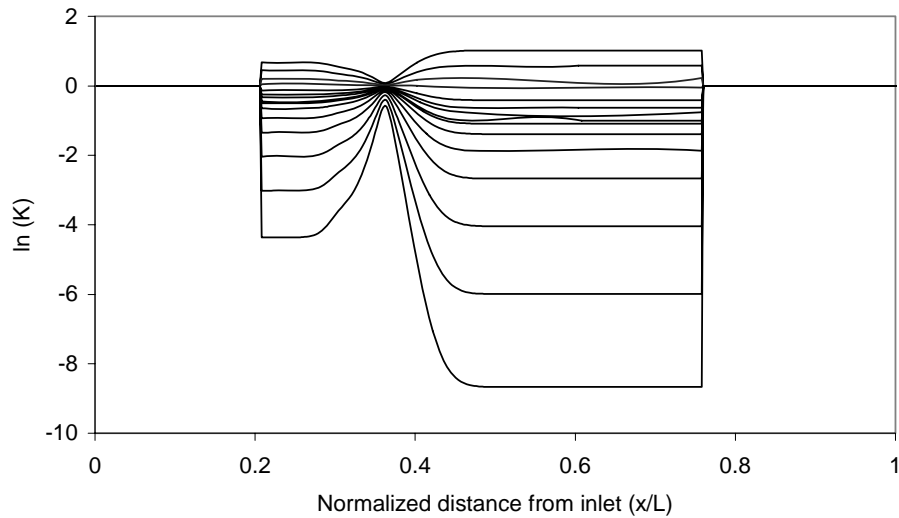


Figure 3.6: K-factor profile along the displacement direction for a v/c gas drive.

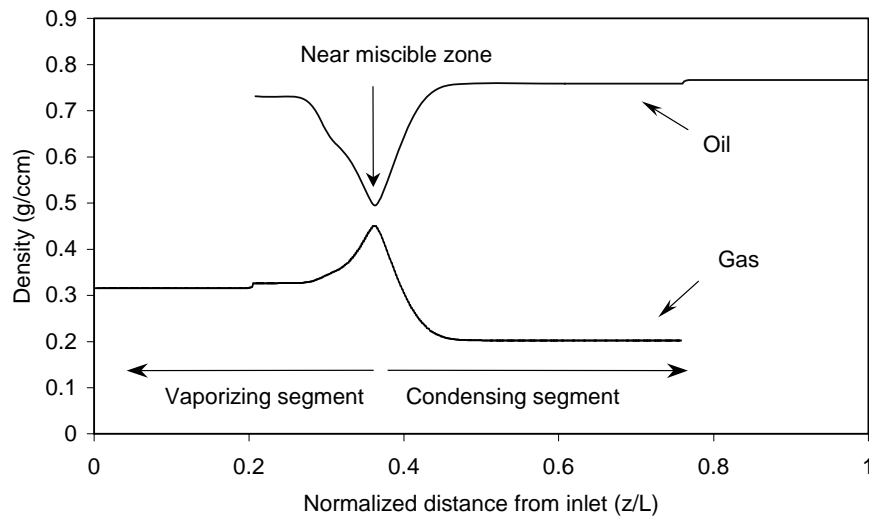


Figure 3.7: Density variation along the displacement direction for a v/c gas drive.

Starting from the injection site, the density of the gas phase increases along the displacement direction due to the vaporization of intermediate components. Then in a near-miscible zone, intermediate components start to migrate back into the liquid phase by condensation, forming a condensing segment.

The discovery of the combined vaporizing and condensing mechanism was a significant milestone in understanding and modeling miscible as well as near-miscible gas injection processes. The significance will become evident from the following presentation and discussion of previously suggested methods for calculation of the minimum miscibility pressure.

3.3 Traditional Determination of the MMP

Ever since the injection of gas became a prospect of enhancing the recovery from oil reservoirs, methods for prediction of the minimum miscibility pressure have been suggested in the literature. Traditionally, the minimum pressure at which the gas should be injected in order to realize a miscible displacement (MMP) has been determined experimentally by slimtube experiments. The experimental apparatus used for slimtube experiments is shown in Figure 3.8:

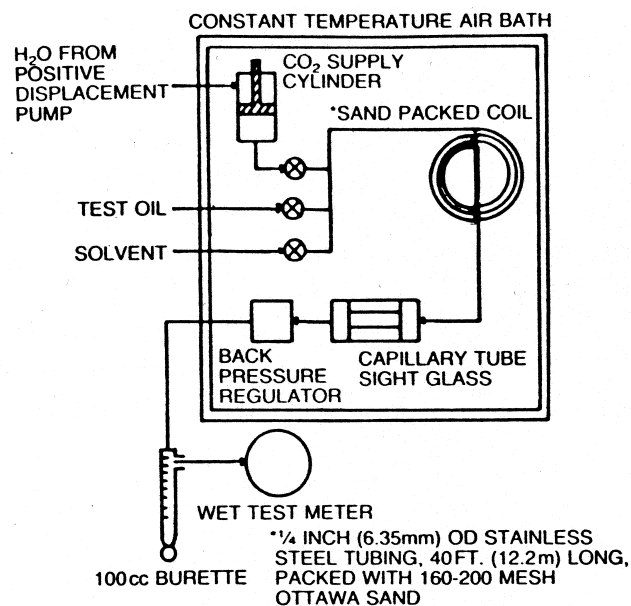


Figure 3.8: Sketch of a slimtube apparatus⁴⁷.

The slimtube apparatus consists of a long steel tube packed with sand to ensure proper mixing of the fluids. The tube is initially saturated with reservoir fluid and placed in a constant temperature air bath. The gas of interest is then injected into the tube at constant velocity or constant pressure drop and the reservoir fluid is displaced. The produced fluids are collected at the outlet and the recovery of the original oil in place (OOIP) is calculated after 1.2 pore volumes have been injected. Unless otherwise mentioned, the recovery is defined as the volume-based ratio of the produced oil and the OOIP under standard conditions (25°C and 1 atm). The apparatus is then cleaned and the procedure is repeated at a different average pressure. By plotting the recovery factors vs. the corresponding average pressure, a picture like Figure 3.9 typically emerges.

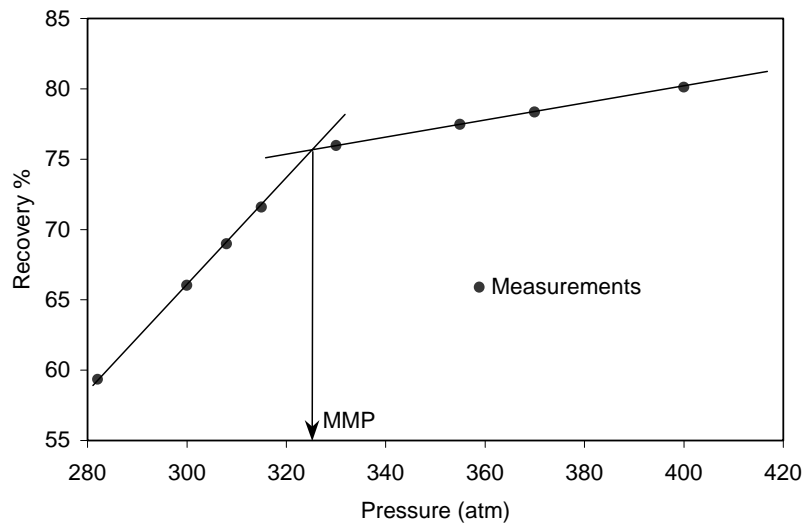


Figure 3.9: Sketch of a typical recovery vs. pressure plot. Definition of the MMP.

The experimental recovery curve exhibits two different regions. At low pressures the recovery increases more rapidly with increasing pressure than at higher pressures. The break point on the recovery curve has traditionally been used to determine the pressure at which a miscible displacement develops, and it was hence considered to be at the MMP. By increasing the injection pressure above the MMP, only a minor increase in the recovery is achieved. Thus the determination of the MMP is of major economic importance when implementation of a gas injection project is considered.

Obviously, the experimental approach to determination of the MMP is very time consuming and consequently expensive. This fact qualifies the massive effort spent on the development of predictive tools. The numerous suggestions for such predictive tools, documented in the literature, can be organized in six main groups:

- Empirical correlation
- Ternary representation/ Limiting tie line approach
- Single cell simulation
- Slimtube simulation
- Multicell simulation
- Semi-analytical methods by the intersecting tie line approach

The different methods will be described and briefly discussed in the following subsections.

3.3.1 Empirical Correlations

Various authors have developed empirical correlations for the purpose of predicting the MMP^{10,11,12,13,25,41,57}. Most of these are based on the theorem of corresponding states or methods derived from this theorem. Experimental MMPs are correlated with properties like pseudocritical temperature and pressure, gas densities and molecular weight of the C₇₊ fraction. Most of the methods are based on studies of pure injection gases (e.g. CO₂) or slightly contaminated injection gases. As in any other application of the corresponding states principle, the predictions become unreliable upon extrapolation. Hence, good results can only be obtained for systems very similar to the reference system. The correlations are easy to use and give a fast result, but as soon as the correlations are used for other systems than the reference, the predicted MMPs are of very little use. Consequently, more general methods for prediction of the MMP are needed.

3.3.2 Ternary Representation/Limiting Tie Line Approach

With the discovery of the vaporizing and the condensing mechanism⁴² in the late 1950s, pseudoternary representations of the phase behavior of gas-oil systems were used to predict

the development of multicontact miscibility in gas injection processes. The properties of such a representation are shown in Figure 3.10.

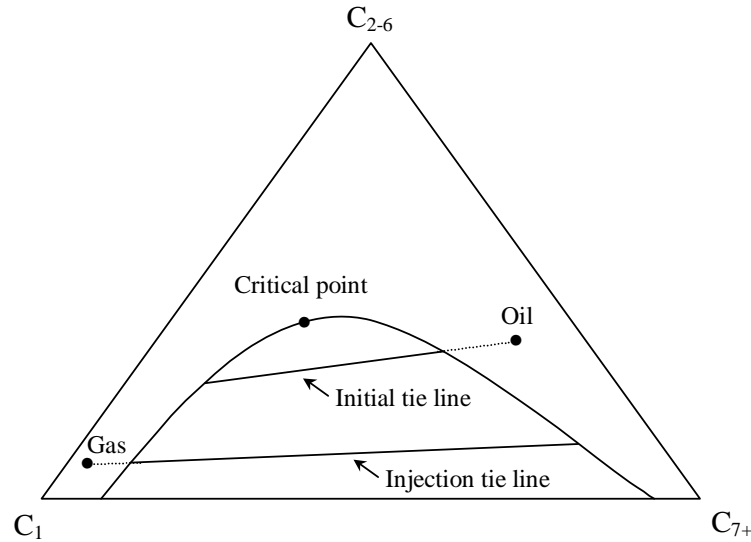


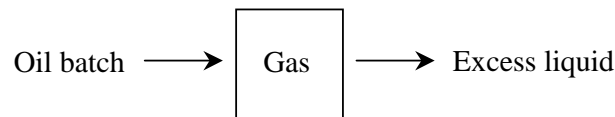
Figure 3.10: Pseudoternary representation of the gas injection process.

Two tie lines denoted the injection and the initial tie line are illustrated in Figure 3.10. These tie lines extend through the injected gas composition and the initial oil composition respectively. A miscible displacement, in the pseudoternary sense, develops at a pressure where one of these tie lines becomes a critical tie line (tangent to the two-phase boundary). In the illustrated case the initial tie line becomes a critical tie line at a lower pressure than that of the injection tie line. This corresponds to vaporizing gas drive in the sense that the initial oil becomes multicontact miscible with a richer gas phase. If the injection tie line becomes critical the mechanism controlling the development of miscibility is a CGD as the injected gas becomes miscible with a lighter oil phase. For the system illustrated in Figure 3.10 the pressure needed for development of a miscible displacement would be lower for the VGD than for the CGD. Hence, in the pseudoternary sense, the VGD_{MMP} would be considered as the MMP. The pressure at which the initial and the injection tie lines become critical can be calculated by using a negative flash algorithm (Whitson and Michelsen⁵⁶) or by using the mixing cell approach described in section 3.3.3

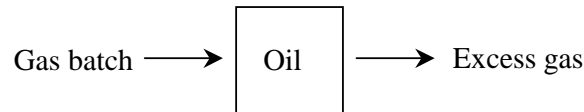
Use of the pseudoternary representation for prediction of the MMP give rise to the problem that the result can only be rigorously correct for true ternary systems because of the partitioning of intermediate components (C_2 - C_6) during the displacement. In other words, the properties of the pseudocomponent C_{2-6} change along the displacement process and the shape of the two-phase region changes accordingly⁵⁸. Another more fundamental problem of using the ternary representation is that the development of miscibility can only take place at the injection site (condensing drive) or at the displacement front (vaporizing drive). Or stated in another way, the ternary representation cannot predict the existence of a combined VGD/CGD mechanism.

3.3.3 Single Cell Simulators

To account for the deficiencies of the pseudoternary approach to determination of the MMP, several methods based on a single mixing cell have been suggested (e.g. Jensen and Michelsen¹⁷). In the mixing cell approach, the thermodynamic behavior of the reservoir fluid and the injected gas is described as a multicomponent system by an equation of state (EOS). The logic of the mixing cell approach is illustrated in Figure 3.11.



a) Forward contact



b) Backward contact (reversed contact)

Figure 3.11: Sketch of the mixing cell approach.

The mixing cell approach consists of two different numerical experiments. In the first case (a) a cell of constant volume, temperature and pressure is filled with the injected gas. A batch of the reservoir fluid is added and the resultant mixture is flashed. The excess volume of the cell is then removed. Any liquid formed by the contact is removed before gas is removed. After removing the excess volume a new batch of fresh oil is added, and the procedure is repeated until the composition in the cell no longer changes. If the mixing cell forms a single phase during any of the contacts, the pressure is above the MMP and a new experiment is performed at a lower pressure. On the other hand, if the simulation converges as a two-phase system, the pressure is below the MMP and a new run is performed at a higher pressure. The pressure can be updated by a simple bisection approach. The $MMP_{\text{one-cell}}$ is defined as the pressure at which the simulation converges at a critical composition. A typical result of a one-cell simulation is illustrated in Figure 3.12.

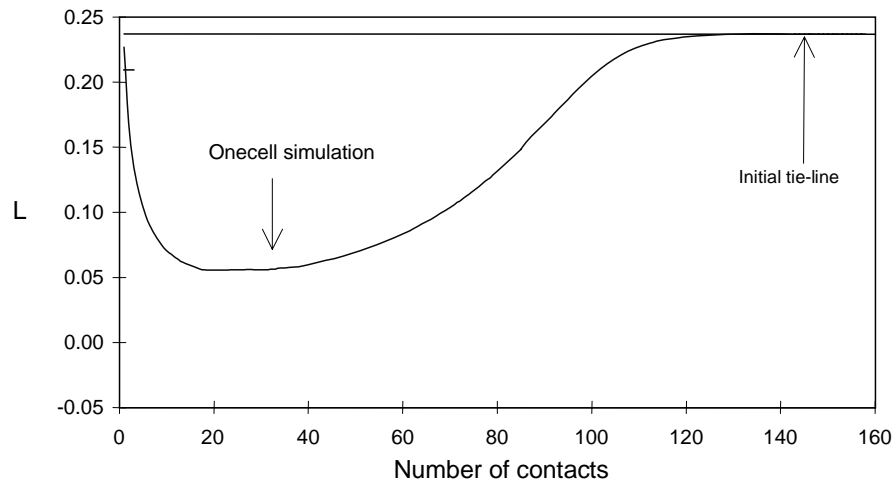


Figure 3.12: One-cell simulation. $P < MMP_{\text{one-cell}}$ (forward contacts).

The y-axis in the figure is the length of the tie line from each contact. The length of a tie line can be defined as

$$L = \sqrt{\sum_{i=1}^{nc} (x_i - y_i)^2} \quad (3.1)$$

where x_i and y_i are liquid and vapor mole fractions. In Figure 3.12 the composition initially moves towards the critical locus and reaches the minimum distance after ~30 contacts. Then the distance increases and the simulation converges at the initial tie line. By increasing the

pressure, the simulation will converge at a composition different from the initial tie line. This is why different values of the MMP in some cases are obtained from one-cell simulations and limiting tie line approaches based on negative flash calculations. Such difference has been reported for reservoir fluids by Jensen and Michelsen¹⁷ and described in detail by Wang and Orr⁵².

In the backward contact scheme (Figure 3.11b) the cell is initially filled with oil and fresh injection gas is added in batches. Excess gas is removed before excess liquid and the rest of the scheme is similar to that of forward contacts.

The physical locations corresponding to the one-cell simulations are the displacement front (forward contacts) and the injection site (backward contacts). If the features of the combined vaporizing and condensing mechanism are recalled, miscibility developed by a combined mechanism cannot take place at the injection site or at the displacement front. Hence, the one-cell simulators can only predict the rigorously true MMP for a pure condensing or pure vaporizing displacement. Pure vaporizing displacements exist for e.g. injection of N_2 or natural gases mainly consisting of CH_4 into oil. For more complex injection gases the displacements are always combined by nature and the use of one-cell simulations will lead to an overestimation of the MMP¹⁶. Pure condensing displacements have not, so far, been reported for multicomponent fluid descriptions.

3.3.4 Slimtube and Multicell Simulations

With the discovery of the combined VGD and CGD mechanism controlling the development of miscibility, Zick⁵⁸ and Stalkup⁴⁴ illustrated that more complex methods have to be used in order to capture the true nature of the general 1-D gas injection process. These methods fall into two categories: A mathematical approach and a physical approach. The mathematical approach is the slimtube simulations where the conservation equations governing 1-D two-phase dispersion-free flow are solved by a finite difference (FD) approach. A variety of different FD methods can be found in the literature, of which the simplest and most widely used is the fully explicit one-point upstream weighting scheme. The slimtube simulations are used to generate recovery curves and the MMP can be determined by the breakpoint on these curves. In the physical approach, the slimtube is described by a sequence of interconnected

tanks as illustrated in Figure 3.13. This approach is referred to as the multicell (MC) approach (Metcalf³³).

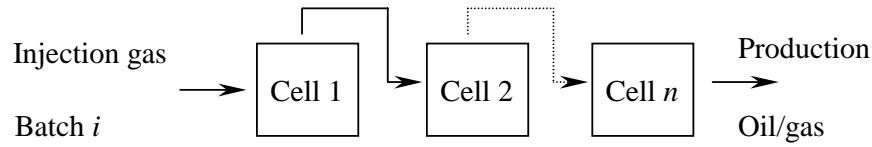


Figure 3.13: Sketch of the multicell approach.

The tanks are initially filled with reservoir fluid and gas is added in batches. Each batch is added to the first cell. The resultant overall composition in the cell is flashed and the excess volume is moved to the neighboring cell. This procedure is repeated for each cell until the production cell (cell n) is reached and a new batch is added to the first cell. The excess volumes are moved according to some specified fractional flow function. As for the FD approach, recovery curves are generated and the MMP can be estimated. It is common to both approaches that the simulation results, and hence the determination of the MMP, are strongly affected by numerical dispersion. Numerical dispersion originates from the discretization of the flow problem. The coarser grid blocks (lower number of cells) used in the simulation the larger the effect of numerical dispersion. The presence of numerical dispersion has the effect of smearing out the recovery curves and make the determination of a break point more difficult/inaccurate. The potential grid size dependence on recovery curves from FD simulations is illustrated in Figure 3.14.

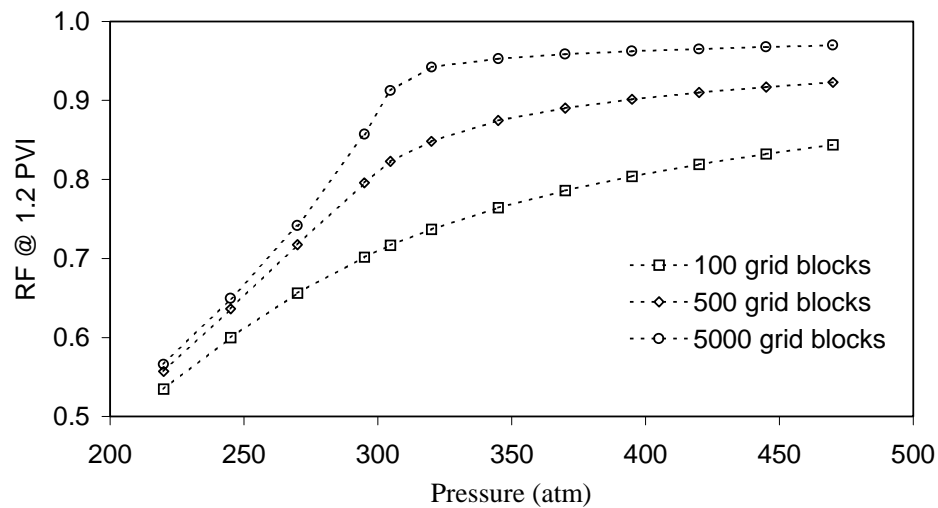


Figure 3.14: Recovery vs. pressure at 1.2 pore volumes injected (PVI). $\Delta\tau/\Delta z = 0.1$.

Hence, the task of determining the MMP by FD/multicell approaches becomes a balance between acceptable accuracy and acceptable CPU time consumption. Various attempts to eliminate the numerical dispersion have been suggested, starting with the paper of Stalkup⁴⁵. The general idea is to extrapolate the recovery factors from coarse grid/cell simulations to an infinite number of grid blocks/cells. A comparison of different extrapolation procedures is found in Høier¹⁶. Even if extrapolation procedures are combined with FD/MC simulations the CPU time consumption for determination of the MMP is still quite extensive. Thus, development of new and faster methods for calculation of the MMP is required.

3.3.5 Semi-analytical Calculation of the MMP

The semi-analytical approach to calculation of the MMP is based on the analytical theory for 1-D dispersion-free two-phase flow outlined in Chapter 2. The backbone of the semi-analytical approach is that the composition path specifying the solution to the 1-D flow problem has to travel through a sequence of key tie lines³⁶. For some systems where the solution to the 1-D problem consists of shocks only, the extensions of these key tie lines (the initial tie line, the injection tie line and nc-3 crossover tie lines) have been proven to intersect rigorously. In the general case and for the purpose of calculating the MMP, the assumption about intersecting key tie lines has proven to be a very good approximation⁵³. Orr et al.³⁸ showed that multicontact miscibility develops at a pressure where one of the key tie lines becomes a critical tie line (shrinks to a point). Dindoruk⁷ used the intersection approach to study the MMP behavior of four-component N₂ systems and Johns and Orr²³ extended the approach to fluid descriptions with up to 11 components, considering only pure component injection gases. Wang and Orr⁵² extended the previous works to multicomponent mixtures with an arbitrary number of components in the injection gas. They used an iterative scheme based on successive substitution to solve their formulation of the intersection equations, but reported numerical problems due to singularities for some systems. Their work formed the basis for a new approach developed in the course of this study. The new approach is also presented in Jessen et al.¹⁸ whereas results from the case study in Section 3.5 are given in Jessen et al.¹⁹

3.4 Global Approach for Calculation of the MMP

A new algorithm has been developed for calculation of minimum miscibility pressure for the displacement of oil by multicomponent gas injection. The algorithm is based on the key tie line identification approach initially addressed by Wang and Orr⁵³. In this work a new global approach is introduced. A number of deficiencies of the sequential approach have been eliminated, resulting in a robust and highly efficient algorithm. The time consumption for calculation of the MMP in multicomponent displacement processes has been reduced significantly and calculation of the MMP can now be performed within a few seconds on a PC for a 15-component gas mixture. Therefore the algorithm is particularly suitable for gas enrichment studies or other case studies where a large number of MMP calculations are required. Predicted results from the key tie line identification approach are shown to be in excellent agreement with slimtube data and with other MC/FD simulators presented in the literature.

3.4.1 Mathematical Approach

In the work of Wang and Orr⁵³ the existence of a point of intersection I is used to specify that two tie lines $A_1 - B_1$ and $A_2 - B_2$ are coplanar (Figure 3.15). Let the end points (A_1, A_2) represent the vapor compositions and (B_1, B_2) the liquid compositions.

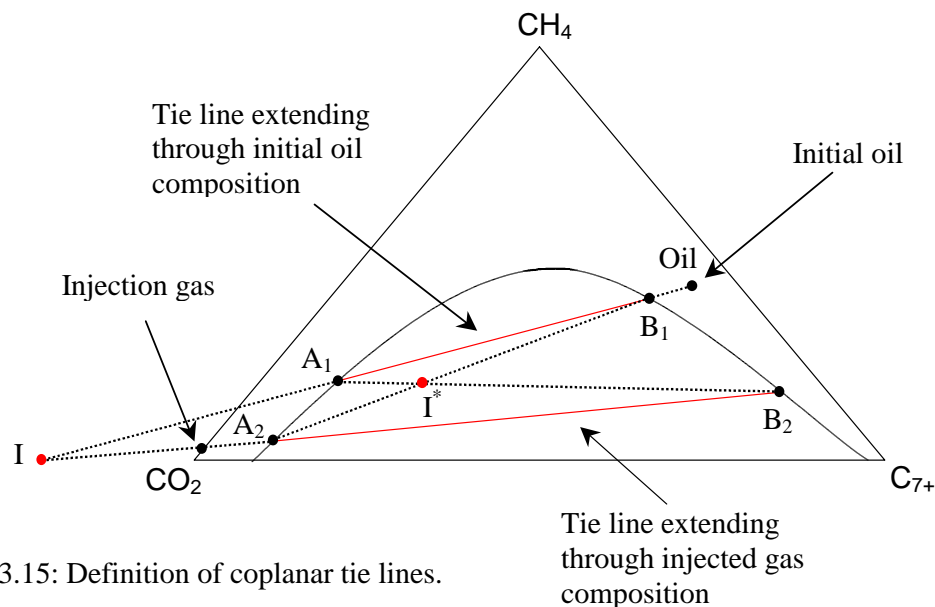


Figure 3.15: Definition of coplanar tie lines.

The coordinates of I must then satisfy

$$\underline{z}(I) = \beta_1 \underline{y}^{(1)} + (I - \beta_1) \underline{x}^{(1)} = \beta_2 \underline{y}^{(2)} + (I - \beta_2) \underline{x}^{(2)} \quad (3.2)$$

In this formulation the intersection point can, however, be located far outside the positive composition space and the corresponding vapor fractions β_1 and β_2 become numerically large when tie lines are close to parallel. In fact, the values of the vapor fractions may even change from minus infinity to plus infinity as tie lines change orientation. This feature will frequently result in numerical difficulties and should therefore be avoided.

We find it preferable to express the colinearity condition by the requirement that a point of intersection I^* between the lines $A_1 - B_2$ and $A_2 - B_1$ must exist (Figure 3.15). In this formulation Eq. 3.2 is replaced by

$$\underline{z}(I^*) = \alpha \underline{y}^{(1)} + (I - \alpha) \underline{x}^{(2)} = \beta \underline{y}^{(2)} + (I - \beta) \underline{x}^{(1)} \quad (3.3)$$

The new formulation of the intersection point constrains the corresponding variables α and β to be in the interval of $[0 ; 1]$, which is far more convenient from a numerical point of view. In the global approach the succession of $nc-1$ intersecting key tie lines is written as

$$x_i^{j+1}(1 - \alpha_j) + y_i^j \alpha_j - x_i^j(1 - \beta_j) - y_i^{j+1} \beta_j = 0, \quad \begin{cases} i = 1, nc - 1 \\ j = 1, nc - 2 \end{cases} \quad (3.4)$$

where i and j specify the component number and the tie line number respectively. The sequence of tie lines must connect the initial tie line and the injection tie line. Hence, we specify the initial oil composition z^{oil} and the injection gas composition z^{inj} by

$$\left. \begin{aligned} z_i^{oil} &= x_i^{j=1}(1 - \beta_{oil}) + y_i^{j=1} \beta_{oil} \\ z_i^{inj} &= x_i^{j=nc-1}(1 - \beta_{inj}) + y_i^{j=nc-1} \beta_{inj} \end{aligned} \right\} i = 1, nc - 1 \quad (3.5)$$

Eqs. (3.4) and (3.5) must be solved subject to the equilibrium constraint:

$$x_i^j \hat{\phi}_i^l - y_i^j \hat{\phi}_i^v = 0, \quad \begin{cases} i = 1, nc \\ j = 1, nc - 1 \end{cases} \quad (3.6)$$

Finally the mole fractions must sum to unity

$$1 - \sum_{i=1}^{nc} x_i^j = 1 - \sum_{i=1}^{nc} y_i^j = 0 \quad j = 1, \dots, nc - 1 \quad (3.7)$$

The MMP is determined as the lowest pressure where one of the tie lines becomes critical.

3.4.2 Solution Strategy

In order to solve the set of Eqs. 3.4-3.7 at a specified pressure, an initial estimate of all variables is required for a Newton-Raphson iteration scheme. This estimate has to be fairly accurate, in particular at pressures close to the MMP, where one tie line is nearly critical. An inaccurate initial estimate is here very likely to result in the “trivial solution” with two equilibrium phases becoming of identical composition, which leads to divergence. To ensure an adequate quality of the initial estimate, the overall calculation is divided into three distinct steps.

In the first step we select a pressure p_{ini} much lower than the assumed MMP in order to guarantee that all equilibrium phases are far from being critical. In addition, we select an approximate injection gas, consisting of the component present in the largest amount in the injection gas concerned, and neglect all other components. Wang and Orr⁵³ have shown that for a pure injection gas the sequence of tie lines can be determined in a simple sequential manner as described below. The tie line extending through the initial oil can easily be located by a negative flash calculation (Whitson and Michelsen⁵⁶). Then the initial tie line is extrapolated to the point where the composition of the most volatile component k (apart from the injected component) equals zero:

$$\beta_k = \frac{x_k}{x_k - y_k} \quad (3.8)$$

Based on the overall composition at β_k the first crossover tie line can be located by performing another negative flash calculation. Then the most volatile among the remaining components is removed and the procedure is repeated until the tie line extending through the injection gas is reached. In the pure component gas injection case, only the heavy component of the oil and the injected component are represented on this tie line.

In the second step we specify the injection gas composition as

$$\underline{z}_{inj} = (1 - \theta) \underline{z}_{inj}^{pure} + \theta \underline{z}_{inj}^{actual} \quad (3.9)$$

where the superscript *pure* indicates the injection gas used in the first step. The solution from the first step corresponds to $\theta = 0$, whereas the solution for the injection gas considered corresponds to $\theta = 1$. By use of the $\theta = 0$ solution as the initial estimate, the solution for a small value of θ is calculated, which is again used to determine consecutive solutions until we arrive at the desired $\theta = 1$ solution. In the final step, the injection gas composition is fixed at the true value and new solutions are determined at increasing pressures, by using that from the previous pressure step as initial estimate, until the MMP is reached. The measurement of the distance from a critical point d_j is calculated in each pressure step for all key tie lines j by

$$d_j = \sqrt{\sum_{i=1}^{nc} (x_i^j - y_i^j)^2} \quad (3.10)$$

To improve the performance of the algorithm the sensitivity equation

$$d\underline{F} = \frac{\partial \underline{F}}{\partial \underline{v}} d\underline{v} + \frac{\partial \underline{F}}{\partial p} dp = 0 \Rightarrow \frac{d\underline{v}}{dp} = - \left[\frac{\partial \underline{F}}{\partial \underline{v}} \right]^{-1} \frac{\partial \underline{F}}{\partial p} \quad (3.11)$$

is solved to find the pressure derivatives of all variables. \underline{v} is the variable vector. No significant computational expense is introduced by solving Eq. 3.11 as all matrices required already exist in a decomposed form. The pressure derivatives are then used to obtain a better estimate for the variables at new pressures and thus lower the number of iterations necessary in each pressure step. Furthermore, the derivatives indicate how much the pressure can be increased in each step. This is accomplished by using the fastest changing composition as a step moderator by making sure that the mole fractions do not extrapolate outside the interval $[0 ; 1]$.

3.4.3 Linear Solver for Newton-Raphson Iteration

To solve the non-linear system of equations described in the previous section a Newton-Raphson scheme is applied with analytical calculation of all elements in the Jacobian matrix. In each iteration the linear system of equations

$$\underline{\underline{J}} \underline{\underline{\Delta}} + \underline{\underline{F}} = \underline{\underline{0}} \quad (3.12)$$

must be solved for the correction vector $\underline{\underline{\Delta}}$. $\underline{\underline{J}}$ is the Jacobian matrix and $\underline{\underline{F}}$ is the trial function vector. The linear system may be solved directly by triangular (LU) decomposition followed by backsubstitution. For small systems (number of equations $N < 100$) this approach is very efficient. As the size of the system is increased, the number of algebraic manipulations for the decomposition increases as N^3 . For a 15-component fluid description the linear system to be solved in each iteration is of the size $N = 448$, and for this size the LU/back procedure is quite expensive. From initial studies of the Newton scheme it was found that the linear solver is the most time consuming part of the algorithm and hence should be the target for optimization in order to speed up the calculation. By analysis of the structure of the linear system it is found that an excessive number of multiplications by zero is performed when a general solver is used. Therefore, a solver specific to the global formulation has been developed. Figure 3.16 gives the structure of the Jacobian matrix for a four-component mixture.

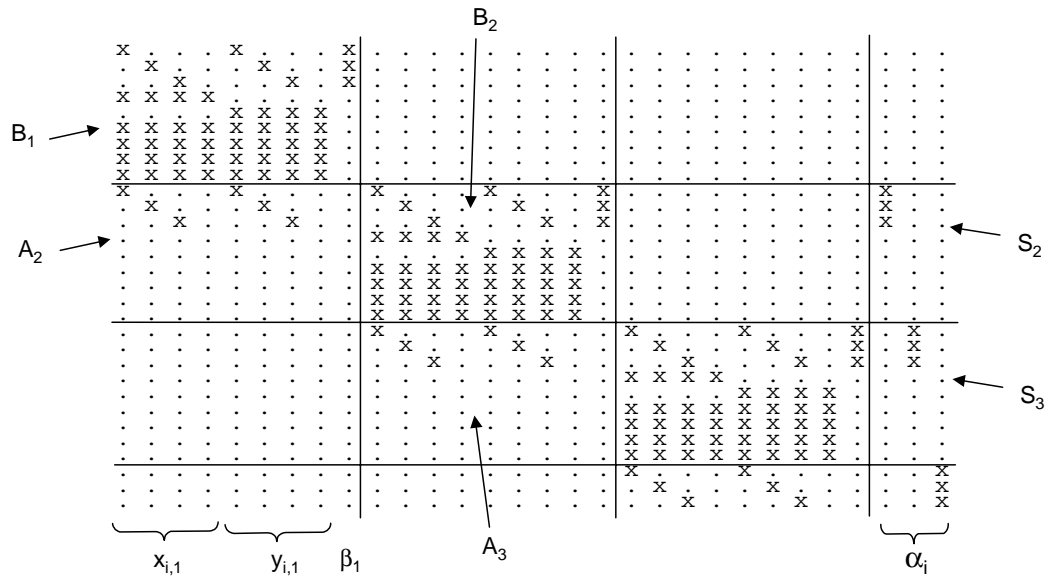


Figure 3.16: Non-zero entries of the Jacobian matrix for linear system (x = non-zero element).

Non-zero entries are marked by x whereas zero entries are indicated by a dot. The structure allows the system of linear equations to be solved in a blockwise manner. By defining the submatrices A , B and S as illustrated in Figure 3.16 the original linear system of equations (3.12) can be rewritten as:

$$B_1\Delta_1 + f_1 = 0 \quad (3.13)$$

$$A_2\Delta_1 + B_2\Delta_2 + S_2\Delta_\alpha + f_2 = 0 \quad (3.14)$$

$$A_3\Delta_2 + B_3\Delta_3 + S_3\Delta_\alpha + f_3 = 0 \quad (3.15)$$

$$A_4\Delta_3 + S_4\Delta_\alpha + f_4 = 0 \quad (3.16)$$

where Δ_i and f_i are subvectors of $\underline{\Delta}$ and \underline{F} . Eq. 3.13 can be solved independently of (3.14-3.16). The correction vector Δ_1 is then inserted into Eq. 3.14, allowing Δ_2 to be expressed explicitly by Δ_α . This elimination procedure is repeated until Δ_α is found from Eq. 3.16. In this manner the full system is solved through a sequence of subsystems for which the LU/back procedure is still efficient. The size of the subsystems for a 15- component mixture is $N = 31$. The difference in time consumption for solving the linear system by the direct LU/back approach and by the blockwise approach described above is illustrated in Figure 3.17.

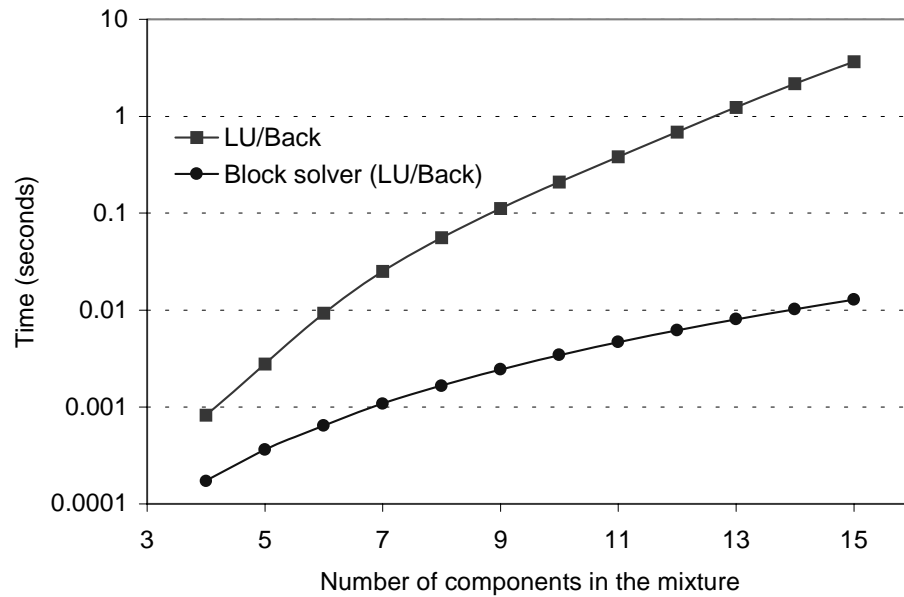


Figure 3.17: Comparison of time consumption for linear equation solvers. 233MHz CPU.

It should be pointed out that the same LU and back substitution routines were used in both cases. The difference in performance is very significant. For a mixture containing 15 components the CPU time consumption, for a single iteration, is reduced by more than a factor of 100.

3.4.4 Modification of Iterative Scheme in the Near-critical Region

As the pressure approaches the MMP it becomes unsafe to use the first order approximation for initial estimates obtained from solving the sensitivity Eq. 3.11, because the variables change rapidly and in a highly non-linear manner in the vicinity of a critical region. A typical behavior of the α 's entering Eq. 3.4 is illustrated in Figure 3.18.

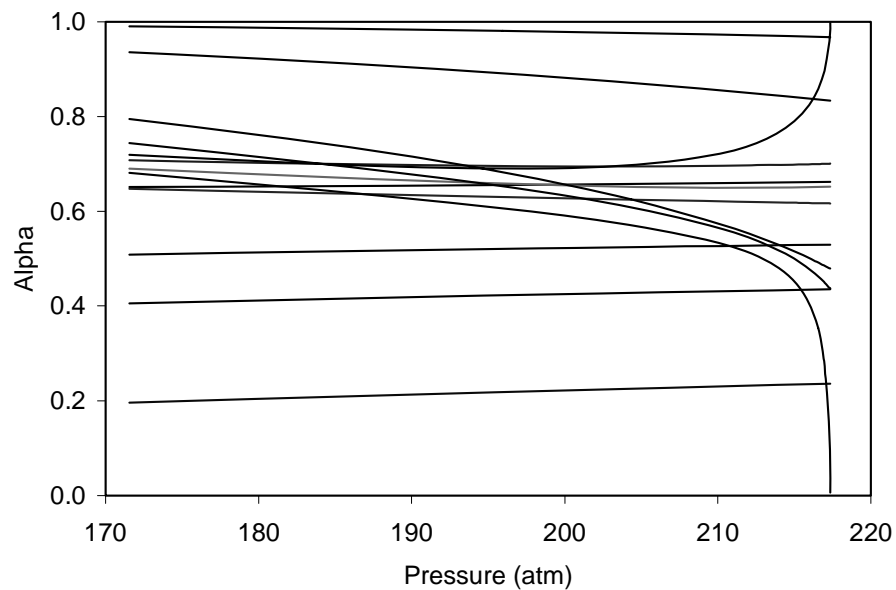


Figure 3.18: Typical variation of α as a function of pressure.

As a tie line becomes critical one α value must approach unity and another must approach zero. These characteristics as well as the highly non-linear behavior are observed in Figure 3.18.

In order to improve the stability of the algorithm a modification of the original formulation is introduced for calculations in the near-critical region. The global formulation for locating the key tie lines can be regarded as the calculation of $nc-1$ coupled phase envelopes. Analogously to the phase envelope calculation of Michelsen³⁴ it is favorable to change specifications in the vicinity of a critical region. Specifying a K -factor and using the pressure as an independent variable prevents getting trapped by the “trivial solution”. The fastest changing K -factor is that of the heaviest component on the shortest key tie line. To specify the K -factor an extra equation must be added to the original formulation. That is

$$f^* = \ln K^* - \ln \left(\frac{y_{nc}}{x_{nc}} \right)_{\min} = 0 \quad (3.17)$$

where the subscript min indicates the shortest tie line and K^* is the specified value. After the specification of a K -factor the resulting problem can be written as

$$\underline{F}'(\underline{v}, p, K^*) = \underline{0} \quad (3.18)$$

The prime on F indicates the extra equation. The Newton-Raphson scheme corresponding to the new formulation includes calculation of a modified correction vector

$$\underline{\Delta}' = \underline{\Delta}_o + \frac{\partial \underline{\Delta}}{\partial p} \Delta p \quad (3.19)$$

where the first term on the right-hand side is the contribution at constant pressure and the second term is the contribution from variation in pressure at constant compositions. The linear set of equations to be solved in each iteration is now written as

$$\frac{\partial \underline{F}}{\partial \underline{v}} \underline{\Delta} + \frac{\partial \underline{F}}{\partial p} \Delta p + \underline{F} = \underline{0} \quad (3.20)$$

$$\frac{\partial f^*}{\partial \underline{v}} \underline{\Delta} + \frac{\partial f^*}{\partial p} \Delta p + f^* = 0 \quad (3.21)$$

$\underline{\Delta}$ can be expressed explicitly by Δp from Eq. 3.20. By substituting of this expression into Eq. 3.21, Δp and subsequently $\underline{\Delta}$ can be evaluated. Although an extra equation is added to the original formulation only an insignificant change in the time consumption is observed. When the solution corresponding to the specified K -factor is found the value of K^* is increased and the procedure is repeated until some stop criterion is satisfied. As the pressure is the primary variable of interest (MMP), it should be pointed out that only very small changes in the pressure are observed when the specified K -factor approaches unity. This is due to the proportionality relation

$$p - p_{critical} \propto (\ln K^*)^2 \quad (3.22)$$

Hence, the calculation should be stopped at $-\ln K^* < 0.05$ in order to avoid unnecessary iterations. It is suggested switching between the iterative schemes when $d_{min} < 0.15$, where min denotes the tie line with the shortest distance to the critical region. Finally to accelerate the convergence in the critical region, improved estimates for the independent variables are obtained for each K^* -step by solving the equations

$$\frac{\partial \underline{F}}{\partial \underline{v}} \frac{d \underline{v}}{d K^*} + \frac{\partial \underline{F}}{\partial p} \frac{dp}{d K^*} + \frac{\partial \underline{F}}{\partial K^*} = 0 \quad (3.23)$$

$$\frac{\partial f^*}{\partial \underline{v}} \frac{d \underline{v}}{d K^*} + \frac{\partial f^*}{\partial p} \frac{dp}{d K^*} + \frac{\partial f^*}{\partial K^*} = 0 \quad (3.24)$$

for the derivatives of \underline{v} and p with respect to K^* .

3.4.5 Examples of MMP Calculation

The global approach described previously has been applied to a number of multicomponent systems ranging from heavy oils to gas condensates. In the numerical experiments presented in the following, phase equilibrium calculations were performed by use of the Peng-Robinson⁴⁰ equation of state. All experiments were run on a Pentium II 233 MHz PC.

Initially, the reservoir fluid from Zick⁵⁸ is used as an example. This selection is due to the documented existence of the combined VGD and CGD mechanism controlling the development of miscibility. The fluid is characterized by the procedure of Pedersen et al.³⁹, using 12 pseudocomponents. The characterized fluid description is given in Table 3.1.

-	T _C (K)	P _C (atm)	ω	k _{CO₂,j}
CO ₂	304.2	72.9	0.228	0.00
CH ₄	190.6	45.4	0.008	0.12
C ₂	305.4	48.2	0.098	0.15
C ₃	369.8	41.9	0.152	0.15
C ₄	425.2	37.5	0.193	0.15
C ₅	469.6	33.3	0.251	0.15
C ₆	507.4	29.3	0.296	0.15
C ₇₊₍₁₎	616.2	28.5	0.454	0.15
C ₇₊₍₂₎	698.9	19.1	0.787	0.15
C ₇₊₍₃₎	770.4	16.4	1.048	0.15
C ₇₊₍₄₎	853.1	15.1	1.276	0.15
C ₇₊₍₅₎	1001.2	14.5	1.299	0.15

Table 3.1: Characterization of Zick⁵⁸ oil including non-zero binary interaction parameters.

Based on the characterization two numerical experiments were carried out. In the first experiment the oil was depleted to 103.4 atm at 358.15 K (Oil 1) and the MMP was determined for displacement by injection of Gas 1 (Table 3.2).

-	X-Oil 1	X-Oil 2	Y _{Gas 1}	Y _{Gas 2}
CO ₂	0.0449	0.0656	0.2218	0.1775
CH ₄	0.2071	0.3711	0.2349	0.3878
C ₂	0.0481	0.0538	0.2350	0.1880
C ₃	0.0409	0.0373	0.2745	0.2196
C ₄	0.0323	0.0261	0.0338	0.0271

C ₅	0.0247	0.0187	0	0
C ₆	0.0298	0.0218	0	0
C ₇₊ (1)	0.2525	0.1791	0	0
C ₇₊ (2)	0.1285	0.0910	0	0
C ₇₊ (3)	0.0855	0.0605	0	0
C ₇₊ (4)	0.0631	0.0447	0	0
C ₇₊ (5)	0.0427	0.0302	0	0

Table 3.2: Oil and injection gas compositions. Based on data from Zick⁵⁸.

In the second experiment the oil was depleted to 206.9 atm at 358.15 K (Oil 2) and the MMP was determined for displacement by injection of Gas 2 (Gas 1 + 20 mole % methane). The results from the experiments are shown in Figures 3.19 and 3.20 whereas the numerical results are presented in Table 3.4.

A second series of experiments for a slightly volatile Oil 3, described in Høier¹⁶, has been performed. The 15-component oil composition and the injection gas composition are given in Table 3.3 whereas the fluid description is given in Appendix A.1. Three experiments, displacing Oil 3 by injection Gas 3, Gas 4 and Gas 5 (53% Gas 3 + 47% Gas 4) at 368.15 K are reported. Calculation results for the first two experiments are given in Figures 3.21 and 3.22. The result from the third experiment is illustrated in Appendix A.2. Numerical values for all experiments are given in Table 3.4.

-	x _{Oil 3}	y _{Gas 3}	y _{Gas 4}
N ₂	0.785	1.58583	1.8579
CH ₄	45.622	92.8772	55.5113
CO ₂	0.265	0.59725	3.79585
C ₂	6.092	3.66376	11.4829
C ₃	4.429	0.38875	13.4119
iC ₄	0.865	0.33887	2.0708
C ₄	2.26	0.08508	6.52458

iC ₅	0.957	0.11535	1.68332
C ₅	1.406	0.02264	2.38398
C ₆	2.097	0.11333	0.5051
C ₇₊ (1)	4.902	0.12047	0.6952
C ₇₊ (2)	9.274	0.0914	0.0766
C ₇₊ (3)	9.88	0.0001	0.00057
C ₇₊ (4)	7.362	0	1.71E-05
C ₇₊ (5)	3.804	0	0

Table 3.3: Compositions of Oil 3 and Gas 3+4. Data from Høier¹⁶.

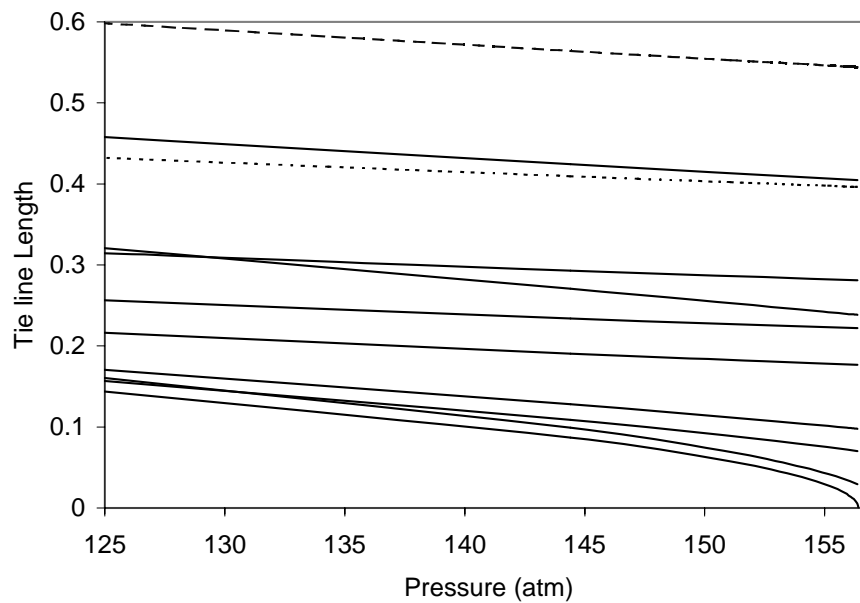


Figure 3.19: Simulation results for Oil 1 displaced by Gas 1. The fourth crossover tie line becomes critical at 156.7 atm (MMP). Injection and initial tie lines are plotted as dotted and broken lines respectively.

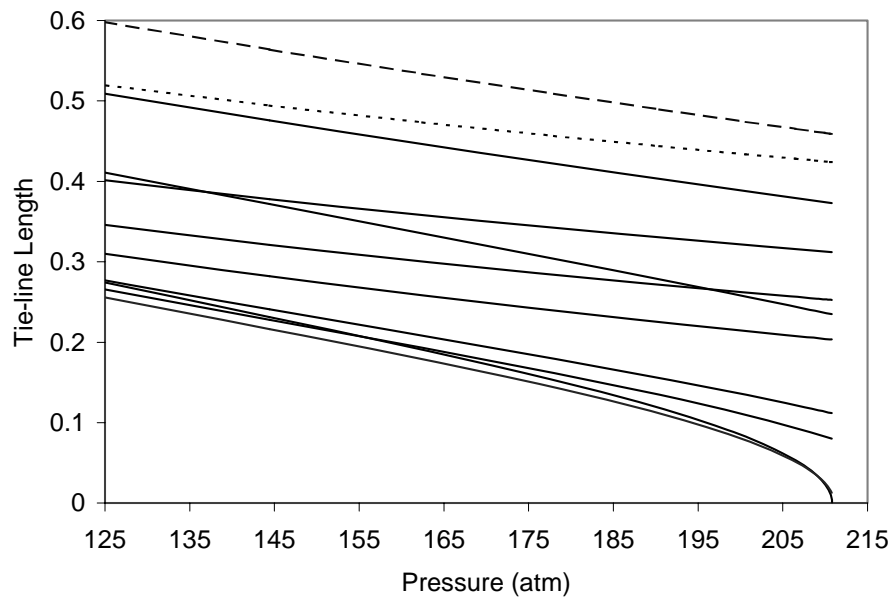


Figure 3.20: Simulation results for Oil 2 displaced by Gas 1. The third crossover tie line becomes critical at 211.0 atm (MMP). Injection and initial tie lines are plotted as dotted and broken lines respectively.

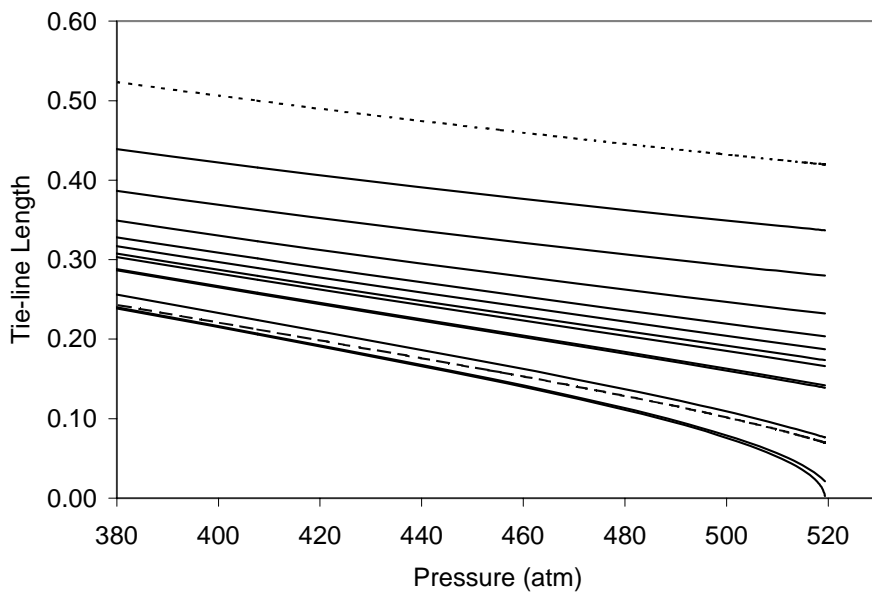


Figure 3.21: Simulation results for Oil 3 displaced by Gas 3. The second crossover tie line becomes critical at 519.3 atm (MMP). Injection and initial tie lines are plotted as dotted and broken lines respectively.

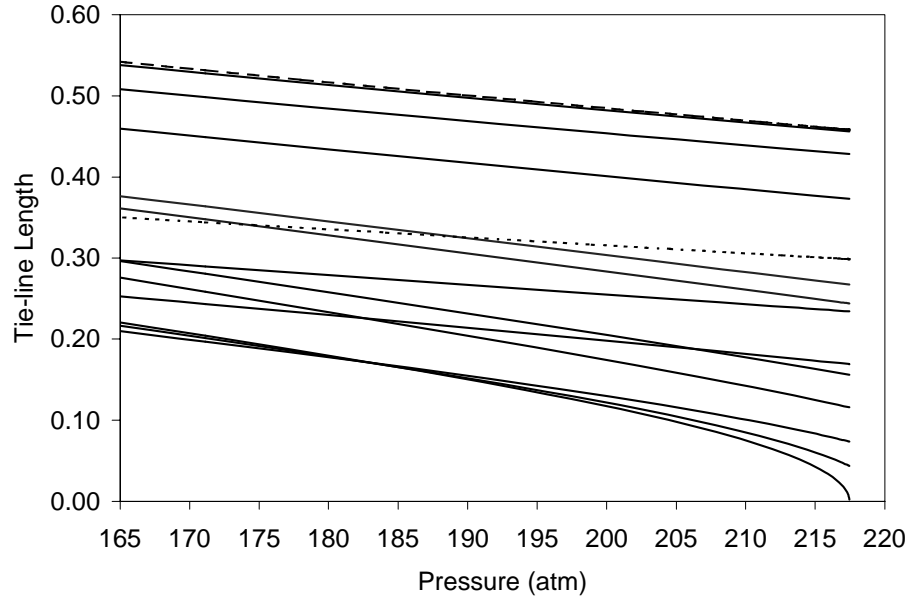


Figure 3.22: Simulation results for Oil 3 displaced by Gas 4. The eighth crossover tie line becomes critical at 217.3 atm (MMP). Injection and initial tie lines are plotted as dotted and broken lines respectively.

Method / Oil	Oil ₁ -Gas ₁	Oil ₂ -Gas ₂	Oil ₃ -Gas ₃	Oil ₃ -Gas ₄	Oil ₃ -Gas ₅
Multicell, Høier ¹⁶	-	-	514.2	231.9	310.9
Slimtube, Høier ^{16*}	-	-	512 ± 7	228 ± 10	302 ± 10
Slimtube, Zick ⁵⁸	152	213.8	-	-	-
Louis Bleriot ^{**}	157	211	524	216	298
Key tie line	156.7	211.0	519.3	217.3	295.7
Calculation Time (Secs)	0.7	0.7	1.9	1.7	1.6

Table 3.4: Comparison with simulation results presented in the literature. P (atm),

* E300 simulation, ** multicell simulation (IVC-SEP program).

The MMP predictions by the presented algorithm are seen to be in excellent agreement with reported slimtube experiments and compositional simulators. In the work of Høier¹⁶ a number of compositional simulations, for different types of fluids, are presented. On the basis of these fluid descriptions the MMPs have been calculated under the same conditions. A general comparison of the MMPs predicted by the presented algorithm and the simulations of Høier¹⁶ and Zick⁵⁸ is given in Figure 3.23.

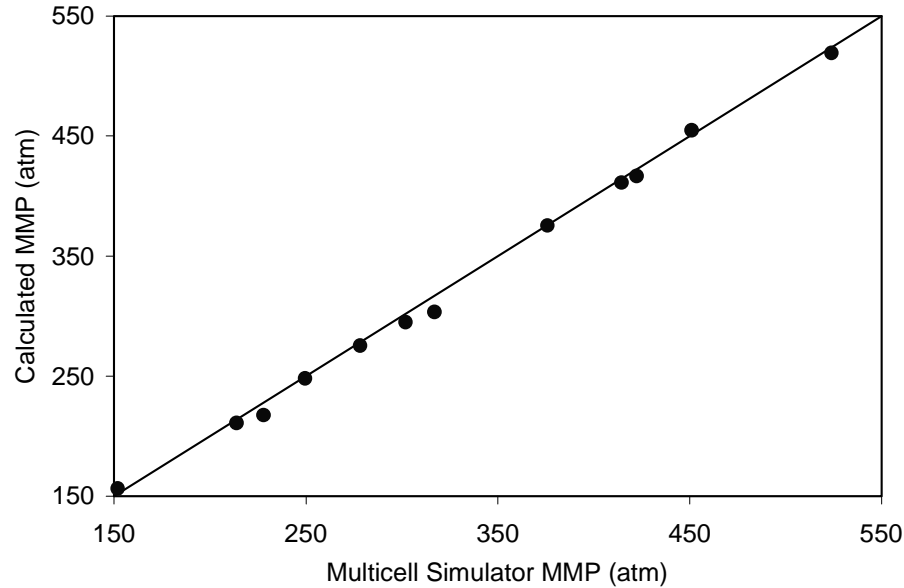


Figure 3.23: Comparison of calculation results with results from the literature^{16, 58}.

3.4.6 Discussion of the Global Approach for Calculation of the MMP

Up to now systems with a maximum of 15 components in the oil description and 15 components in the injected gas have been investigated. The average time consumption for the MMP calculations is around a few seconds. Wang and Orr⁵³ describe a sequential approach for solving the key tie line intersection equations. The sequential approach, based on an outer loop for updating K -factors by successive substitution and an inner loop for solving the intersection equations, is much more time-consuming than the global formulation of this work. Wang and Orr⁵³ report typical computation times of about 30 minutes with a Dec-Alpha workstation. The large difference in time consumption is caused by the use of successive substitution for updating K -factors, which is impractical for near-critical calculations. Furthermore, the sequential approach cannot achieve the convergence speed of a full Newton-

Raphson iteration. The repeated solution of the intersection equations offers very good initial estimates in each pressure/ K^* step and no more than five iterations are needed by the global approach even for the near-critical region.

It should be emphasized that none of the presented calculation examples exhibit pure vaporizing or pure condensing mechanisms controlling the development of miscibility. This is evident from the fact that the critical tie line in all cases differs from the initial and the injection tie lines.

3.5 Application of the New MMP Algorithm

The modest time consumption for calculations of the MMP by the global approach makes the algorithm particularly useful in connection with gas enrichment studies as well as other studies where compositional simulators are significantly more costly. To illustrate in more detail some areas of application of the new algorithm, a case study relevant to considerations made by the reservoir engineer prior to any full scale modeling of a gas injection project is presented. Before any modeling work can be done, a reservoir fluid sample is sent to the PVT laboratory in order to obtain information about component distributions, densities, bubble-point pressures, swelling tests etc. This is the experimental basis for the generation of a fluid description entering the thermodynamic model (EOS) for prediction of phase equilibrium. Normally, a characterized fluid description is generated. This fluid description is then tuned to match experimental data from the PVT laboratory. Most of the standard PVT experiments give little or no information about the phase equilibrium in the critical/near-critical region(s). If it is recalled that prediction of the MMP is in fact prediction of a point on the critical locus some interesting questions could be:

- To what extent will the prediction of the MMP be affected when a given fluid description is tuned to match other experimental data?
- Does it make any difference what parameters are used to tune the thermodynamic model?
- How sensitive is the predicted MMP to the number of components used in the fluid description?

All phase equilibrium calculations of the following subsections have been performed using the SRK EOS⁴³. A real reservoir fluid described in Table 3.5 forms the basis of this study. Initially, the fluid is characterized by the method of Pedersen et al.³⁹, using 15 pseudo-components. The characterized fluid description is given in Tables 3.6 and 3.7. At the reservoir temperature (387.45 K), the fluid is reported to have a saturation pressure (P_{sat}) of 251.7 atm.

Component	Mole (%)	ρ (Kg/m ³)	M_w (g/mole)
N ₂	0.45		
CO ₂	1.64		
CH ₄	45.85		
C ₂	7.15		
C ₃	6.74		
i-C ₄	0.84		
n-C ₄	3.11		
i-C ₅	1.03		
n-C ₅	1.65		
C ₆	2.52		
C ₇	3.77	729.4	92
C ₈	4.28	750.9	106
C ₉	2.70	773.9	120
C ₁₀	1.69	783.5	137
C ₁₁₊	16.58	796.8	288

Table 3.5: Fluid description for case study.

	T _c (K)	P _c (atm)	ω	M_w (g/mole)	x-Oil 4	y-Gas 6	y-Gas 7
N ₂	126.200	33.6000	0.0400	28.016	0.450	0.49	0.67
CO ₂	304.200	72.9000	0.2280	44.010	1.640	1.82	2.44
CH ₄	190.600	45.4000	0.0080	16.043	45.850	81.39	68.16
C ₂	305.400	48.2000	0.0980	30.069	7.150	9.15	10.32
C ₃	369.800	41.9000	0.1520	44.096	6.740	4.67	9.50
i-C ₄	408.100	36.0000	0.1760	58.123	0.840	0.50	1.09
n-C ₄	425.200	37.5000	0.1930	58.123	3.110	1.24	3.75
i-C ₅	460.400	33.4000	0.2270	72.150	1.030	0.20	0.95
n-C ₅	469.600	33.3000	0.2510	72.150	1.650	0.26	1.31
C ₆	507.400	29.3000	0.2960	86.177	2.520	0.09	0.91
C ₇	632.800	30.2987	0.1842	109.007	12.440	0.19	0.90
C ₁₁	659.605	23.4598	0.4773	175.327	6.320	0.00	0.00
C ₁₆	703.646	19.2900	0.8197	256.674	5.024	0.00	0.00
C ₂₃	766.497	16.7852	1.2114	370.099	3.240	0.00	0.00
C ₃₃	892.990	15.1302	1.3718	590.374	1.996	0.00	0.00

Table 3.6: Characterized fluid description.

	CH ₄	C ₂	C ₃ to C ₃₃
N ₂	0.02	0.06	0.08
CO ₂	0.12	0.15	0.15

Table 3.7: Non-zero interaction parameters.

3.5.1 Effect of Tuning and Lumping

The predicted saturation pressure based on the initial characterized fluid description is 259.1 atm. In order to obtain a better match on the predicted P_{sat} the fluid description was tuned by five different approaches/parameters resulting in five tuned fluid descriptions. The parameters were

- The molecular weight of the plus fraction (re-characterization)
- The critical temperature T_c of the heaviest component in the characterized fluid description
- The critical pressure P_c of the heaviest component in the characterized fluid description
- The acentric factor ω of the heaviest component in the characterized fluid description
- The binary interaction parameter k_{ij} between CH₄ and the heaviest component in the characterized fluid description

The values of the tuned parameters for the five new fluid descriptions are given in Table 3.8.

Parameter	Initial value	Tuned value	P_{sat} (atm)	MMP (atm)	Dev %
Experimental	-	-	251.7	370.1	0.0
No tuning	-	-	259.1	363.7	1.7
M_w (g/mole)	288.00	268	251.7	351.6	5.0
T_c (K)	892.99	830.50	251.7	365.1	1.4
P_c (atm)	15.13	12.38	251.7	370.8	-0.2
ω	1.372	1.1331	251.7	366.1	1.1
k_{ij} (CH ₄ -C ₃₃)	0.00	-0.0856	251.7	366.5	1.0

Table 3.8: Tuned parameters and a comparison of calculated MMPs for various tuning approaches.

In order to match the experimental P_{sat} when the molecular weight (M_w) of the plus fraction is used as a parameter a reduction of 7% is needed. This is of the same magnitude as the uncertainty of the experimental determination and hence considered to be reasonable. In the T_c -tuned description a reduction of 7 % is necessary to match the P_{sat} , whereas a reduction of 18% is needed in the P_c -tuned model. The magnitude of the latter is somewhat high but can still be accepted. For the ω_{nc} -model, the tuned value is 17 % lower than the characterized value. Finally, a k_{ij} -value of -0.086 is needed in the last tuning approach.

An experimental swelling test where the reservoir fluid Oil 4 is mixed with Gas 6 (Table 3.6) is compared with predictions of the different models in Figure 3.24.

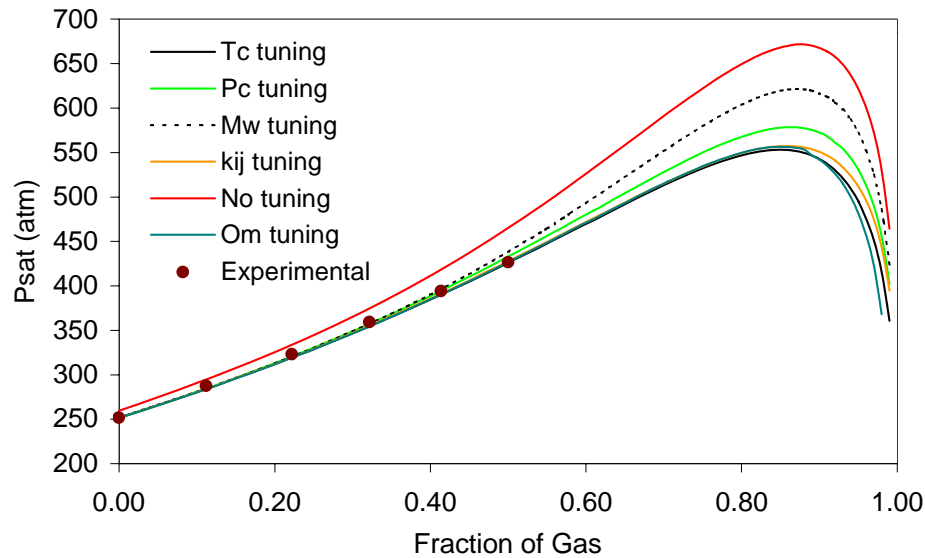


Figure 3.24: Swelling test simulations for different tuning approaches.

Predictions of the T_c -tuned model and the k_{ij} -tuned model are seen to give the best accuracy. The MMP based on slimtube experiments where Gas 6 (Table 3.6) is injected into reservoir fluid has been reported to be 370.1 atm. Calculated values of the MMP for the original fluid description as well as for the five tuned models are given in Table 3.8. It is seen that no significant difference in the predicted MMPs is observed from using different parameters for tuning the characterized fluid description. Further, it is seen that the M_w -tuned model introduces the largest error in the predicted MMP. This is somewhat in contrast to the

swelling test performance where the M_w -model is superior to the untuned model. Based on the investigated system it is concluded that a high accuracy in the prediction of a swelling test does not ensure a correct prediction of the MMP.

Although increasingly powerful computers are developed, the number of components used in three-dimensional compositional simulators is still limited to a maximum of about eight. Therefore, it is necessary to reduce the number of components used in the fluid description by a lumping procedure. The influence of lumping on the prediction of the MMP has been investigated for the reservoir fluid. Through a number of calculations with decreasing number of components, the variation in the MMP predictions has been determined. In this work, the clustering procedure of Montell and Gouel³⁷ combined with property calculation of Leibovici³⁰ is applied. Relative errors in P_{sat} and MMP for the tuned models are shown in Figures 3.25 and 3.26 respectively.

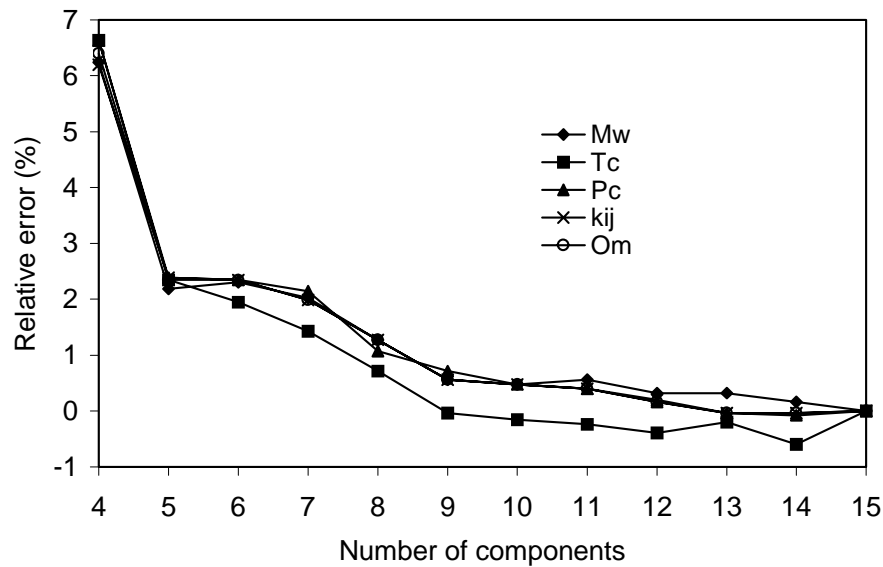


Figure 3.25: Lumping study. Relative error in P_{sat} vs. number of components.

The relative errors in the predicted P_{sat} do not exceed 3 % as long as more than four components are used in the fluid description. The same pattern is seen for the relative errors in the predicted MMP. Equivalent variation in the relative error, biased by the error from the 15-component fluid descriptions, is seen for all models. This also indicates that the method of tuning has very little impact on the prediction of the MMP. On basis of the investigated

reservoir fluid, it is concluded that the key tie line approach has a low sensitivity to the number of components used in the fluid description.

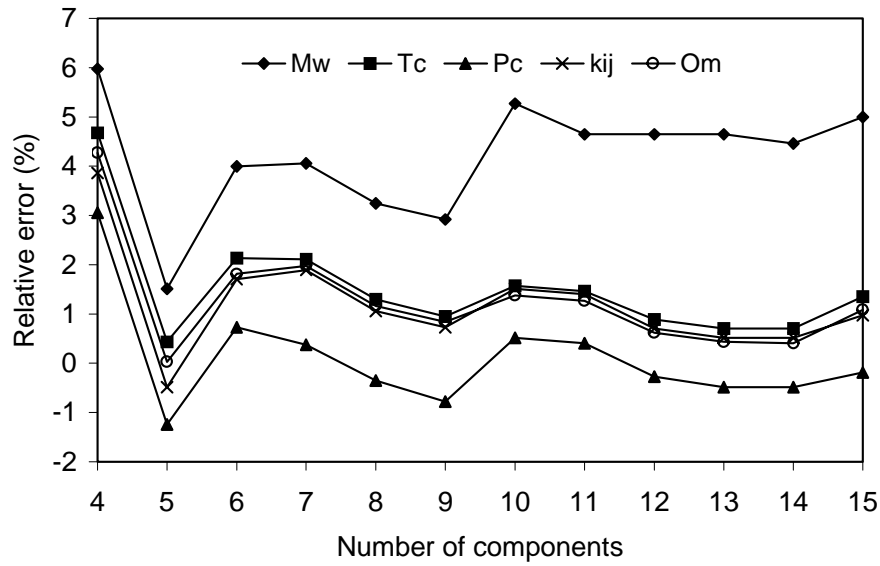


Figure 3.26: Lumping study. Relative error in MMP vs. number of components.

3.5.2 Gas Enrichment Study

If more than one potential injection gas is available, a gas enrichment study is necessary to determine which gas mixture should be injected into the reservoir. In this study a rich gas (Gas 7, Table 3.6) is considered as solvent. The fraction E of solvent added to the original injection gas is defined by

$$y_{inj} = y_{gas}(1 - E) + y_{solvent}E \quad (3.25)$$

A series of MMP calculations for different values of the solvent fraction has been made by use of the T_c -tuned model. Figure 3.27 shows the MMP as a function of the solvent fraction along with an indication of which key tie line controls the development of miscibility. At low values of the solvent fraction, the MMP decreases slowly up to a fraction around 0.1. In this region the 4th key tie line controls the miscibility process. Afterwards the MMP drops off rapidly until a solvent fraction of around 0.4 is reached. At this level of enrichment the MMP is reduced by 90 atm to approximately 280 atm. The development of miscibility is now

controlled by the 9th key tie line. Further enrichment of the injection gas does not affect the MMP. Hence, in this case, no further enrichment is necessary if the solvent gas can be used for other profitable purposes.

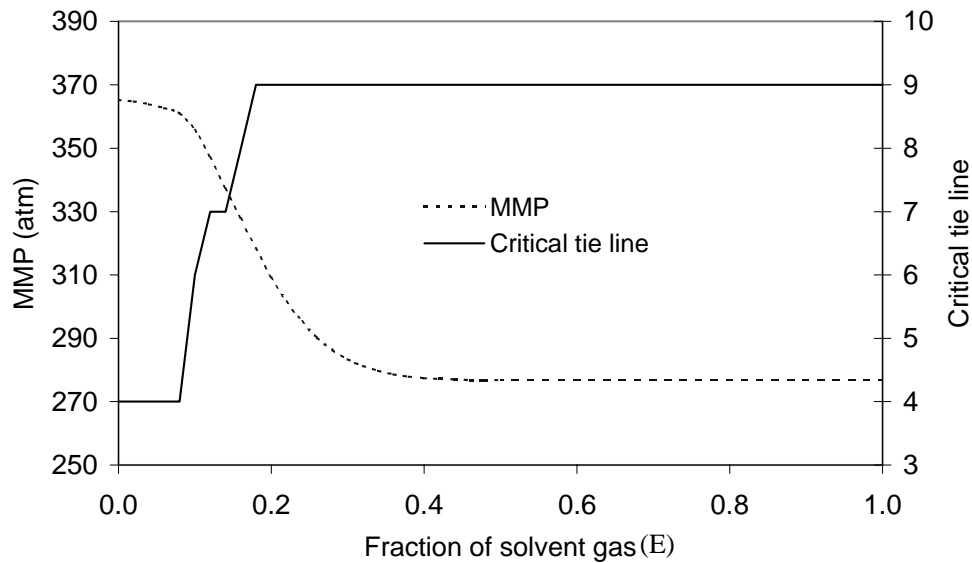


Figure 3.27: Gas enrichment study. MMP vs. fraction of solvent Gas 7.

In the gas enrichment study illustrated in Figure 3.27 the MMP is a monotonic, decreasing function of the fraction of solvent gas (E).

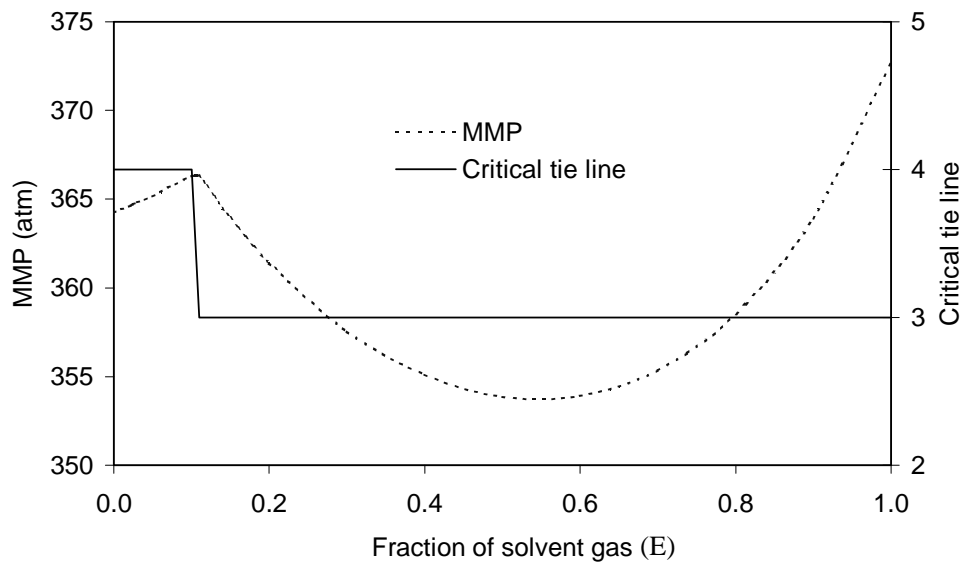


Figure 3.28: Gas enrichment study. MMP vs. fraction of solvent gas (25 % N₂ + 75% CO₂).

This is not always the case and the entire MMP vs. E needs to be investigated in order to locate the true minimum value of the MMP. As an illustration, a solvent gas consisting of 25 % N_2 and 75 % CO_2 is considered. The MMP vs. E plot of this solvent is given in Figure 3.28. The MMP vs. E curve initially increases as the fraction of solvent is increased. Then, at an enrichment level around 0.1 the curve breaks and starts to decrease. The value of the MMP decreases until it reaches the minimum value at around $E = 0.58$ and starts, again, to increase until the maximum value of MMP is reached at $E = 1.0$. Thus, Figure 3.28 illustrates that the MMP vs. E relationship is not necessarily monotonic.

3.6 Summary

A brief introduction to the different approaches used for prediction of the minimum miscibility pressure over the last decades has been given. The overview aims to stress that more complex methods, like the FD/MC methods or the semi-analytical method, must be used to ensure a proper prediction of the MMP in general.

A new global approach to calculation of the MMP has been presented. The algorithm is based on the semi-analytical approach and allows prediction of the MMP for gas injection processes using any number of components in the fluid description. The new approach has been tested on a number of different systems. All calculations have been verified with an in-house multicell compositional simulator. Most of the investigated systems have been bubble-point systems but also a few dew-point systems (gas condensates) have been investigated. For the latter systems the number of grids used in the compositional simulators has a large influence on the predicted MMP¹⁶. For gas condensates, MMPs predicted by the key tie line approach are found to be in good agreement with reported simulation results, but more condensate systems should be investigated before further conclusions are made.

The global approach is superior to previously presented MMP algorithms in terms of the CPU requirement. Calculation times have been reduced to a few seconds on a PC. Thus, the algorithm offers an efficient tool for reservoir engineers studying gas injection processes.

Examples based on a case study are given to illustrate the use of the algorithm. The effects of tuning and lumping on the predicted MMP have been investigated. For this case study the variables used for tuning the fluid description to experimental PVT data did not influence the predicted MMP significantly. This may not hold true for all systems. The lumping study showed that the number of components used in the fluid description only had a minor effect on the predicted MMP as long as four or more components were used. As for the effect of tuning, this may not hold true for all systems. The lumping study verifies the fact that four or more components are needed in the fluid description in order to represent a combined v/c displacement.

The algorithm was used in two gas enrichment studies with the aim of determining the optimal mixture of available injection gases. In the first enrichment study the MMP was found to be a monotonous function of the enrichment factor, while the second study exhibited a strongly non-monotonous behavior. The two cases are given to illustrate the need for more than a few points on the MMP vs. E curve and hence the need for a fast MMP algorithm.

4. Approximate Semi-analytical Solutions to the 1-D Gas Injection Problem (NVC)

In this chapter the algorithm for approximation of key tie lines, developed during the calculation of the MMP (Chapter 3), will be combined with the analytical theory of 1-D gas injection processes (Chapter 2) to obtain approximate semi-analytical solutions to the governing mass conservation equations. The simplified version of the conservation equations described in Section 2.1 is initially addressed. Due to the simpler mathematics involved in solving the NVC formulation of the flow problem, the NVC form serves as a proper starting point for generating algorithms for the general formulation. Further, it will be demonstrated how solution construction tools from a no volume change (NVC) algorithm can be used in a volume change (VC) algorithm by introducing minor modifications.

4.1 Grouping of Analytical Solutions

Solutions to the 1-D gas injection problem can be divided into two main groups. The first group describes fully shelf-sharpening systems where all key tie lines are connected by shocks. The second group describes systems where some key tie lines are connected by continuous variation along a nontie line path (rarefaction or spreading wave). The two groups are dealt with in separate subsections

All analyses and examples in this chapter are based on a fractional flow function given by

$$f = \frac{S^2}{S^2 + \mu_r (1 - S - S_{or})^2} \quad (4.1)$$

The residual oil saturation S_{or} is fixed at 0.2 and the vapor to liquid phase relative viscosity μ_r is calculated by the Lohrenz-Bray-Clark³¹ correlation. The NVC algorithms for fully self-sharpening systems and systems with nontie line rarefactions are also presented in Jessen et al.²⁰

4.2 Self-sharpening Systems

Fully self-sharpening systems are characterized by the feature that all key tie lines are connected by shocks. For such systems the key tie line intersection approach is rigorously accurate because the extensions of a pair of key tie lines connected by a shock must intersect³⁸. Two types of shocks occur. When the shock velocity matches the tie line eigenvalue ($\lambda_{\text{tie line}} = df/dS$) on one side of the shock, the shock is known as a tangent shock. When the shock velocity differs from the wave velocities on both sides of the shock, the shock is called a genuine shock. Both types of shocks occur in typical solutions. Because the tie lines which make up the solution can be found by the intersecting tie line approach^{18,53}, a full solution can be constructed if the shock composition points can be determined on each of the key tie lines. The only remaining question is: On which tie line does the solution construction begin? In the following, that tie line will be referred to as the “primary” tie line.

Solution construction begins with finding the tangent shocks that connect the primary tie line to adjacent tie lines just upstream and downstream. For problems in which the injection gas composition lies on the vapor side of the two-phase region, the composition path lies on the vapor side of the equivelocity curve (where $f=S$)¹⁵. For such compositions, $f > S$.

It is now demonstrated that the primary tie line must be the shortest of the key tie lines. To prove the truth of this statement, consider the simple ternary vaporizing gas drive (Figure 4.1a) in which oil (composition **a**) is displaced by gas (composition **e**). Two key tie lines make up the solution: The tie line extending through the initial oil composition, and the tie line extending through the gas composition. In this example, the tie lines are connected by a shock because a rarefaction between the oil tie line and the gas tie line would violate the velocity rule. The corresponding overall fractional flow curves for the two key tie lines are shown in Figure 4.1b, and the saturation profile for the solution is shown in Figure 4.1c. In this case, the leading shock is a tangent shock, found by constructing the chord from point **a** in Figure 4.1b, which is tangent to the fractional flow curve for the oil tie line. The shock from point **c** on the oil tie line is found by constructing a chord from point X which is tangent to the fractional flow curve for the oil tie line. Point X (Figure 4.1a) is the intersection point of the two key tie lines. Point X in Figure 4.1b lies on the $Q_I = G_I$ line.

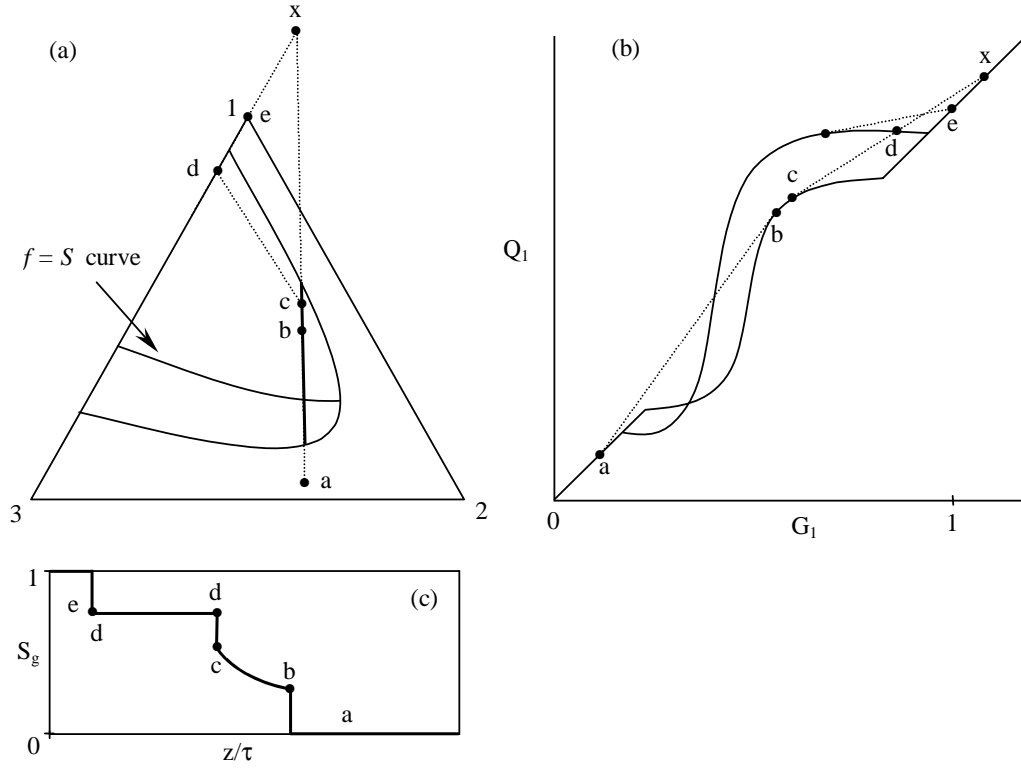


Figure 4.1: Construction of tangent shocks. Existence of primary tie line.

The composition of point **d**, the landing point on the gas tie line is given by the intersection of the chord with the fractional flow curve of the gas tie line. It should be noted that point **d** lies above the composition at which a chord constructed from the gas composition, point **e**, would be tangent to the fractional flow curve for the gas tie line. A continuous variation from point **d** to that tangent point would violate the velocity rule, so a genuine shock from point **d** to point **e** is required. The velocity of that shock is given by the slope of the chord from point **d** to point **e**.

The tangent drawn from point X to point **c** in Figure 4.1b satisfies the following equations⁷:

$$\frac{Q_i^c - Q_i^d}{G_i^c - G_i^d} = \frac{Q_i^c - Q_i^x}{G_i^c - G_i^x} = \frac{Q_i^d - G_i^x}{G_i^d - G_i^x} = \frac{f^c - S^{cx}}{S^c - S^{cx}} = \frac{f^d - S^{dx}}{S^d - S^{dx}} = \frac{df^c}{dS^s} \quad (4.2)$$

where S^{cx} and S^{dx} refer to the saturations at point X measured on the tie lines containing points **c** and **d**:

$$S^{cx} = \frac{G_1^x - g_{1l}^c}{g_{1v}^c - g_{1l}^c} \quad S^{dx} = \frac{G_1^x - g_{1l}^d}{g_{1v}^d - g_{1l}^d} \quad (4.3)$$

Figure 4.1b shows that the tangent constructed from point **c** to X intersects the overall fractional flow curve for the injection gas tie line at point **d**. If, on the other hand, the chord had been drawn from point X to the tangent point on the gas tie line, the extension of the chord would not intersect the overall fractional flow curve for the oil tie line. Thus, it is not possible to satisfy the shock equations if the tangent has been constructed to the gas tie line, but it is possible to do so for the oil tie line. Analysis of the shock equations indicates that it is always possible to satisfy the shock equations for this example if $S^{cx} > S^{dx}$. The length of the tie lines controls that restriction. In this example, the oil tie line is short and the gas tie line is longer, so $g_{1v}^c - g_{1l}^c > g_{1v}^d - g_{1l}^d$. Because the differences in g_{1l}^c and g_{1l}^d are small, the length of the tie lines dominates the saturations in Eq. 4.3. Thus, if a shock between two tie lines is a tangent shock, the tangent must be constructed to the shorter of the two tie lines.

Similar reasoning can be applied sequentially to each adjacent pair of tie lines, with the result that in fully self-sharpening systems the shortest of the $n_c - 1$ key tie lines must be a tie line which is connected to tie lines just upstream and downstream by tangent shocks, with the tangents constructed from the intersection points to the shortest tie line. Therefore, the shortest tie line is the primary tie line.

The algorithm for construction of fully self-sharpening 1-D solutions is:

1. Locate all key tie lines by using the tie line intersection approach. The global solution algorithm of Jessen *et al.*¹⁸ presented in the previous chapter was used here.
2. Locate the primary (shortest) key tie line and start tracing the solution upstream and downstream. For each adjacent pair of tie lines, the possibility of a tangent construction is initially investigated. The construction procedure is illustrated in Figure 4.2.
3. Downstream construction: A tangent construction is made by solving Eq. 4.2 for (S_I, λ_I) on the primary tie line from the first downstream intersection point (I_1) . The landing point on the downstream tie line (S_2, λ_1) is subsequently found by solving Eq. 4.2 with the shock velocity fixed.

4. For the next downstream pair, intersecting at I_2 , a new tangent construction is examined. From this point and forward the tangent construction may be invalid due to a violation of the velocity rule. That is, if the end point of the previous construction (S_2, λ_1) has a velocity which is higher than the jump or landing point from the new shock construction (S_3, λ_2). In such a case, the new pair of tie lines is connected by a genuine shock, which is followed by a constant state. If, on the other hand, two tangent constructions are made to the same tie line the tangent points are connected by either a direct jump or by continuous variation along the tie line.
5. Step 4 is repeated until the tie line extending through the initial oil is reached. The solution path often enters (and leaves) the two-phase region by a tangent shock. However, for some systems, (Figure 4.1, for example), variation along the tie line violates the velocity rule and a direct jump is used.
6. From the primary tie line, the solution path is traced upstream by the approach of steps 3 and 4.

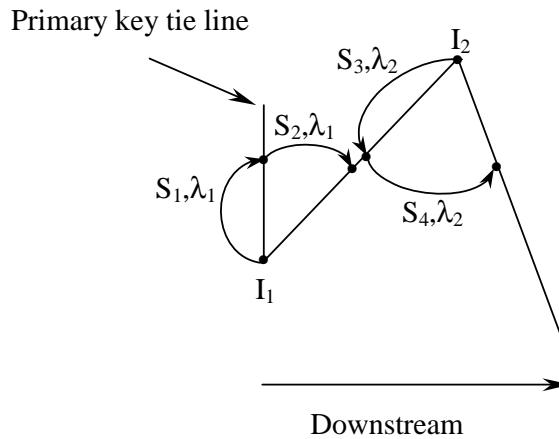


Figure 4.2: Illustration of downstream solution path construction.

4.3 Solution Example for Fully Self-sharpening System

To illustrate the application of the algorithm for construction of self-sharpening solutions, the Oil 4/Gas 6 system given in Table 3.6 is revisited. The reservoir temperature is 387.45 K at which the bubble point pressure of the original oil is 252 atm. The pure component critical

volumes V_c , used for the prediction of phase viscosities, are calculated by specifying the critical compressibility factor of all components to be 0.307. The 1-D solution for the displacement of Oil 4 by Gas 6 at 275 atm is desired. The 14 key tie lines (those extending through the oil and gas compositions and 12 crossover tie lines) are determined, and the third crossover tie line is identified as the primary (shortest) tie line, the starting point for shock construction. The saturation profile is shown in Figure 4.3, and the details of the solution are given in Table 4.1.

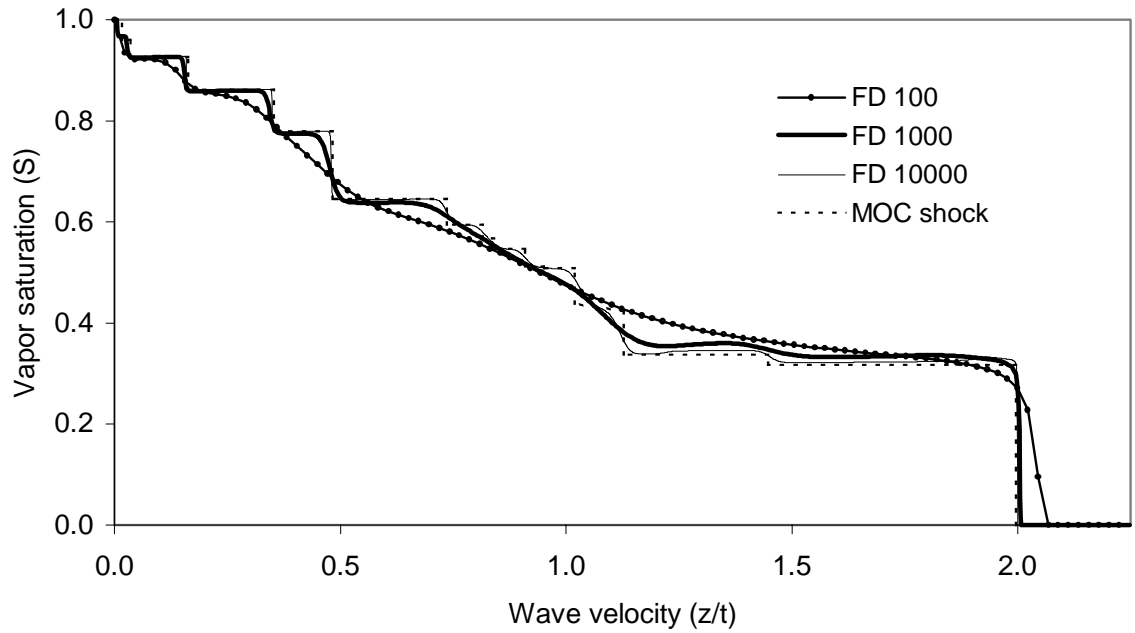


Figure 4.3: Comparison of analytical and numerical saturation profiles for displacement of Oil 4 by Gas 6 at 275 atm and 387.45 K. The finite difference (FD) solutions were obtained with 100, 1000, and 10000 grid blocks and $\Delta z/\Delta t = 10$.

The primary tie line is connected to the first downstream tie line by a tangent shock (d_1). The remaining downstream part of the solution consists of genuine shocks, constant states, and a direct jump from the oil tie line to the initial oil composition.

The upstream part of the solution starts with a tangent shock (d_2) connecting the primary tie line to the next crossover tie line. The remaining upstream shocks are all genuine shocks with associated constant states, and another genuine shock connects the injection gas tie line to

Point	Tie line	$\mu_{\text{gas}}/\mu_{\text{oil}}$	Log (K_{nc})	Z_{nc}	S	λ
Oil	Initial	0.1719	-5.80352	0.019957	-	1.9972 - ∞
a	Initial	0.1719	-5.80352	0.011376	0.321	1.4501 - 1.9972
b	1	0.1758	-5.70171	0.010801	0.344	1.2170 - 1.4501
c	2	0.1740	-5.73387	0.010972	0.338	1.1270 - 1.2170
d ₁	3	0.1879	-5.46043	0.008974	0.424	1.1270
d ₂	3	0.1879	-5.46043	0.008732	0.438	1.0187
e	4	0.1782	-5.64053	0.007761	0.509	0.9505 - 1.0187
f	5	0.1774	-5.65381	0.007727	0.512	0.9086 - 0.9505
g	6	0.1674	-5.83705	0.007376	0.547	0.8407 - 0.9086
h	7	0.1608	-5.95911	0.007205	0.567	0.8155 - 0.8407
i	8	0.1500	-6.16425	0.007001	0.595	0.7360 - 0.8155
j	9	0.1281	-6.60241	0.006702	0.646	0.4823 - 0.7360
k	10	0.0705	-7.72998	0.006246	0.780	0.3521 - 0.4823
l	11	0.0391	-8.54209	0.006109	0.862	0.1630 - 0.3521
m	12	0.0219	-9.01158	0.006151	0.927	0.0351 - 0.1630
n	Inj.	0.0150	-9.12906	0.008519	0.960	0.0163- 0.0351
o	Inj.	0.0150	-9.12906	0.000049	1	0- 0.0163
Gas	Inj.	0.0150	-9.12906	0.000000	-	0

Table 4.1: MOC solution for displacement of Oil 4 by Gas 6 at 275 atm and 387.45 K.

the injection gas composition. A continuous variation connects the two shock points (d₁ and d₂) on the primary tie line.

In order to confirm the analytical solution, a series of finite difference (FD) simulations was performed. Single-point upstream weighting with a Courant number ($\Delta z/\Delta t$) of 10 was used in all the simulations, which were run on a 450 MHz PC. The FD simulation scheme is described in Appendix A.3. The new two-phase PT flash algorithm developed by Michelsen³⁵ was used in the FD simulator to speed up the numerical solutions. The numerical saturation profiles from simulations using 100,1000 and 10000 grid blocks are compared with the analytical profile in Figure 4.3. The CPU time required to construct the analytical solution was 0.9 second, compared to 4.4 seconds, 5.4 minutes and 7.8 hours used respectively in the numerical simulations. The coarse grid simulation (100 grid blocks) is not able to describe the details but only the general tendency of the dispersion-free solution. More details are captured by use of 1000 grid blocks and an excellent agreement is observed when 10000 grid blocks

are used. However, the CPU cost for capturing the true dispersion-free saturation profile by numerical simulators is substantially higher.

4.4 Systems with Nontie-line Rarefactions (Spreading Waves)

The shock solution described in the previous sections can be found even when a rarefaction connects one or more pairs of tie lines. In many problems, rarefaction segments appear which are short, and wave velocities change little over the length of the rarefaction. In such cases, the shock solution is an excellent approximation of the exact solution. For problems with longer rarefactions, a more accurate approximate solution can be obtained by the procedure described in this section.

It should be recalled that at any given point in the two-phase region, the n_c-1 eigenvalues represent characteristic wave velocities of compositions subject to variation in the corresponding eigenvector direction. Tie lines are eigenvectors and the remaining n_c-2 admissible directions can be integrated to obtain nontie-line paths. When a nontie-line rarefaction exists in the 1-D solution, the solution path switches from a key tie line path and travels along a nontie-line path to end up at a neighboring key tie line. The velocity rule dictates that a path switch, from a tie line path to a nontie-line path, can only occur at an equal eigenvalue point of mixed type. That is a point in compositional space where a tie line eigenvalue coincides with a nontie-line eigenvalue. For a given tie line the number of equal-eigenvalue points of mixed type is $2(n_c-2)$. Half of them can immediately be disregarded, as they are located on the liquid side of the equivelocity curve. The equal eigenvalue points can be located directly by solving the eigenvalue problem along a given tie line. The direct approach is quite time consuming and therefore the indirect method of Dindoruk⁷ (described in Section 2.3.4) for location of equal eigenvalue points is recommended for problems of the current type.

In the following we assume that two key tie lines, known in advance, are connected by a spreading wave. The question is then: At which equal eigenvalue point does the tie line path switch to the nontie-line path? The appropriate equal eigenvalue point can be selected by a geometrical interpretation of the displacement problem. When a rarefaction is present, the key tie lines are bound to a surface in compositional space of tie lines intersected by the path

between the key tie lines. The nontie-line rarefaction traverses this surface. As illustrated later, experience shows that the tie line surface is only gently curved and can be approximated nicely by a plane determined by the key tie lines. Hence, at the correct equal eigenvalue point no other eigenvectors, besides the tie-line eigenvector and the eigenvector related to the matching nontie-line eigenvalue, will point in the direction of the plane R spanned by the neighboring key tie lines. In practice this is done by checking angles between the normal vector to R and the eigenvectors. It should be noted that for systems with five or more components in the mixture, the normal vector to R is no longer uniquely determined and must be found by e.g. a minimization approach. In this work the approach described in Appendix A.4 was used to determine the normal vector.

After the selection of equal eigenvalue point, the nontie-line path is traced to the next key tie line by integration of the nontie-line eigenvector. For the general case, however, the presence of a spreading wave is not known in advance. Hence, a tool for predicting the existence of nontie-line rarefactions is needed.

4.5 Prediction of Spreading Waves in 1-D Solutions

If two key tie lines are connected by a rarefaction, the path switch from the tie line path to the nontie-line path must occur at an equal eigenvalue point on the tie-line closest to the critical locus. This is due to the intrinsic symmetric behavior around critical points. In the work of Dindoruk⁷, continuous variation along nontie-line paths is linked to the envelope curve generating the ruled surface traveled by the nontie-line path. This envelope curve is illustrated in a two-dimensional projection of the general case in Figure 2.8. The tie lines belonging to the one-parameter family $\phi_k(\psi)$ on the k 'th ruled surface are all tangents to the envelope curve E_k . The overall volume fraction of a given component i at the point of tangency on the envelope curve can be written as

$$G_i = (g_{iv} - g_{il})\theta_k(\psi) + g_{il} \quad (4.4)$$

where $\theta_k(\psi)$ is the superficial vapor volume fraction at the point of tangency.

Dindoruk⁷ derives an expression for the variation of the nontie-line eigenvalue λ_k along the nontie-line path in the vicinity of the equal eigenvalue point:

$$\lim_{\lambda_k \rightarrow \lambda_t} \frac{d\lambda_k}{d\psi} = \frac{f - S}{(S - \theta_k)^2} \frac{d\theta_k}{d\psi} \bigg|_{\lambda_k = \lambda_t} \quad (4.5)$$

where λ_t is the tie line eigenvalue at the equal eigenvalue point. While Eq. 4.5 applies strictly only near the equal eigenvalue point, the indicated sign of the left-hand side applies over the entire nontie-line path.

4.5.1 The Fanning Rule (Envelope Rule)

Eq. 4.4 shows that a critical point must be a point on the envelope curve. This fact makes it possible to predict the sign of the derivative of the superficial vapor saturation with respect to ψ and hence the variation of λ_k , once the orientation of the key tie lines is known. The absolute distance from the two-phase boundary to the envelope curve increases as the nontie-line path is traced from an equal eigenvalue point. The sign of the superficial vapor fraction depends on whether the tie lines of the ruled surface are fanning from the liquid side or the vapor side of the two-phase region or, equivalently, whether the envelope curve is located on the vapor or the liquid side of the two-phase region. Ultimately, the shape of the fractional flow curve and the velocity rule are used to determine whether a path switch at an equal eigenvalue point is admissible. It should be recalled that the velocity rule states that a high-speed wave must be found downstream of a low-speed wave. For systems in which the injection composition lies on the vapor side of the phase envelope and the initial composition on the liquid side, the solution path (after the leading shock) lies on the vapor side of the equivelocity curve ($f > S$). This fixes the sign of the numerator on the right hand side of Eq. 4.5, and hence the derivative of the nontie-line eigenvalue has the same sign as the derivative of the superficial vapor saturation θ_k . Application of the fanning (envelope) rule in combination with the velocity rule results in four distinct cases shown in Figures 4.4-4.7.

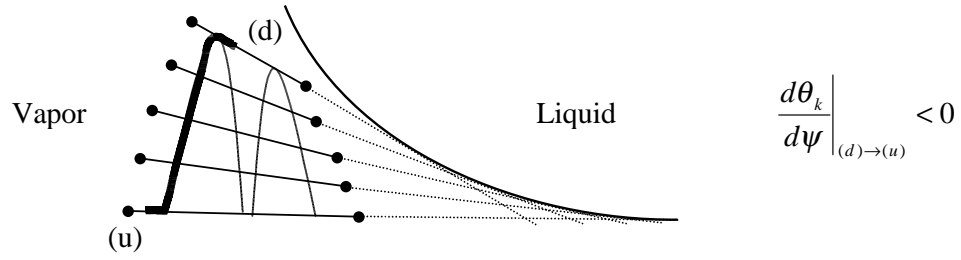


Figure 4.4: Vaporizing wave with liquid side envelope. Upstream (u), downstream (d).

The first case illustrated in Figure 4.4 is a vaporizing wave where the envelope curve is located on the liquid side of the two-phase region. As the nontie-line path is traced from the equal eigenvalue point located downstream (d) towards the injection point located upstream (u), the superficial vapor saturation θ_k decreases. This is consistent with the velocity rule and hence the path switch is allowed and a spreading wave will be present in the 1-D solution.

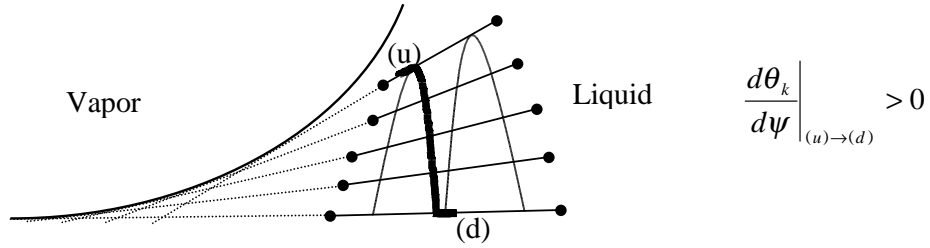


Figure 4.5 Condensing wave with vapor side envelope.

Figure 4.5 shows a condensing wave in which θ_k is increasing as the nontie-line path is traced from an upstream point (u) towards the initial oil. This is consistent with the velocity rule and hence a spreading wave will form in the solution.

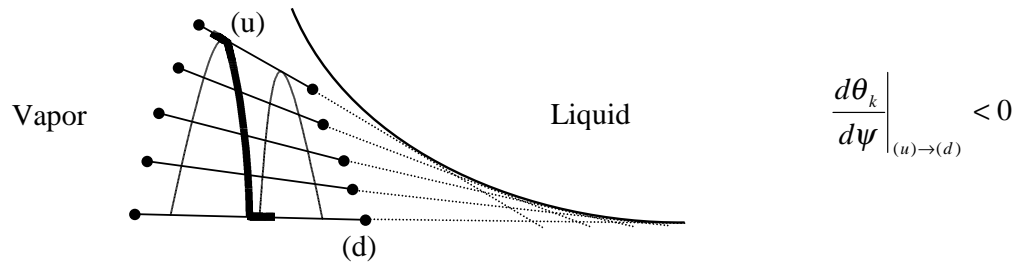


Figure 4.6 Condensing wave with liquid side envelope.

In the condensing drive illustrated in Figure 4.6, θ_k is a decreasing function of the nontie-line path when traced from an upstream point (u) towards the initial oil. This is a violation of the velocity rule, as the upstream part of the wave will eventually catch up with the downstream part. In other words, the wave is self-sharpening. The upstream and downstream key tie lines must consequently be connected by a shock. Depending on the compatibility with the solution this can be either a tangent shock or a genuine shock.

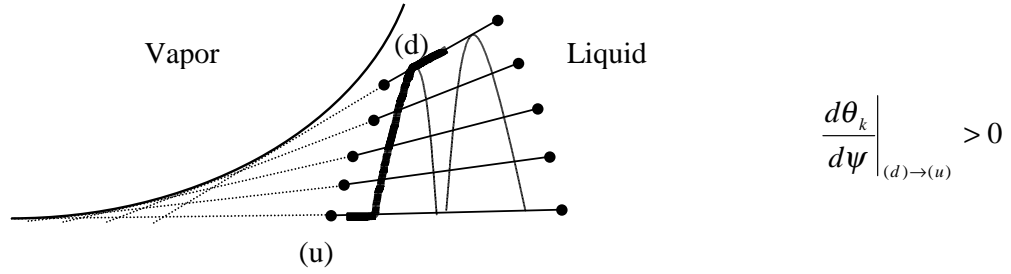


Figure 4.7: Vaporizing wave with vapor side envelope.

Figure 4.7 shows a vaporizing wave with the envelope curve located on the vapor side of the two-phase region. As the nontie-line path is traced from an upstream point (u) towards the injection point, the nontie-line eigenvalue increases. Again this behavior will result in a sharpening wave, a path switch at the equal eigenvalue point is not allowed and a shock is required.

The general feature of the four cases presented above is that a spreading wave will only form if the nontie-line path, starting at the equal eigenvalue point, is moving away from the envelope curve. Whether a rarefaction appears between two key tie lines can be summarized easily in terms of tie line length and whether the intersection point lies on the liquid or the vapor side of the two-phase region. Table 4.2 gives a summary of this.

Type	Tie line length		Intersection	Wave
	Upstream	Downstream		
Vaporizing	Long	Short	Liquid side	Rarefaction
Vaporizing	Long	Short	Vapor side	Shock
Condensing	Short	Long	Liquid side	Shock
Condensing	Short	Long	Vapor side	Rarefaction

Table 4.2: Summary of the fanning (envelope) rule.

Vaporizing segments occur when a longer key tie line lies upstream of a shorter key tie line (see Figures 4.4 and 4.7), and in vaporizing segments, a rarefaction occurs when the intersection between the key tie lines lies on the liquid side of the two-phase region. In condensing segments, a shorter key tie line is upstream of a longer one (see Figures 4.5 and 4.6), and a rarefaction occurs when the intersection is on the vapor side. Additional analysis is required to determine whether rarefactions appear if either the initial oil or the injection gas composition is in the two-phase region.

4.5.2 Algorithm for Systems with Nontie-line Rarefactions

The algorithm for constructing 1-D solutions, taking into account the existence of spreading waves, is as follows:

1. Locate all key tie lines by the tie line intersection approach.
2. Apply the fanning rule to each neighboring pair of key tie lines. If no rarefactions are predicted, switch to the simplified algorithm for fully self-sharpening systems.
3. For each predicted rarefaction, locate the equal eigenvalue point and integrate the eigenvalue problem to obtain the corresponding nontie-line path.
4. Locate the primary key tie line and start the shock construction downstream. Switch points between the nontie-line paths, and the tie line paths are introduced in the solution requirements in parallel with the velocity rule. The downstream solution is traced until the initial oil composition is reached.
5. Continue constructing the upstream solution by the approach of step 4 until the injection gas composition is reached.

4.6 Solution Example with Nontie-line Rarefaction

The appearance of nontie-line rarefactions is commonly observed in the solution path for displacements when N_2 is present in the injected gas. To illustrate the limits of the algorithm used for constructing fully self-sharpening solutions, pure N_2 is now injected into the reservoir fluid (Oil 4) at the same temperature and pressure as previously. The saturation profile generated by the algorithm for fully self-sharpening systems is compared with coarse and fine grid numerical simulations in Figure 4.8. The saturation profile from the fine grid simulation clearly indicates a nontie-line rarefaction between the initial tie line and the first crossover tie line. Figure 4.8 further illustrates the saturation profile obtained by combining an integration of the nontie-line path with shock constructions as described previously. Details of the shock solution are given in Appendix A.5.

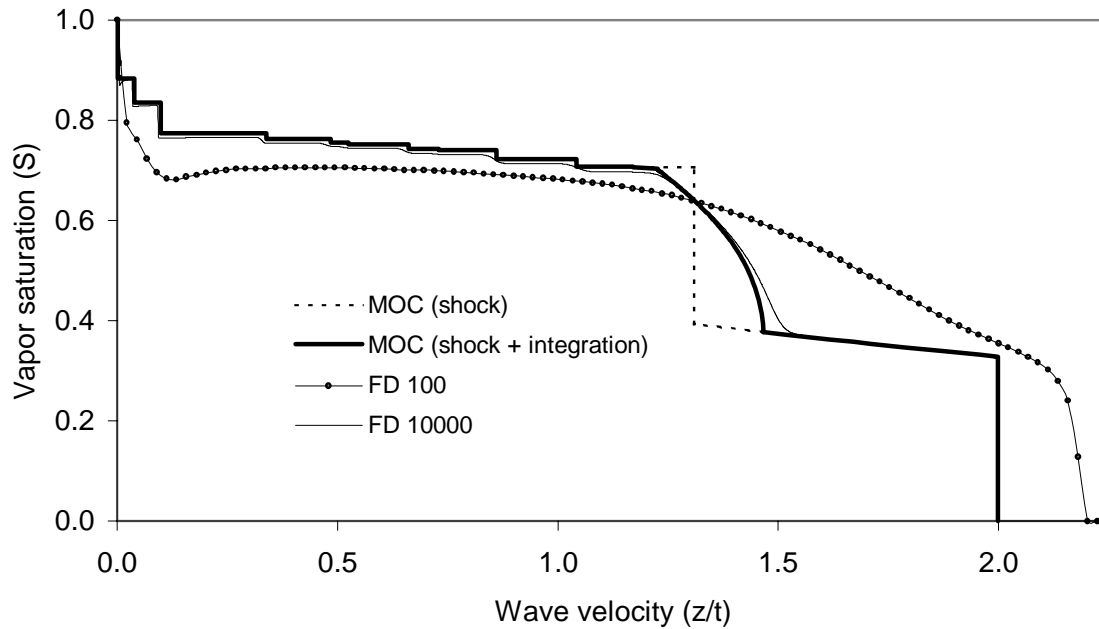


Figure 4.8: Comparison of analytical solutions (with and without integration) with numerical saturation profiles for the displacement of Oil 4 by pure N_2 at 275 atm and 387.45 K. The finite difference (FD) solutions were obtained using 100 and 10,000 grid blocks and $\Delta z/\Delta t = 10$.

For this system, the tie line extending through the initial oil is the primary tie line. Application of the fanning rule indicates that a nontie-line rarefaction connects the initial tie line and the

first crossover tie line. The nontie-line path ends at an overall composition approximately located on the adjacent tie line. The inaccuracy of the approximation introduced by assuming intersecting key tie lines is quite small, as Table 4.3 shows.

-.	x (shock)	x(rarefaction)	Error %	y (shock)	y(rarefaction)	Error %
N ₂	0.23695463	0.23657449	0.16	0.86905145	0.87052697	0.17
CO ₂	0.00892119	0.00896803	0.52	0.01255008	0.01262557	0.60
CH ₄	0.00000000	0.00000000	-	0.00000000	0.00000000	-
C ₂	0.06295753	0.06196958	1.59	0.05199391	0.05114823	1.65
C ₃	0.07434362	0.07361960	0.98	0.03517118	0.03476156	1.18
i-C ₄	0.01007617	0.00998769	0.89	0.00333684	0.00329854	1.16
n-C ₄	0.03922843	0.03896883	0.67	0.01076864	0.01066283	0.99
i-C ₅	0.01382016	0.01374001	0.58	0.00260091	0.00257527	1.00
n-C ₅	0.02260102	0.02248533	0.51	0.00376605	0.00373032	0.96
C ₆	0.03645991	0.03630629	0.42	0.00382992	0.00379312	0.97
C ₇	0.20213968	0.20233382	0.10	0.00585749	0.00581241	0.78
C ₁₁	0.10787320	0.10827271	0.37	0.00095891	0.00095155	0.77
C ₁₆	0.08952057	0.09020739	0.76	0.00011148	0.00011053	0.86
C ₂₃	0.05901420	0.05964260	1.05	0.00000305	0.00000300	1.37
C ₃₃	0.03608969	0.03692364	2.26	0.00000009	0.00000009	0.88

Table 4.3: Comparison of tie lines found by MOC integration and by the tie line intersection approach. Oil 4 displaced by pure N₂ at 387.45K and 275 atm.

The observed deviation is of an order of magnitude where the numerical evaluation of the coefficient matrix \underline{A} (Eq. 2.27) and the step by step integration may contribute significantly. To avoid violation of the mass conservation equations, the first crossover tie line is connected to the end point of the nontie-line path by a genuine shock. The downstream solution consists of a continuous variation along the initial tie line and a tangent shock to the initial oil. Genuine shocks and constant states make up the upstream part of the solution until the injection tie line is reached. Finally, the solution is completed by a direct jump to the injection composition.

Figure 4.8 shows that the fully self-sharpening solution is a much more refined approximation than that obtained by a coarse grid (FD 100) numerical simulation.

4.7 Significance of Spreading Waves in the 1-D Solutions

It was pointed out in the previous section that even if a spreading wave is present in the 1-D solution, the fully self-sharpening solution could give a far more refined approximation than coarse grid FD simulation. This fact combined with the additional complication of including the nontie-line path integration suggests that some spreading waves may be disregarded in the approximate solutions. This section illustrates how the key tie line information can be used to select significant spreading waves and disregard insignificant ones. It has been proven that spreading waves traveling a ruled surface where all tie lines intersect at the same point upon extension have a constant characteristic wave velocity²⁴ (nontie-line eigenvalue). In such cases the spreading wave is identical to a nontie-line shock of which the latter is far more convenient when a solution is constructed. It should be recalled that ruled surfaces are also developable surfaces⁵⁴. The characteristic of a developable surface is that two tie lines on the surface located infinitely close to each other will intersect. This suggests that the variation of eigenvalues along a nontie-line path can be neglected if two key tie lines are located close to each other. On the limit where two key tie lines coincide this will be rigorously true. The angle between two neighboring key tie lines can be used as a measurement of the distance to be traveled by the nontie-line path. In the previous section Oil 4 was displaced by pure N₂ to illustrate the application of the general NVC algorithm. In the calculation example the angle between the initial and the first crossover tie lines is 80.2 deg. Hence, the nontie-line path has to travel quite a distance, which results in a significant variation of the corresponding wave velocity. Next the displacement of Oil 4 by a gas containing 85 % CH₄ and 15 % N₂ at 275 atm and 387.45 K is considered. The simulation result is illustrated in Figure 4.9 whereas the details of the shock solution can be found in Appendix A.6. For this displacement the fanning rule predicts a spreading wave connecting the initial and the first crossover tie lines. In this case the angle between the two key tie lines is 12.0 deg. Accordingly, the significance of the spreading wave is smaller than in the displacement by pure N₂. This is clearly seen from Figure 4.9. In fact the numerical simulation using 1000 grid blocks is less refined than the solution consisting only of shocks. In summary of this section, the displacement of Oil 4 by pure CH₄ at 275 atm and 387.45 K is studied.

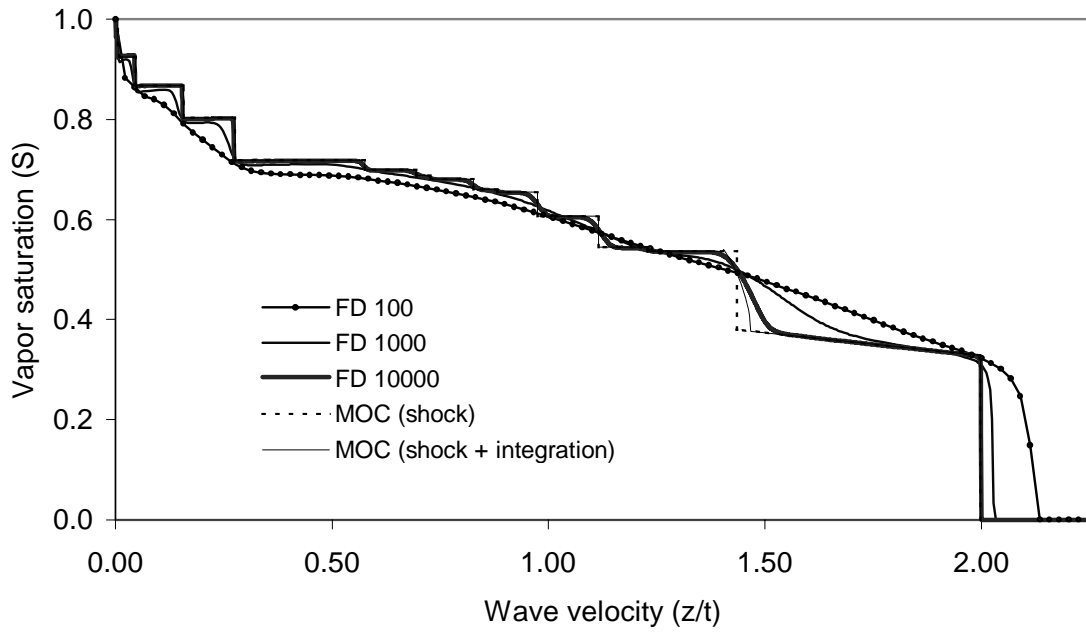


Figure 4.9: Comparison of analytical and numerical saturation profiles for displacement of Oil 4 by 85% CH_4 and 15% N_2 at 275 atm and 387.45 K. The finite difference (FD) solutions were obtained with 100, 1000, and 10000 grid blocks and $\Delta z/\Delta t = 10$.

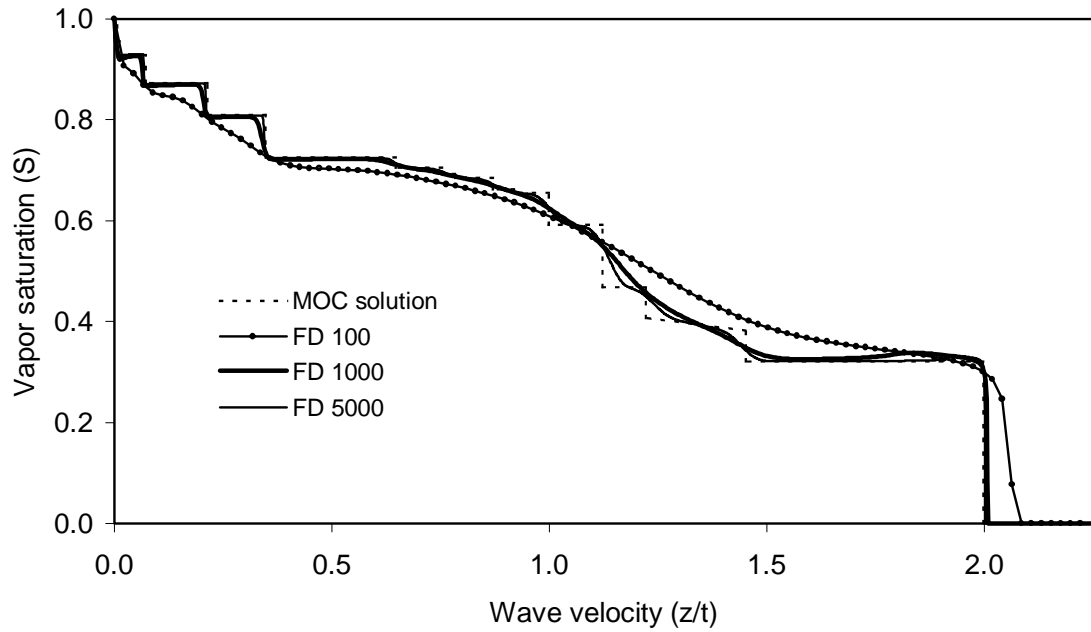


Figure 4.10: Comparison of analytical and numerical saturation profiles for displacement of Oil 4 by pure CH_4 at 275 atm and 387.45 K. The finite difference (FD) solutions were obtained with 100, 1000, and 5000 grid blocks and $\Delta z/\Delta t = 10$.

The details of the shock solution are given in Appendix A.7 and a comparison of analytical and numerical saturation profiles is shown in Figure 4.10. For this displacement the initial and the first crossover tie lines are no longer connected by continuous variation. On the other hand the fanning rule predicts the presence of two spreading waves: One connecting the first and the second crossover tie lines and one connecting the second and the third crossover tie lines. These segments are in fact predicted for all the displacements of Oil 4 considered up to now. The angles between the key tie lines holding the predicted segments are very small and Figure 4.10 clearly justifies that these waves are replaced by shocks. A summary of the insignificant spreading waves predicted by the fanning rule is given in Table 4.4.

System	Angle between crossover tie lines (deg.)	
	2 and 3	3 and 4
Oil 4 - Gas 6	0.20	3.7×10^{-2}
Oil 4 - N ₂	0.33	0.40
Oil 4 - 85% CH ₄ /15% N ₂	0.99	2.00
Oil 4 - CH ₄	0.96	2.13

Table 4.4: Prediction of insignificant nontie-line rarefactions. Angles between key tie lines.

Based on this analysis it is recommended to discard spreading waves predicted by the fanning rule if the angle between the neighboring key tie lines is less than 10 deg. The diminutive gain in accuracy of the approximate solutions obtained by including such segments does not qualify the extra complexity added to the solution construction. Throughout the rest of this work insignificant nontie-line rarefactions will be disregarded without further notice.

4.8 Example of Curvature of Surface Traveled by a Spreading Wave

This section illustrates, by a calculation example, the modest curvature of a surface traveled by a nontie-line path. For this purpose Oil 3 (Table 3.3) is displaced by pure N₂ at 300 atm and 368.15 K. The saturation profile of the MOC solution is compared with FD solutions in Figure 4.11 whereas the details of the MOC solution are given in Appendix A.7.

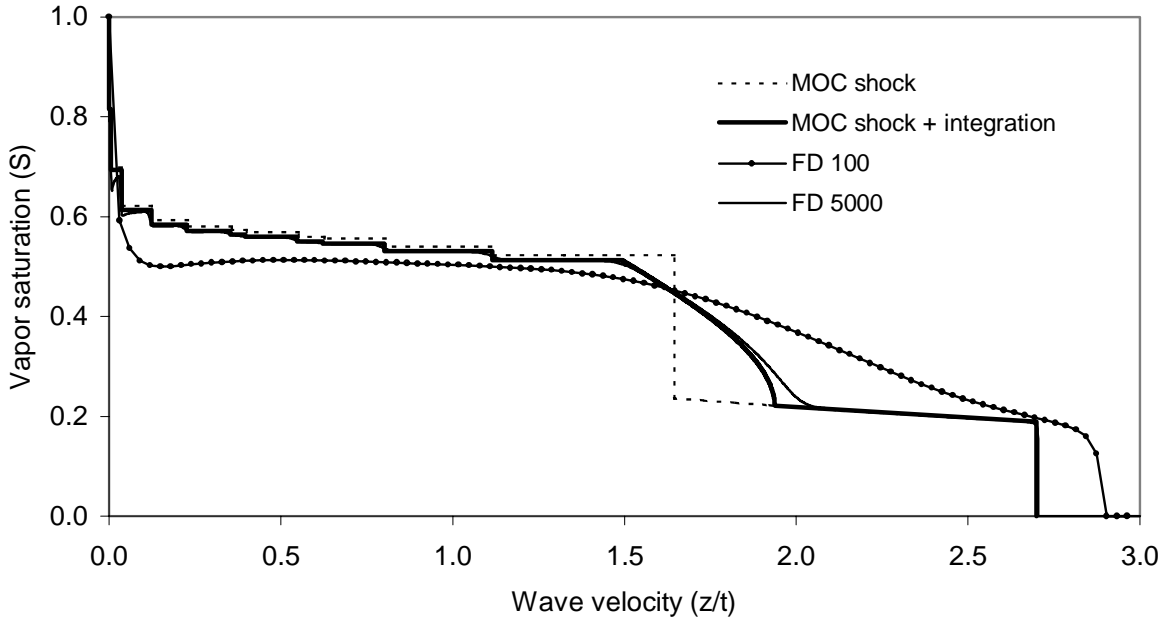


Figure 4.11: Comparison of analytical and numerical saturation profiles for displacement of Oil 3 by pure N_2 at 300 atm and 368.15 K. The finite difference (FD) solutions were obtained with 100 and 5000 grid blocks and $\Delta z/\Delta t = 10$.

In the solution the initial tie line is connected to the first crossover tie line by a spreading wave. Based on the key tie line intersection approach, a plane R spanned by the initial tie line and the first crossover tie line can be defined. The question is then: To what extent does the nontie-line path connecting the two key tie lines deviate from the plane R? The deviation of the nontie-line path can be quantified, at any given point, by the angle γ between the normal vector \underline{n} to the plane R and the nontie-line eigenvector. Further the distance to the landing tie line, in this case the first crossover tie line, can be defined as

$$l = \sum_{i=1}^{nc} (x_i^u - x_i^d)^2 + (y_i^u - y_i^d)^2 \quad (4.6)$$

The superscripts u and d refer to the landing point and the current point on the nontie-line path respectively. x and y are equilibrium mole fractions of the liquid and the vapor phase on a given tie line. A plot of the distance and the angle γ vs. the nontie-line eigenvalue is given in Figure 4.12.

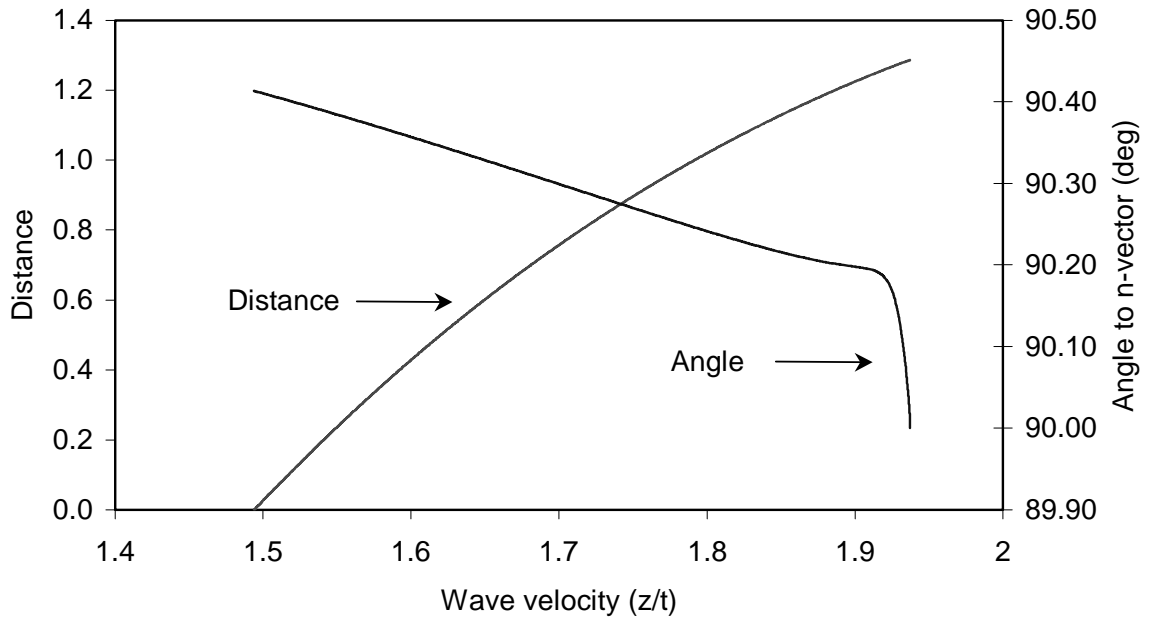


Figure 4.12: Deviation of nontie-line path from the plane spanned by neighboring key tie lines.

The equal eigenvalue point is located at $(S, \lambda) = (0.221, 1.937)$. At this point the angle to the n-vector is 90 deg, while the distance to the first crossover tie line is 1.287. Initially, the angle to the n-vector increases steeply as the nontie-line path is traced in the eigenvector directions. This may be due to the error introduced by the stepwise approach for tracing the nontie-line path. In other words, a step in the tangent vector direction will deviate more from the exact path at points with high curvature. This is sketched in Figure 4.13. As the nontie-line path is traced away from the equal eigenvalue point the change in γ becomes more flat. This indicates that the final deviation is biased by the error introduced at the start of the tracing.

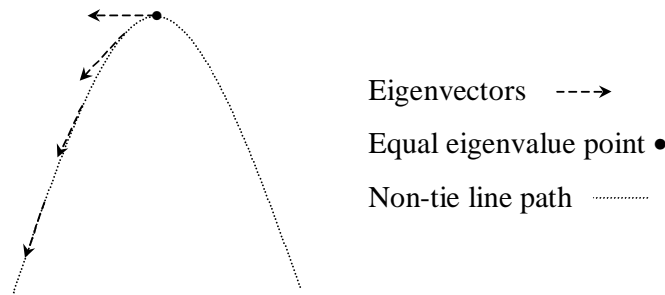


Figure 4.13: Sketch of tangent vectors (eigenvectors) and nontie-line path.

In the given calculation example the ultimate deviation from R is only 0.4 degree although a large variation in the eigenvalue results in tracing the nontie-line path. This observation confirms that the assumption about intersecting key tie lines is a very good approximation indeed. Different step sizes ε have been tested in the scheme for tracing a nontie-line path:

$$\underline{G}_{new} = \underline{G}_{old} + \varepsilon \underline{Y}_{non-tie\ line} \quad (4.7)$$

In the scheme of Eq. 4.7 eigenvectors are normalized prior to any step. It is recommended to use a step size in the interval $[10^{-4}; 10^{-2}]$. The smallest step size should be used in the vicinity of the equal eigenvalue point.

4.9 Analytical Solution below the Saturation Pressure of the Initial Oil

For all the solutions presented in the previous sections the gas was injected into the oil at a pressure above the bubble-point pressure of the oil. To demonstrate that analytical solutions can also be constructed for systems where the initial oil is unstable, the displacement of Oil 4 by pure CO₂ at 200 atm and 387.45K is considered. The bubble-point pressure of Oil 4 is 252 atm and hence the initial oil forms a two-phase system. Injection of CO₂ into Oil 4 represents a fully self-sharpening system and the analytical solution is made up entirely of shocks. The saturation profile obtained by the analytical approach is compared with coarse and fine grid FD simulations in Figure 4.14.

Details of the analytical solution are given in Appendix A.9. The second crossover tie line is identified as the primary tie line. The upstream solution consists of a tangent shock connecting the primary tie line and the third crossover tie line. Genuine shocks and a direct jump, from the injection tie line to the injection gas composition, make up the remainder of the upstream solution. The downstream construction starts with a tangent shock connecting the first and the second crossover tie lines. Hence, continuous variation along the second crossover tie line connects the up- and downstream constructions. The first crossover tie line and the initial tie line are connected by a genuine shock. The landing point S_1 from the genuine shock, connecting the first crossover tie line to the initial tie line, is located below the inflection point on the ff-curve whereas the saturation corresponding to the initial oil S_o is located above the inflection point.

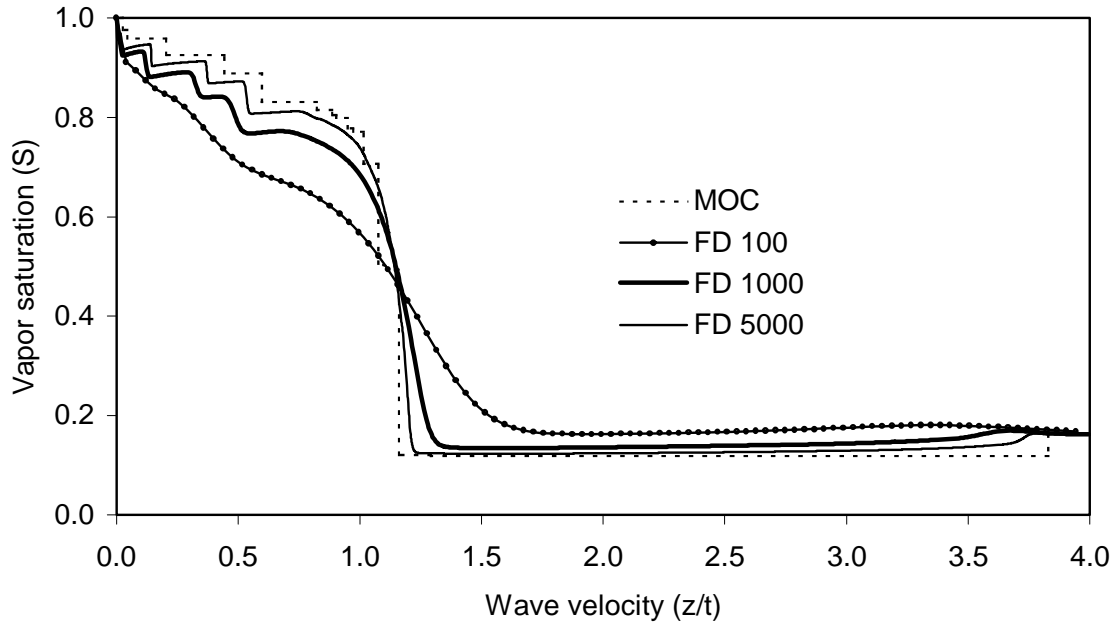


Figure 4.14: Comparison of analytical and numerical saturation profiles for displacement of Oil 4 by pure CO_2 at 200 atm and 387.45 K. The finite difference (FD) solutions were obtained with 100, 1000, and 5000 grid blocks and $\Delta z/\Delta t = 10$.

This means that the velocity rule would be violated if the two points (S_1 , S_0) were connected by continuous variation, and a direct jump from point S_1 to S_0 is the only possible solution.

4.10 Recovery Curves from Analytical 1-D Solutions

So far, all the presented approximate semi-analytical solutions to the 1-D gas injection problem have been given as relations between vapor saturation and characteristic wave velocity $S(\lambda)$. This form of presenting 1-D solutions is very general in the sense that no consideration has to be made regarding the amount of injected gas or specification of any position along the displacement. From a reservoir engineering point of view, the recovery of OOIP for a given gas injection process is of greater interest than any characteristic wave velocity. Consequently, this section demonstrates how recovery curves can be generated through construction of semi-analytical solutions.

To use the analytical solutions for calculation of recovery for a given 1-D displacement process, attention should again be turned to the physical system sketched in Figure 2.1. It is seen from the dimensionless variables (z, τ) introduced in Eq. 2.3 that the outlet of the slimtube is located at $z = 1$ and that τ corresponds to the number of pore volumes injected (PVI). The traditional recovery factor of the OOIP after 1.2 PVI is used in this work. The recovery factor based on the MOC solutions can be calculated by setting up a simple mass balance over the slimtube. By specifying one pore volume the OOIP and the amount/composition of the fluids left in the slimtube after the displacement can be determined. After injecting 1.2 PV of gas, compositions with a wave velocity less than or equal to 1.2^{-1} will still be in the slimtube.

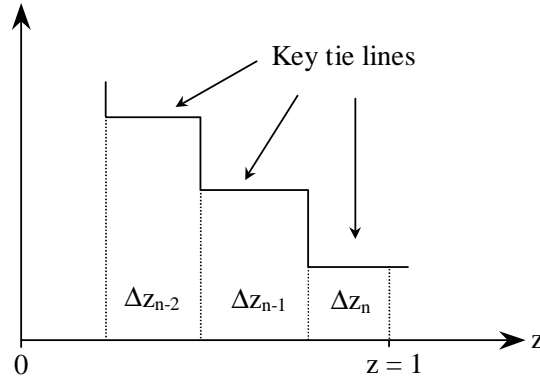


Figure 4.15: Determination of amount and composition of fluid left in slimtube after 1.2 PVI.

In more general terms, the self-similar nature of the analytical solution allows the saturation profiles to be scaled with respect to the number of PVI (τ). A sketch of a re-scaled saturation profile is given in Figure 4.15. The saturation profile is then divided into n segments (Δz_i) of constant vapor saturation, corresponding to a specific overall composition on a known key tie line. The vapor saturation for each segment is converted to mole fractions of vapor (β) and the component overall mole fractions can be calculated from the key tie line information. For the recovery factors the “true” vapor and liquid volumes predicted by the EOS are used to determine the mole numbers in each segment by

$$N_i = \frac{\Delta z_i P}{z_{eos} R_{gas} T} \quad (4.8)$$

If a segment contains two equilibrium phases z_{eos} is calculated by

$$z_{eos} = z_l(1 - \beta) + z_v\beta \quad (4.9)$$

where the subscripts l and v refer to the liquid and vapor phase compressibility factors respectively. The total number of moles left in the slimtube after the displacement (N_{left}) is found by summing Eq. 4.8 over all segments, whereas the overall composition, in mole fractions, is calculated by

$$\underline{Z}_{left} = N_{left}^{-1} \sum_{i=1}^n N_i \underline{Z}_i \quad (4.10)$$

When the number of moles and the composition of the fluid left in the slimtube after the displacement are known, the produced amount/composition can be calculated by mole and component balances. The produced oil and gas are then flashed to standard conditions and the recovery factor can be calculated. To confirm the recovery curves determined by semi-analytical calculations, a similar approach has been applied to determination of the recovery factor from numerical simulations. Initially, the displacement of Oil 4 by Gas 6 is considered. For this system the predicted MMP is 365 atm. The recovery curve obtained by semi-analytical calculations is compared with numerical simulations in Figure 4.16.

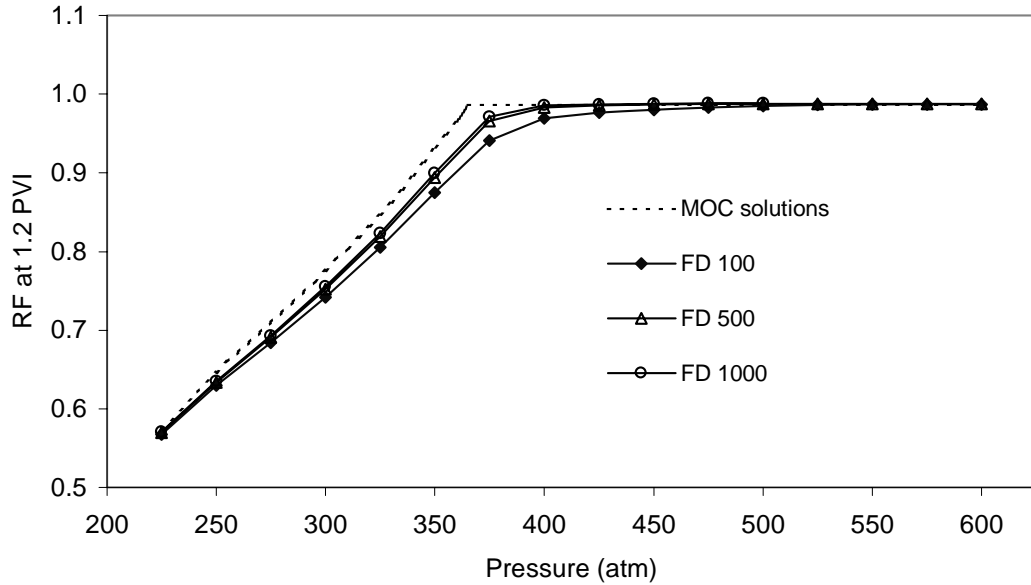


Figure 4.16: Comparison of semi-analytical and numerical recovery curves for the displacement of Oil 4 by Gas 6 at 387.45 K. The finite difference (FD) solutions were obtained with 100, 500, and 1000 grid blocks and $\Delta z/\Delta t = 10$.

The recovery curves from the FD simulation approach the dispersion-free solution (MOC) rapidly as the number of grid blocks is increased. If the MMP was determined by location of the break point on the recovery from coarse grid numerical simulations, only a small over prediction would occur in the current case. The deviation between the analytical recovery curve and the numerical recovery curves is largest at the MMP because effects of numerical dispersion become stronger as a point in the critical locus (MMP) is approached⁵¹.

Similar features are found for the displacement of Oil 4 by pure CH_4 and by pure CO_2 . The MMPs for these displacements are 371 atm and 226 atm respectively. Analytical and numerical results are given in Figures 4.17 and 4.18.

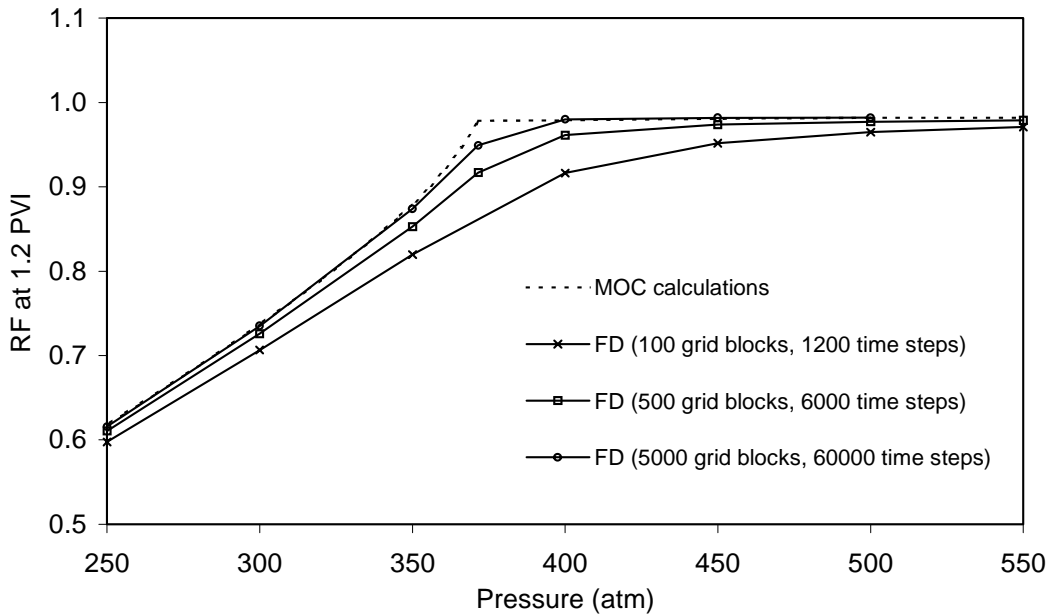


Figure 4.17: Comparison of analytical and numerical recovery curves for displacement of Oil 4 by pure CH_4 at 387.45 K. The finite difference (FD) solutions were obtained with 100, 500, and 5000 grid blocks and $\Delta z/\Delta t = 10$.

The displacement of Oil 4 by pure CH_4 and pure CO_2 appears to be slightly more sensitive to numerical dispersion, and more refined numerical simulations are needed to capture the dispersion-free recovery curve.

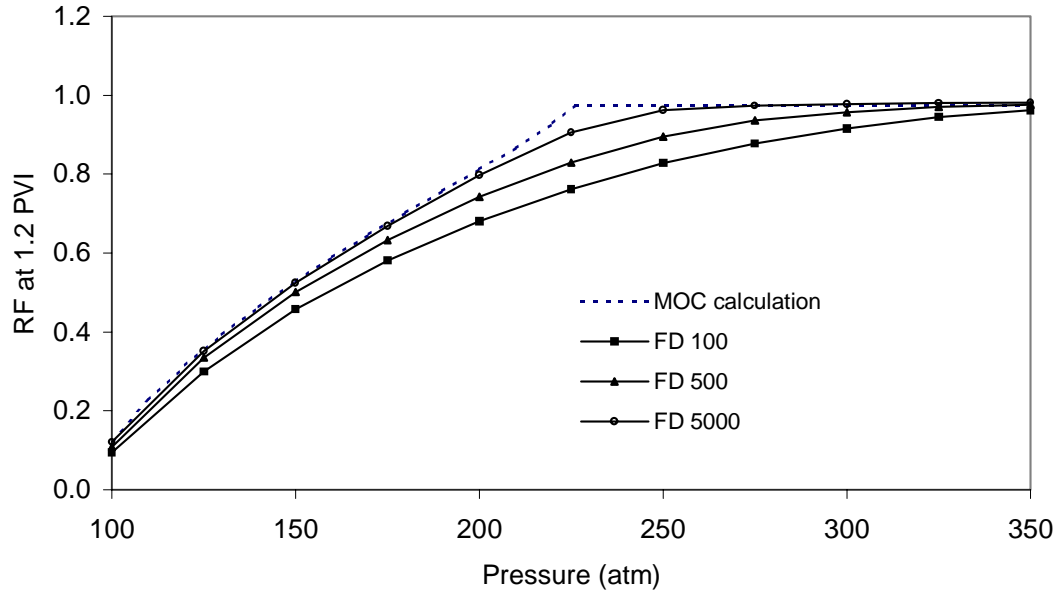


Figure 4.18: Comparison of analytical and numerical recovery curves for displacement of Oil 4 by pure CO_2 at 387.45 K. The finite difference (FD) solutions were obtained with 100, 500 and 5000 grid blocks and $\Delta z/\Delta t = 10$.

A completely different picture arises when Oil 4 is displaced by pure N_2 . For this system the MMP predicted by the global approach is 380 atm. The recovery curve obtained by MOC

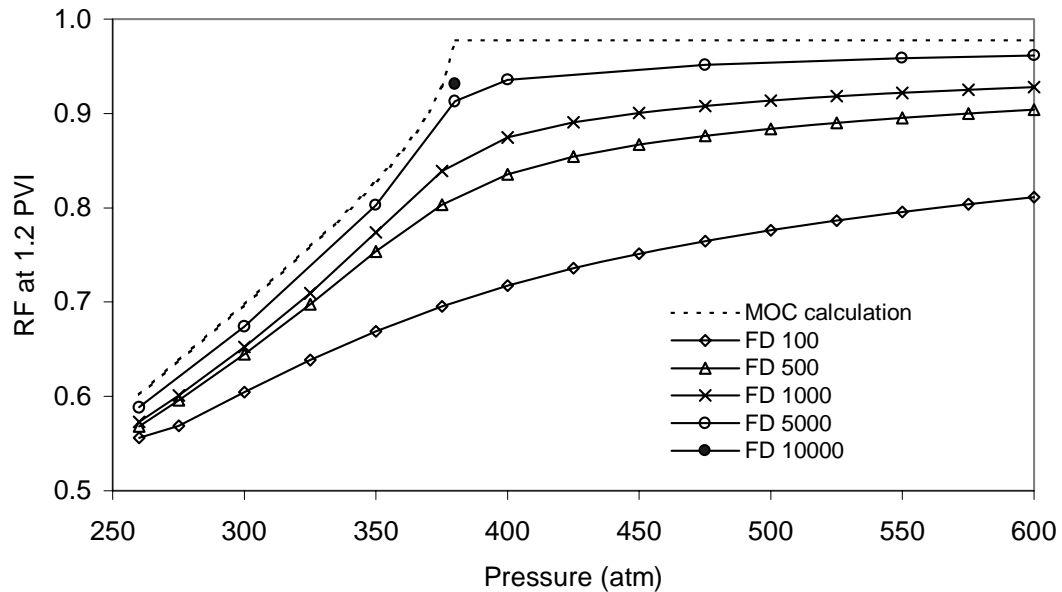


Figure 4.19: Comparison of analytical and numerical recovery curves for displacement of Oil 4 by pure N_2 at 387.45 K. The finite difference (FD) solutions were obtained with 100, 500, 1000, 5000 and 10000 grid blocks and $\Delta z/\Delta t = 10$.

calculations is compared with numerical simulations in Figure 4.19. For this system the effect of numerical dispersion is seen to be very significant. At the MMP the recovery predicted by numerical simulations with 100, 1000 and 10000 grid blocks is 70%, 85% and 93 %. This very substantial variation in the recovery factor suggests that otherwise feasible gas injection projects might be abandoned, if coarse grid numerical simulations form the basis of a project evaluation. The existence of a system-dependent sensitivity to numerical dispersion has been reported by several authors^{32,45,51} and will be discussed further in Chapter 6. Sensitivity to numerical dispersion, similar to that of the previous system, is found for the displacement of Oil 3 by pure N_2 .

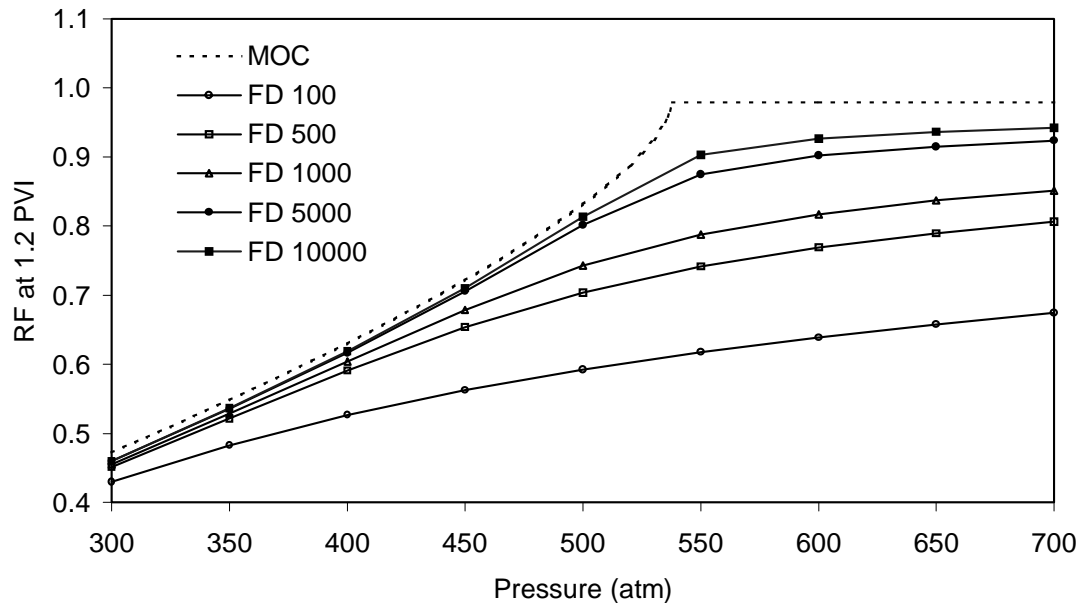


Figure 4.20: Comparison of analytical and numerical recovery curves for displacement of Oil 3 by pure N_2 at 368.15 K. The finite difference (FD) solutions were obtained with 100, 500, 1000, 5000 and 10000 grid blocks and $\Delta z/\Delta t = 10$.

The time consuming part of constructing 1-D analytical solutions is the location of key tie lines. Hence, in terms of required CPU time the MOC approach is superior to coarse grid numerical simulations for the purpose of generating recovery curves. This is partly due to the fact that key tie lines from a previous solution (pressure) are easily traced to a higher pressure whereas the FD simulations have to be restarted for each pressure step.

4.11 Supplementary NVC Solutions

In this section additional semi-analytical solutions based on the NVC assumption are presented. The additional solutions serve as additional validation of the algorithms given in the previous sections. Four cases are described in which Oil 3 is displaced by Gas 3, Gas 5, pure CH_4 and a 75%-25% mixture of CO_2 and CH_4 .

4.11.1 Displacement of Oil 3 by Gas 3 at 300 atm and 368.15 K

A comparison of the analytical and the numerical solutions is given in Figure 4.21 while the details of the MOC solution are given in Appendix A.10.

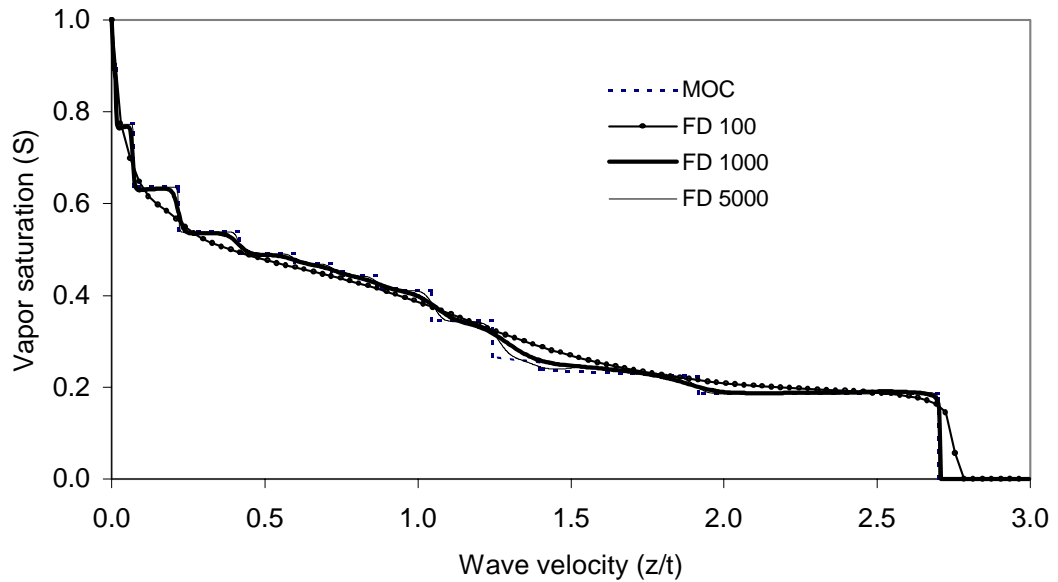


Figure 4.21: Comparison of analytical and numerical saturation profiles for displacement of Oil 3 by Gas 3 at 300 atm and 368.15 K. The finite difference (FD) solutions were obtained with 100, 1000, and 5000 grid blocks and $\Delta z/\Delta t = 10$.

The displacement of Oil 3 by Gas 3 is somewhat different from the previously presented solutions in the sense that three tangent constructions are included. The second crossover tie line is identified as the primary tie line. The downstream construction starts with a tangent construction connecting the second and the first crossover tie lines. The next pair of key tie

lines (the first crossover tie line and the initial tie line) is also connected by a tangent shock. The tangent part of this shock is located on the first crossover tie line and hence two points on this tie line are connected by continuous variation. Finally, the initial oil is connected to the initial tie line by a direct jump. The upstream part of the solution starts with a tangent shock connecting the primary tie line and the third crossover tie line. The two points on the primary tie line are connected by continuous variation along the tie line. The rest of the upstream solution is made up by genuine shocks followed by a direct jump to the injection gas composition.

4.11.2 Displacement of Oil 3 by Gas 5 at 250 atm and 368.15 K

A comparison of the analytical and numerical solutions is given in Figure 4.22 while the details of the MOC solution are given in Appendix A.11.

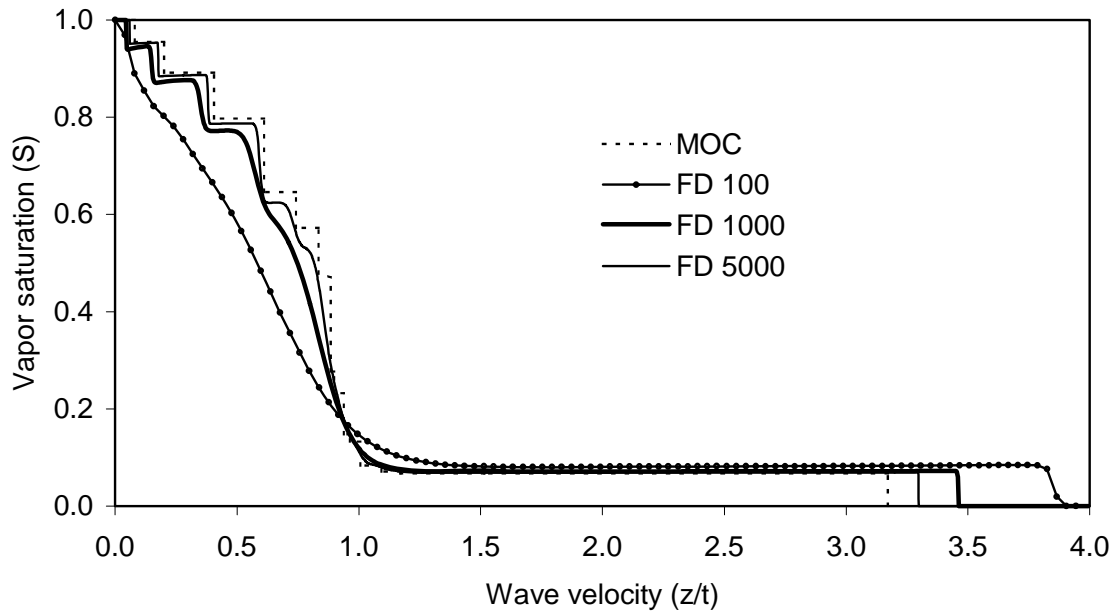


Figure 4.22: Comparison of analytical and numerical saturation profiles for displacement of Oil 3 by gas 5 at 250 atm and 368.15 K. The finite difference (FD) solutions were obtained with 100, 1000, and 5000 grid blocks and $\Delta z/\Delta t = 10$.

In this case the eighth crossover tie line is the primary one. The downstream solution starts with a tangent shock connecting the primary tie line and the seventh crossover tie line.

Genuine shocks and a direct jump to the initial oil make up the rest of the downstream solution. The upstream solution is similar to the downstream solution. That is, a tangent construction to the primary tie line followed by a sequence of genuine shocks until the injection tie line is reached. Finally, the injection gas is reached through a direct jump. The up- and downstream parts of the solution are connected by continuous variation along the primary tie line.

4.11.3 Displacement of Oil 3 by Pure CH_4 at 300 atm and 368.15 K

A comparison of the analytical and the numerical solutions is given in Figure 4.23 while the details of the MOC solution are given in Appendix A.12.

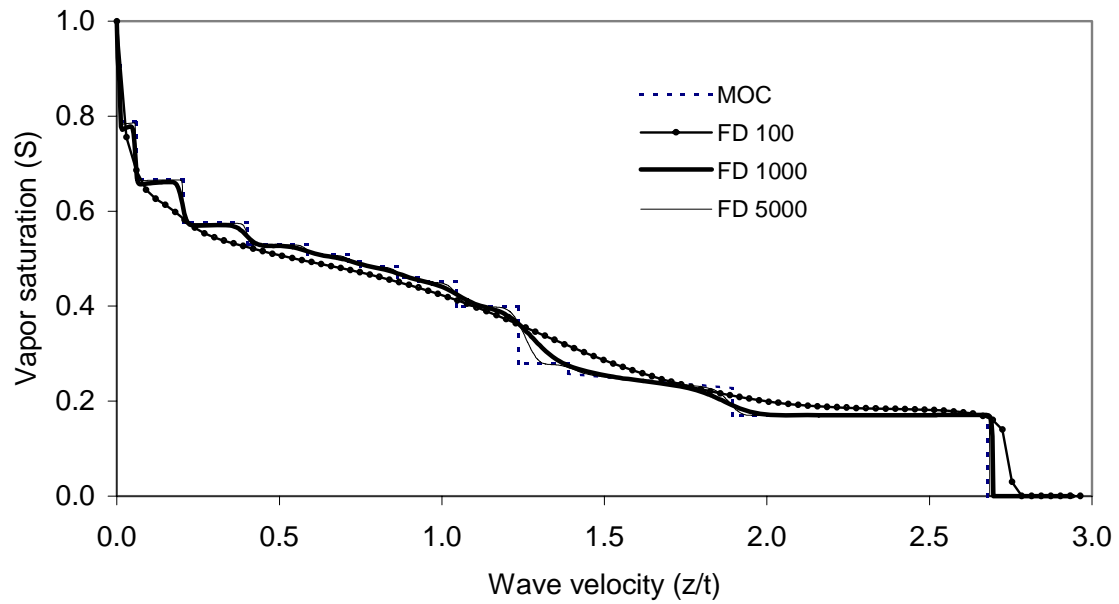


Figure 4.23: Comparison of analytical and numerical saturation profiles for displacement of Oil 3 by pure CH_4 at 300 atm and 368.15 K. The finite difference (FD) solutions were obtained with 100, 1000, and 5000 grid blocks and $\Delta z/\Delta t = 10$.

The structure of the analytical solutions for this system is identical to the previous one. In this case, however, the primary tie line is the first crossover tie line.

4.11.4 Displacement of Oil 3 by 75% CO₂ and 25% CH₄ at 275 atm and 368.15 K

The MMP for the displacement of Oil 3 by the CO₂-CH₄ mixture is predicted to be 291 atm. The displacement at 275 atm is therefore close to being a multicontact miscible. This is evident from the comparison of analytical and numerical simulations given in Figure 4.24.

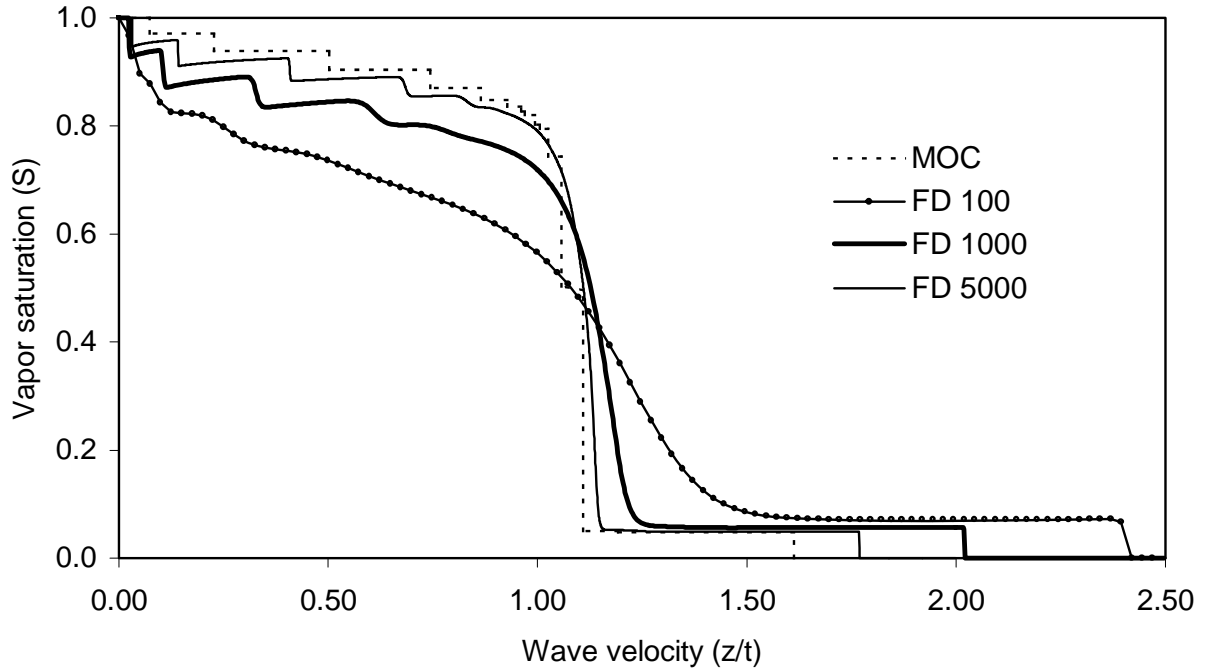


Figure 4.24: Comparison of analytical and numerical saturation profiles for displacement of Oil 3 by 75% CO₂ and 25% CH₄ at 275 atm and 368.15 K. The finite difference (FD) solutions were obtained with 100, 1000, and 5000 grid blocks and $\Delta z/\Delta t = 10$.

As the pressure approaches the MMP the saturation profile becomes gradually steep. At the MMP the profile will be a step function with a wave velocity of 1. Figure 4.24 clearly shows the effects of numerical dispersion in the near-critical region. Even the FD simulation using 5000 grid blocks has difficulties capturing the dispersion-free profile. The structure of the analytical solution, constructed from the second crossover tie line (primary), is identical to that of Section 4.10.2. Details of the MOC solution are found in Appendix A.13.

4.12 Summary

A new approach to constructing approximate analytical solutions to the 1-D gas injection process is presented. The new approach is based on a combination of the analytical theory of 1-D gas injection problems with no volume change on mixing and the tie line intersection approach studied in Chapter 3. Two algorithms are developed for the construction of approximate analytical solutions.

The first algorithm is based on the assumption that all key tie lines, defining the 1-D solution geometrically in the compositional space, are connected by shocks and hence must intersect pairwise. Construction of fully self-sharpening solutions is bound to start at a primary tie line. Proof is given that a primary tie line exists and that the primary tie line must be the shortest of the key tie lines. The solutions generated by the algorithm are rigorously correct for fully self-sharpening systems. For displacements which include nontie line rarefactions, the solutions obtained by the algorithm are approximate, but they are much more accurate than solutions obtained by conventional finite difference compositional simulation unless impractical fine computational grids are used. The computation time required for construction of fully self-sharpening solutions is demonstrated to be orders of magnitude lower than for the corresponding numerical simulations.

To obtain a more refined approximation for displacements with nontie line rarefactions a tool is developed for the prediction of such segments. The presence of a rarefaction between key tie lines can be determined easily from the lengths of the upstream and downstream tie lines and from the position of the intersection point on the vapor side or the liquid side of the two-phase region. This approach is referred to as the fanning rule, which forms the basis of the general algorithm for construction of analytical solutions. In the general algorithm, shock constructions are combined with nontie line path integration, resulting in far more accurate approximations of the 1-D displacement problems with significant spreading waves. Through a study of the curvature of the ruled surface traveled by a nontie line rarefaction, it is demonstrated that the tie line intersection approach is very accurate even for systems with significant rarefaction.

The new algorithms are used for generating recovery curves. In this connection, the existence of a system dependent sensitivity to numerical dispersion for FD simulations is observed.

5. Approximate Analytical 1-D Solutions with Volume Change (VC)

In this chapter the intersecting key tie line approach is combined with tools from the general analytical theory of 1-D gas injection processes. It will be demonstrated how this combination allows the construction of approximate analytical solutions taking into account volume change on mixing (VC). The reader is assumed to be familiar with the content of Chapters 2-4. The analysis and the development of algorithms in this chapter are restricted to consider only the construction of fully self-sharpening solutions: All segments of the approximate solutions are based on shock constructions. Nevertheless, the fanning rule presented in the previous chapter applies directly to the general displacement problem, in which components are allowed to change volume as they are partitioned between the equilibrium phases. Hence, by checking for emergence of significant nontie line rarefactions, the quality of the approximations obtained by constructing fully self-sharpening solutions can be monitored. For all the calculation examples presented in this chapter, molar densities predicted by the applied EOS are used directly without any volume correction.

5.1 Shocks in the Two-phase Region

In the general formulation of the conservation equations a shock balance is given by

$$\Lambda = \frac{v_d^{II} F_i^{II} - v_d^I F_i^I}{C_i^{II} - C_i^I}, \quad i = 1, \dots, nc \quad (5.1)$$

with

$$F_i^I = f(\rho_y y_i - \rho_x x_i) + \rho_x x_i \quad (5.2)$$

and

$$C_i = S(\rho_y y_i - \rho_x x_i) + \rho_x x_i \quad (5.3)$$

ρ_x and ρ_y refer to the liquid and vapor phase molar densities corresponding to the liquid and vapor phase compositions on the tie line connecting \underline{x} and \underline{y} . The superscripts I and II in Eq. 5.1 denote the two key tie lines connected by the shock. An extra degree of complexity is added to the shock balance equation as the total velocity (v_d) varies across a shock front. In general the variation in the total velocity is caused by changes in the phase densities

throughout the displacement. Variation in the compositional space along a tie line does accordingly not affect the total velocity, as the equilibrium phase densities are constant.

Shock balances in the form of Eq. 5.1 were applied successfully in the work of Dumoré⁹ and Monroe et al.³⁶ whereas Dindoruk⁷ presented the first detailed analysis. He demonstrated that two tie lines connected by a shock intersect in the molar concentration space at a fictitious point $\rho_s Z_{s,i}$ defined by

$$\rho_s Z_{s,i} = (\rho_y y_i \theta + (1-\theta) \rho_x x_i)^I \quad (5.4)$$

and

$$\rho_s Z_{s,i} = \alpha (\rho_y y_i \theta + (1-\theta) \rho_x x_i)^{II} \quad (5.5)$$

where α is given by

$$\alpha = \frac{v_d^{II} - \Lambda}{v_d^I - \Lambda} \quad (5.6)$$

The fictitious nature of the concentration point $\rho_s Z_{s,i}$ is due to the fact that tie lines can intersect outside the physical concentration space. Dindoruk⁷ further demonstrated that the fictitious vapor saturations θ^I and θ^{II} entering Eqs. 5.4-5 are related to the shock velocity and the corresponding total velocities on the opposite sides of the shock by

$$\frac{v_d^I f^I - \Lambda S^I}{v_d^I - \Lambda} = \theta^I \quad (5.7)$$

and

$$\frac{v_d^{II} f^{II} - \Lambda S^{II}}{v_d^{II} - \Lambda} = \theta^{II} \quad (5.8)$$

The superficial vapor saturations entering Eqs. 5.7 and 5.8 can be determined directly from key tie line information by simple component balances.

Consider a neighboring pair of key tie lines (*I* and *II*). Let tie line *I* be the shorter one and hence the starting point for a shock construction. Eq. 5.7 can be rewritten in the form

$$\Lambda^* = \frac{\Lambda}{v_d^I} = \frac{f^I - \theta^I}{S^I - \theta^I} \left(= \frac{df^I}{dS^I} \right) \quad (5.9)$$

which is similar in structure to the shock balance equation in the NVC formulation (Eq. 2.33). If the key tie lines are connected by a tangent shock, the scaled shock velocity (Λ^*) can be determined by a tangent construction to the fractional flow curve as indicated in Eq. 5.9. If on

the other hand the shock is, a genuine shock the saturation S^I and consequently the fractional flow of vapor f^I will be known in advance and Eq. 5.9 can be used to calculate the scaled shock velocity directly. The landing point on key tie line II can be determined through a reformulation of Eq. 5.8 in terms of the scaled shock velocity:

$$\frac{v_d^I}{v_d^{II}} \Lambda^* = \frac{f^{II} - \theta^{II}}{S^{II} - \theta^{II}} \quad (5.10)$$

Prior to calculation of the landing point on tie line II the ratio between the total velocities on the opposite sides of the shock must be evaluated. This is done by calculating α from Eqs. 5.4 and 5.5 by use of any component present on both sides of the shock. The ratio of total velocities is then given by

$$\frac{v_d^{II}}{v_d^I} = \alpha(1 - \Lambda^*) + \Lambda^* \quad (5.11)$$

and the landing point is subsequently obtained by solving Eq. 5.10 for the vapor saturation S^{II} . From the shock construction scheme outlined above it is evident that the routines, developed in the course of solving NVC problems, can be applied to VC problems without modifications.

5.2 Shocks due to Phase Appearance and Disappearance

For shocks due to phase appearance (leading shocks) and disappearance (trailing shocks), the shock balance given in Eq. 5.1 is applied with superscripts I and II , indicating the single-phase side and the two-phase side respectively. This shock balance was initially studied by Welge.⁵⁵ The overall molar density and overall flux of a component i at a point in the single-phase region can be written as

$$F_i^I = C_i^I = \rho_z Z_i \quad (5.12)$$

where ρ_s is the EOS based molar density at the point Z . By inserting Eqs. 5.12 and 5.2 in Eq. 5.1 the following expression is derived:

$$\frac{v_d^{II} f^{II} - \Lambda S^{II}}{v_d^{II} - \Lambda^{II}} = \frac{\rho_s Z_i \frac{v_d^I - \Lambda}{v_d^{II} - \Lambda} - \rho_x x_i}{\rho_y y_i - \rho_x x_i} = \theta \quad (5.13)$$

By introducing a fictitious molar density ρ_s^* defined by

$$\rho_s^* = \rho_s \frac{v_d^I - \Lambda}{v_d^{II} - \Lambda} = (\rho_y - \rho_x)\theta + \rho_x \quad (5.14)$$

it is evident that ρ_s^* must be located on the extension of a line passing through the points ρ_x and ρ_y , and that this line is a key tie line (initial or injection tie line). This reasoning is similar to the analysis by Dindoruk⁷. The fictitious vapor saturation θ corresponding to ρ_s^* can be calculated from key tie line information. By rewriting Eq. 5.13 the shock velocity can be related to the landing point in the two-phase region by

$$\Lambda^* = \frac{\Lambda}{v_d^{II}} = \frac{f^{II} - \theta}{S^{II} - \theta} \left(= \frac{df^{II}}{dS^{II}} \right) \quad (5.15)$$

The scaled shock velocity can thus be solved for either as a semi-shock by tangent construction to the fractional flow curve (as indicated in Eq. 5.15) or as a genuine shock where S^{II} and f^{II} are known a priori. After solving for the scaled shock velocity, the relationship between the total velocities at points I and II is found from

$$\frac{v_d^I}{v_d^{II}} = \frac{\rho_s^*}{\rho_s} (1 - \Lambda^*) + \Lambda^* \quad (5.16)$$

5.3 Algorithm for Construction of Fully Self-sharpening Solutions (VC)

In Sections 5.1 and 5.2, tools were described for calculation of the shock velocity scaled with respect to dimensionless total velocity on one side of the shock. However, for the purpose of constructing full solutions to 1-D problems, actual shock velocities must be used to rule out non-physical shock solutions by application of the velocity rule. In other words, the dimensionless total velocity on one side of a shock must be known prior to any shock constructions. As for the NVC formulation of the 1-D problem, a fully self-sharpening solution must start with a tangent construction to the primary tie line. Thus the dimensionless total velocity of the primary tie line must be determined. In Chapter 2 the conservation equations were written in terms of a dimensionless time variable τ given by

$$\tau = \frac{v_{inj} t}{L\phi} \quad (5.17)$$

In the formulation of Chapter 2 the displacement problem is thus scaled with respect to the injection velocity. Consequently, the determination of v_d on the primary tie line requires the full solution to be known. This paradox can be resolved due to the self-similarity of the analytical solutions and the linear dependence between the overall flux and the total velocity (Eq. 2.6). Any solution to the conservation equations can be rescaled with respect to any given total velocity without changing the structure of the solution. By rescaling the conservation equations with respect to the total velocity on the primary tie line, the up- and downstream parts of the solution can be constructed by use of the tools described in previous sections. Once a solution to the rescaled problem is found, the solution to the original formulation is determined by scaling the characteristic wave velocities with respect to the injection velocity. For convenience the total velocity on the primary tie line can be set equal to 1. The solution scaled with respect to the injection velocity is found from

$$\lambda = \frac{\lambda_{rescaled}}{v_{inj}} \quad (5.18)$$

$$v_d = \frac{v_{d,rescaled}}{v_{inj}} \quad (5.19)$$

The velocity v_{inj} entering Eqs. 5.18 and 5.19 is the injection velocity predicted by the rescaled solution. The algorithm for construction of fully self-sharpening solutions is hence:

1. Determine all key tie lines by the global approach.
2. Locate the primary key tie line and fix the total velocity for this tie line.
3. Construct the up- and downstream parts of the solution by solving the shock balances for each adjacent pair of key tie lines. Start both segments by a tangent construction to the primary tie line.
4. Rescale the characteristic wave velocities and the total velocities of the obtained solution with respect to the injection velocity.

5.4 Examples of Analytical Solutions with Volume Change on Mixing

The new approach to constructing semi-analytical solutions to the 1-D displacement problem, taking into account volumetric effects, has been applied to a number of gas-oil systems. It should be recalled that no density information is required to locate the key tie lines defining the geometry of a given displacement process. The key tie lines used for constructing solutions to the VC formulation of the conservation equations are therefore identical to those used for solving the NVC problems. This similarity suggests that the general structure of the analytical solutions in the VC formulation is identical to that of the simplified NVC formulation. The truth of this is apparent from the following calculation examples.

Initially, the displacement of Oil 4 by Gas 6 is considered. The gas is injected into the oil at 275 atm and 387 K. By application of the fanning rule no significant nontie line rarefactions are predicted, and the fully self-sharpening solution is thus expected to be a very good approximation. As for the NVC solution, the shock constructions start at the third crossover tie line by tangent constructions to the second and fourth crossover tie lines.

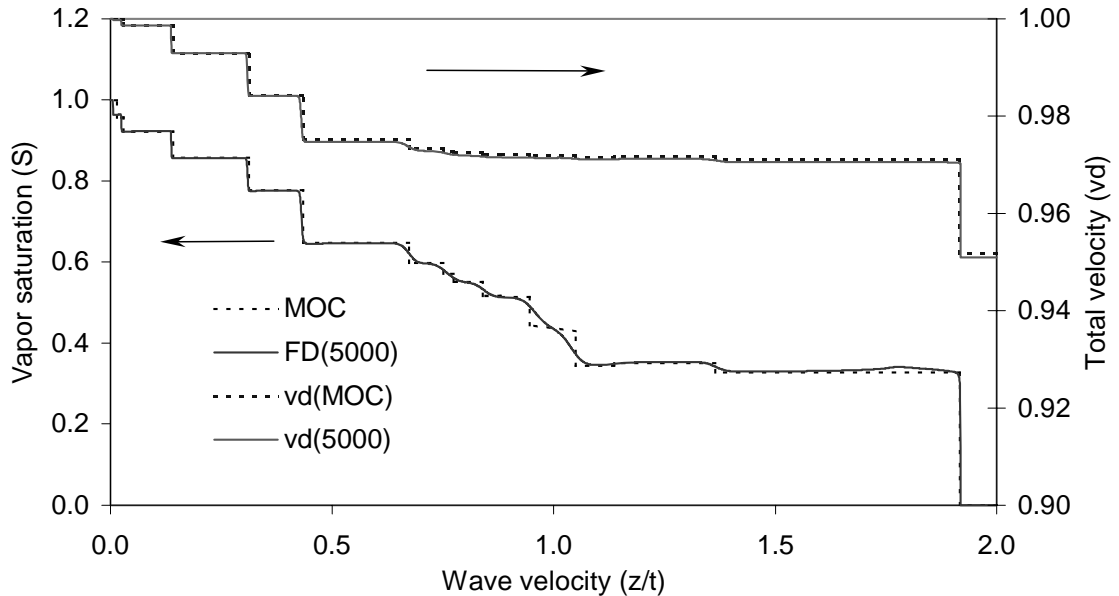


Figure 5.1: Comparison of analytical and numerical solutions for the displacement of Oil 4 by Gas 6 at 275 atm and 387.45 K including volumetric effects. The FD solution was obtained with 5000 grid blocks and $\Delta z/\Delta \tau = 10$.

Genuine shocks and direct jumps in and out of the two-phase region make up the remainder of the up- and downstream solution. The analytical solution is compared with a fine grid numerical simulation in Figure 5.1 while details of the solution are found in Appendix A.14. Excellent agreement is found between the analytical solution and the numerical simulation. A comparison of the VC solution with the NVC solution reported in Chapter 4 is illustrated in Figure 5.2.

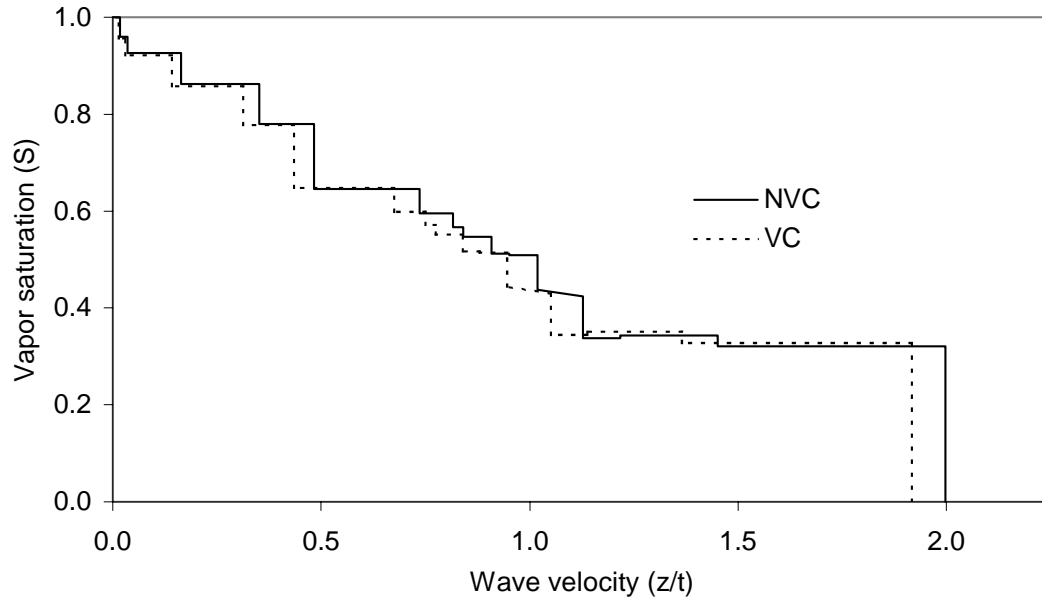


Figure 5.2: Comparison of analytical VC and NVC solutions for the displacement of Oil 4 by Gas 6 at 275 atm and 387.45 K.

The general structure of the NVC and the VC solutions is seen to be identical. In the given example the characteristic waves of the VC solution are moving slower than in the NVC solution. In terms of the displacement process, the breakthrough time (time elapsed prior to any production of gas) predicted by the VC solution would be larger than for the NVC solution. That this is no general feature is shown by the next example.

To illustrate the limitations of the self-sharpening solutions with volume change, the displacement process in which pure N_2 is injected into Oil 3 at 275 atm and 387 K is examined. The analytical solution is compared with fine and coarse grid numerical simulations in Figure 5.3 while the VC and the NVC solutions are compared in Figure 5.4.

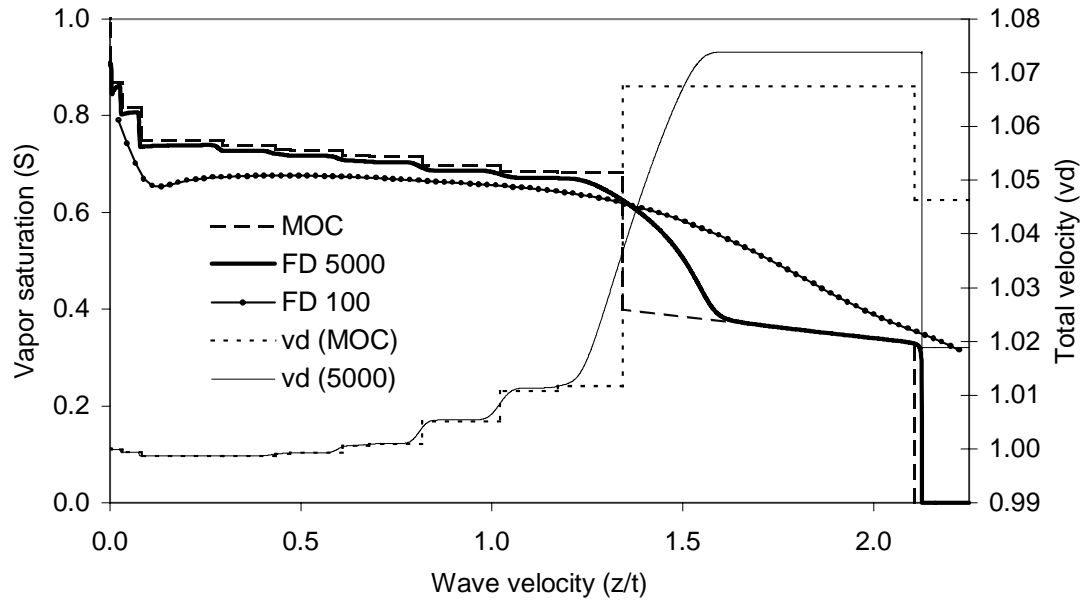


Figure 5.3: Comparison of analytical and numerical solutions for the displacement of Oil 4 by pure N_2 at 275 atm and 387.45 K including volumetric effects. The FD solutions were obtained with 100 and 5000 grid blocks and $\Delta z/\Delta \tau = 10$.

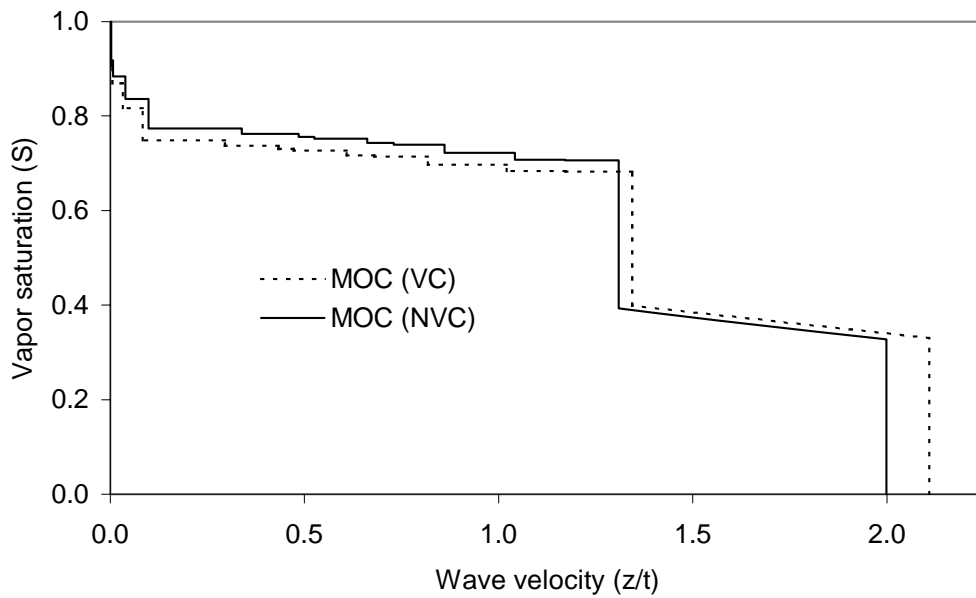


Figure 5.4: Comparison of analytical VC and NVC solutions for the displacement of Oil 4 by pure N_2 at 275 atm and 387 K.

Details of the analytical solution are found in Appendix A.15. For this example the fanning rule predicts the existence of a significant nontie line rarefaction connecting the initial tie line and the first crossover tie line. Nevertheless, it is possible to construct a solution consisting of shocks only. It is seen from Figure 5.3 that analytical solution based on pure shock constructions fails to match exactly the fine grid numerical simulation. However, the analytical solution still offers a far more refined approximation to the fine grid simulation than the coarse grid simulation does. The analytical approximation will be particularly useful if the displacement process is continued after breakthrough. For this example the breakthrough will occur after 0.48 PVI (corresponding to $\lambda_{\text{front}} = 2.1$). Hence, for calculation of recovery curves after injection of 1.2 PVI, where all waves with characteristic velocities larger than 1.2^{-1} have been produced, the analytical solution will be a good approximation to the fine grid numerical simulation. The quality of this approximation is demonstrated in Section 5.5.

The similarity in the general structure of the analytical solution for the VC and NVC problems is illustrated in Figure 5.4. In contrast to the previous example, where the characteristic waves of the NVC had higher velocities than the VC waves over the entire range, the NVC waves of the current case have lower velocities in one region of the solution and higher in another.

Next the analytical shock solution for the displacement of Oil 3 by Gas 3 at 300 atm and 368.15 K is generated. The NVC solution for this displacement process is described in Section 4.10.1. This system differs from the other systems presented in Chapter 4 in the sense that three tangent constructions are present in the solution. Again the same structure is found for the VC solution. The saturation and the total velocity profile are compared with equivalent numerical simulations in Figure 5.5. Details of the analytical solution along with a comparison of the NVC and the VC solutions are given in Appendix A.16. No significant nontie line rarefactions are predicted by the fanning rule so that good agreement is expected between the semi-analytical and fine grid numerical simulation. Figure 5.5 clearly shows that this is the case. The downstream solution construction starts with a tangent shock connecting the primary tie line (second crossover tie line) to the first crossover tie lines. A second tangent construction connects the first crossover tie line to the initial tie line and, finally, the downstream construction is completed by a direct jump to the initial oil.

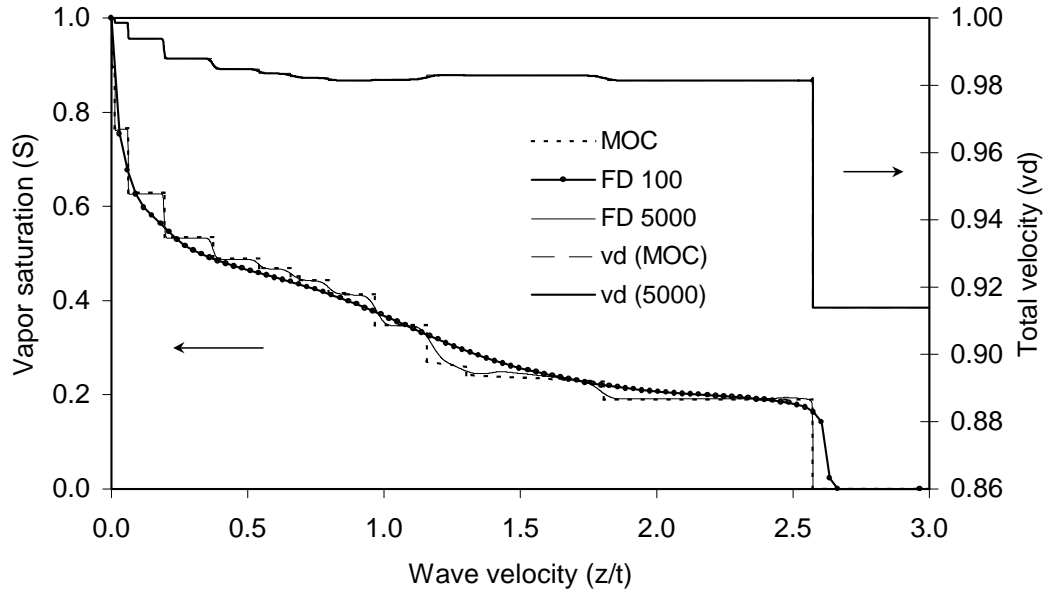


Figure 5.5: Comparison of analytical and numerical solutions for the displacement of Oil 3 by Gas 3 at 300 atm and 368.15 K including volumetric effects. The FD solutions were obtained with 100 and 5000 grid blocks and $\Delta z/\Delta \tau = 10$.

The upstream solution construction starts with a third tangent construction connecting the primary tie line to the fourth crossover tie line, followed strictly by genuine shocks and a direct jump to the injection gas composition.

Finally, a near-miscible displacement process is considered in which Oil 3 is displaced by a mixture of 75% CO_2 and 25% CH_4 . The gas mixture is injected at 275 atm and 368.15 K. These conditions are 16 atm below the pressure at which a multicontact miscible displacement would develop ($\text{MMP} = 291$ atm). The analytical solution is compared with numerical simulations in Figure 5.6. As pointed out previously numerical dispersion becomes significant as a miscible displacement is approached. This is evident from Figure 5.6. Although the saturation profiles from the numerical simulations converge towards the analytical solution as the number of grid blocks is increased, not even the fine grid numerical solution is able to capture the details of the analytical solution completely. The specifics of the analytical solution and a comparison with the NVC solution are given in Appendix A.17.

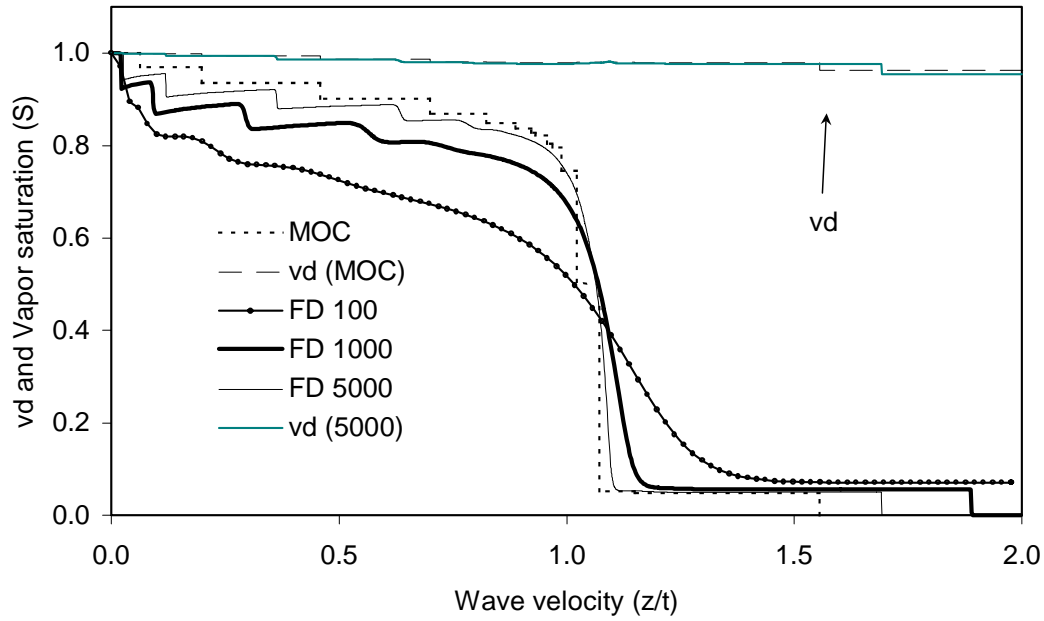


Figure 5.6: Comparison of analytical and numerical VC solutions for the displacement of Oil 3 by Gas 3 at 275 atm and 368.15 K. The FD solutions were obtained with 100, 1000 and 5000 grid blocks and $\Delta z/\Delta \tau = 10$.

5.5 Recovery Curves from Analytical Solutions with Volume Change on Mixing

In this section the results obtained from applying the new VC algorithm to generation of recovery curves are presented. The approach to calculation of the recovery factor from analytical solutions described in Chapter 4 can be used directly for the VC solutions of this chapter. Initially, the displacement process where Gas 6 is injected into Oil 3 at 387.45 K is studied. The recovery curve obtained from analytical solutions is compared with numerical simulations in Figure 5.7. As the number of grid blocks is increased in the FD simulations the corresponding recovery curves converge rapidly towards the dispersion-free recovery curve. The largest deviation is found near the MMP (365 atm) where the effect of numerical dispersion becomes more significant.

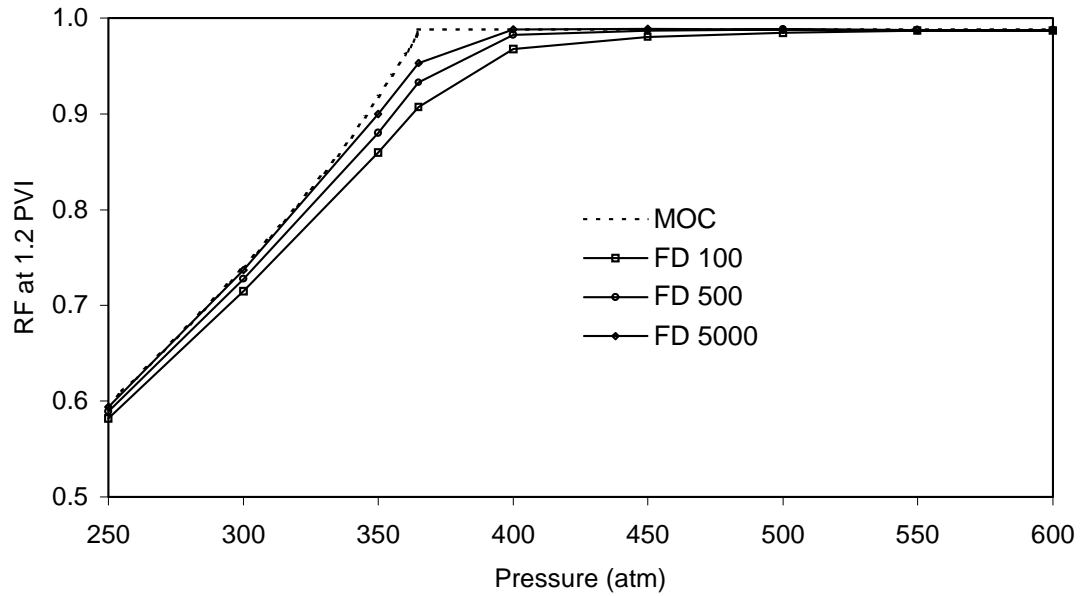


Figure 5.7: Comparison of recovery curves for the displacement of Oil 4 by Gas 6 at 387.45 K generated by semi-analytical calculations and FD simulations. The FD solutions were obtained with 100, 500 and 5000 grid blocks and $\Delta z/\Delta \tau = 10$.

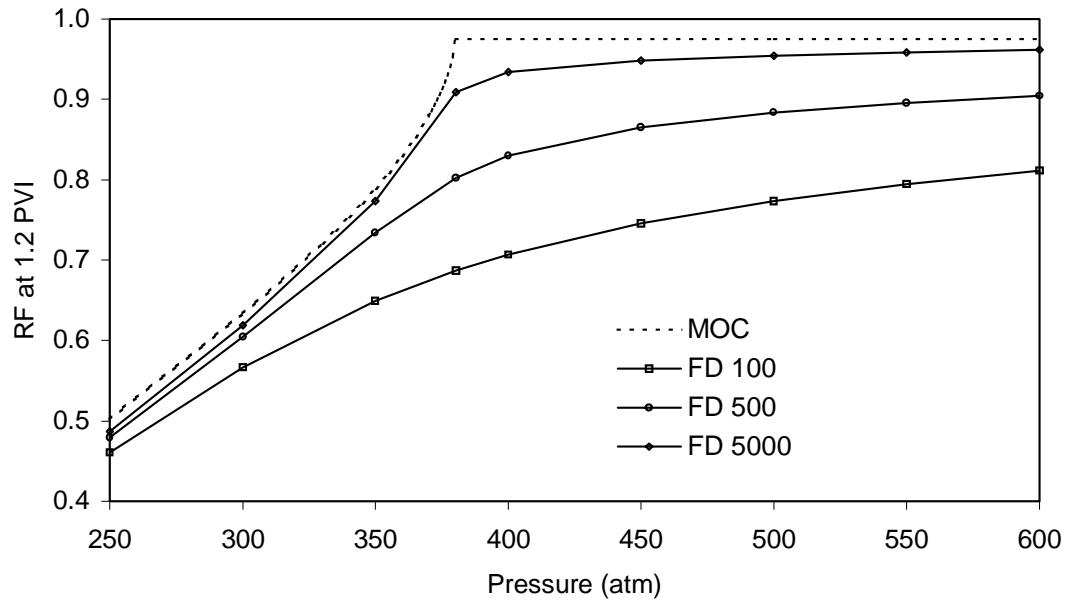


Figure 5.8: Comparison of recovery curves for the displacement of Oil 4 by pure N_2 at 387.45 K generated by semi-analytical calculations and FD simulations. The FD solutions were obtained with 100, 500 and 5000 grid blocks and $\Delta z/\Delta \tau = 10$.

The second example of recovery curves generated by analytical calculations and FD simulations given in Figure 5.8 is based on the displacement of Oil 3 by pure N_2 at 387.45 K. The analytical solution to this displacement problem was presented in the previous section. It was described how the analytical solution fails to capture the details of the fine grid FD simulation because of the existence of a significant nonlinearity rarefaction in the solution. Figure 5.8 shows excellent agreement between the recovery curves predicted by fine grid FD simulations and the pure shock solutions. The high quality of the approximate analytical solution is due to the fact that only the low-velocity part ($\lambda < 1.2^{-1}$) of the saturation profiles (e.g. Figure 5.3) is used for calculation of the recovery. The convergence of the FD simulation towards the dispersion-free solution is observed to be much slower for the injection of pure N_2 than for the injection of Gas 6 considered in the previous example. An identical pattern was observed for the NVC solutions to the two gas injection problems. Hence, there appears to be a system specific sensitivity to the effects of numerical dispersion. The nature of this phenomenon is addressed in Chapter 6.

5.5 Summary

In this chapter the general analytical theory of 1-D gas injection problems is combined with the intersecting tie line approach in order to obtain semi-analytical solutions. Thus, the assumption about ideal mixing used for construction of 1-D solutions in Chapter 4 is relaxed. The analysis and the development of solution construction tools are restricted to considering only fully self-sharpening solutions. In other words, the analytical solutions are assumed to consist only of shock constructions. The shock balances in the general (VC) formulation are more complex than in the NVC formulation since the overall convective velocity varies across a shock front.

Tools for construction of shocks in the two-phase region along with tools for construction of shocks due to phase appearance and disappearance are presented. The shock balance equations are rewritten in a form which allows direct application of the routines developed in the course of constructing NVC solutions.

In order to construct full solutions to the 1-D problem the general formulation of the conservation equations has to be rescaled with respect to the convective velocity of the

primary tie line. An approach to rescale the conservation equations is described as well as a new general algorithm for construction of pure shock solutions with VC.

The new algorithm is applied to four different oil-gas systems. It is demonstrated how the fanning rule developed in Chapter 4 can be used to predict the quality of the approximate solutions by checking for the emergence of significant spreading waves. Very good agreement between analytical and fine grid numerical solutions is observed. It is demonstrated that even though significant spreading waves exist in a true solution, the approximation of a pure shock solution is far more refined than coarse grid numerical simulations.

Analytical solutions from the new algorithm are used for generation of recovery curves which can be used to predict the upper recovery limit (dispersion-free) for a given displacement process. The analytical recovery curves are in excellent agreement with results from fine grid FD simulations.

Finally, the existence of a system dependent sensitivity to numerical dispersion in FD simulations is observed.

6. On System-dependent Sensitivity of Numerical Dispersion in FD Simulations

The effects of numerical dispersion in conventional finite difference compositional simulations have been studied extensively ever since computers were first applied to prediction of reservoir performance or, ultimately, generation of production forecasts. The papers of Stalkup^{45,46} and Lim *et al.*³² are examples of such studies. This chapter focuses on the apparent system specific sensitivity to numerical dispersion observed for the numerical simulation reported in Chapters 4 and 5. Analysis of this phenomenon will be restricted to considering the impact of numerical dispersion on FD solutions for 1-D displacement problems in homogeneous porous media. Further, this study considers only the simple but still often applied one-point upstream weighting formulation of the mass conservation equations. Numerical dispersion in this type of simulation emerges partly from truncation errors introduced by the finite difference representation of the convective term²⁶, and partly from the fact that FD simulations of this kind basically correspond to a sequence of interconnected mixing cells. Aris and Amundson¹ demonstrated the asymptotic equivalence of mixing cells in series and the convection-diffusion equation. In mixing cell terminology, it is characteristic of numerical dispersion that material entering one cell can be allowed to enter the next cell faster than normal flow would allow. The magnitude of the artificial dispersion is of the order $\Delta z/2$, which for reservoir scale modeling often exceeds what is physically realistic⁴⁶.

Walsh and Orr⁵¹ demonstrated, on the basis of 1-D ternary displacements problems, that the sensitivity to of numerical dispersion for a given system is related to the phase behavior of the system in terms of the size and the shape of the two-phase region. The basic ideas of Walsh and Orr⁵¹ are combined with the intersecting tie line approach and extended to apply to miscible displacements of multicomponent systems. Consider the displacement of Oil 5 given in Table 6.1 by pure N₂ at 305 atm and 344 K.

	P _C (psia)	T _C (F)	ω	Oil 5	k(N ₂ ,j)		
N ₂	493	-232.42	0.04	0	-	-	-
CH ₄	667.8	-116.63	0.0104	0.5	0.031	-	-
C ₄	550.7	305.65	0.201	0.1624	0.12	0.027	-
C ₁₀	305.7	652.1	0.49	0.3376	0.12	0.042	0.008

Table 6.1: Properties of Oil 5. Data from Dindoruk⁷

Dindoruk⁷ analyzed in detail the analytical VC solution to the system at a pressure well below the MMP. The geometrical structure of the displacement process is shown in Figure 6.1. The figure illustrates the key tie lines predicted by the global approach (red lines) along with an FD solution path obtained by use of 1000 grid blocks and $\Delta z/\Delta \tau = 10$ (blue line). At the given temperature the MMP for the current system is predicted to be 309 atm. Thus, the displacement process shown in Figure 6.1 is near-miscible as seen from the length of the initial tie line. The mechanism controlling the development of miscibility is a pure vaporizing drive and hence an enriched gas becomes locally miscible with the initial oil.

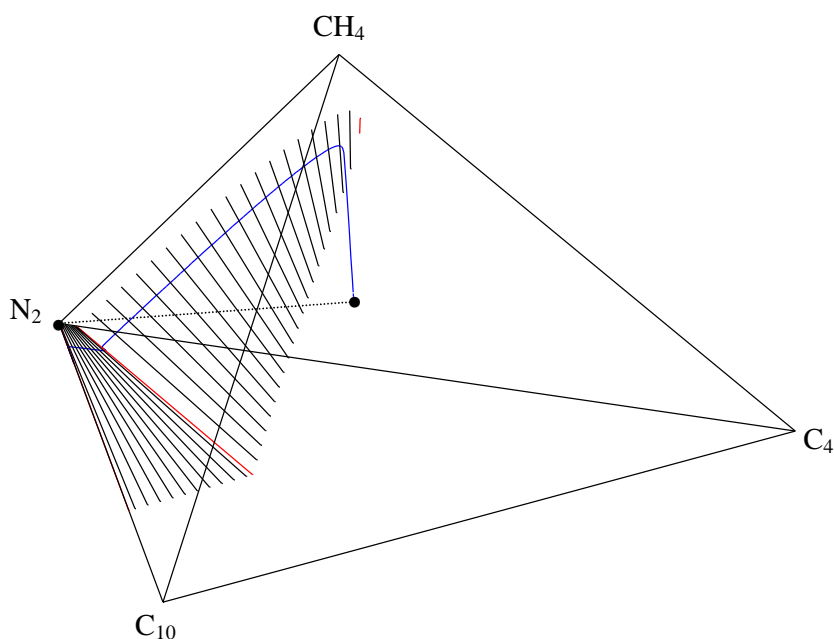


Figure 6.1: Displacement of Oil 5 by pure N_2 at 305 atm and 344 K. The red lines are the key tie lines predicted by the global approach. The blue line is the result of a 1000 grid FD simulation with $\Delta z/\Delta \tau = 10$.

The initial oil is located on the $CH_4 - C_4 - C_{10}$ surface of the quaternary diagram. The initial tie line is also located on this surface and the dispersion-free analytical solution (not included) would have to enter the two-phase region by a shock along this tie line. The initial tie line is connected to the crossover tie line by a nontie line rarefaction. In this case the crossover tie

line is located on the $N_2 - C_4 - C_{10}$ surface. A shock must connect the crossover tie line to the injection tie line, which is located on the $N_2 - C_{10}$ line of the phase diagram.

The recovery curve for this displacement process has been generated by analytical calculations and is compared with coarse and fine grid numerical simulations in Figure 6.2.

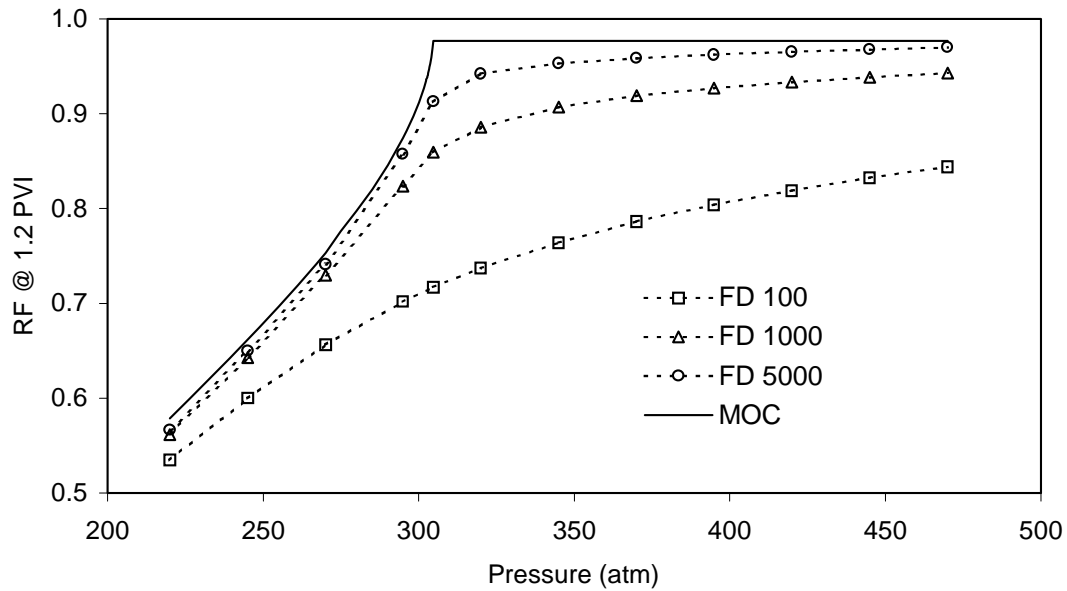


Figure 6.2: Comparison of recovery curves from analytical and FD simulations for the displacement of Oil 5 by pure N_2 at 344 K. The FD simulations were performed with 100, 1000 and 5000 grid blocks and $\Delta z/\Delta \tau = 10$.

Figure 6.2 clearly demonstrates that FD simulation of the displacement process illustrated in Figure 6.1 is strongly affected by numerical dispersion if coarse grid blocks are used. The geometrical structure of the displacement process (Figure 6.1) can be used to explain this high sensitivity to numerical dispersion. At the beginning of the FD simulation N_2 is mixed with the initial oil along the dilution line connecting the two compositions (dotted line). As the oil is mixed with the injected N_2 , the composition path starts to move along the dilution line until the boundary of the two-phase region is reached. The orientation of the tie lines in the two-phase region forces the liquid composition of the first two-phased contact down towards the $N_2 - C_4 - C_{10}$ surface (and the injection tie line), whereas the corresponding gas phase is moving upwards toward the initial tie line. In the case concerned the presence of numerical dispersion will allow a gas with low enrichment of C_4 , from previous contacts with liquid

compositions still rich in C_4 , to contact an even richer liquid phase. Such a contact corresponds to a line of similar direction as that of the dilution line in compositional space. Thus, numerical dispersion will force the composition path downward in the direction of the $N_2 - C_4 - C_{10}$ surface and away from the initial tie line. This suggests that the orientation of the dilution line relative to the direction of the initial tie line (critical tie line) plays an important role regarding the sensitivity of the current system. To investigate if this relationship has any influence on the sensitivity to numerical dispersion, a 50/50 mixture of N_2 and CH_4 is used as injection gas. The geometrical structure of this displacement process is given in Figure 6.3

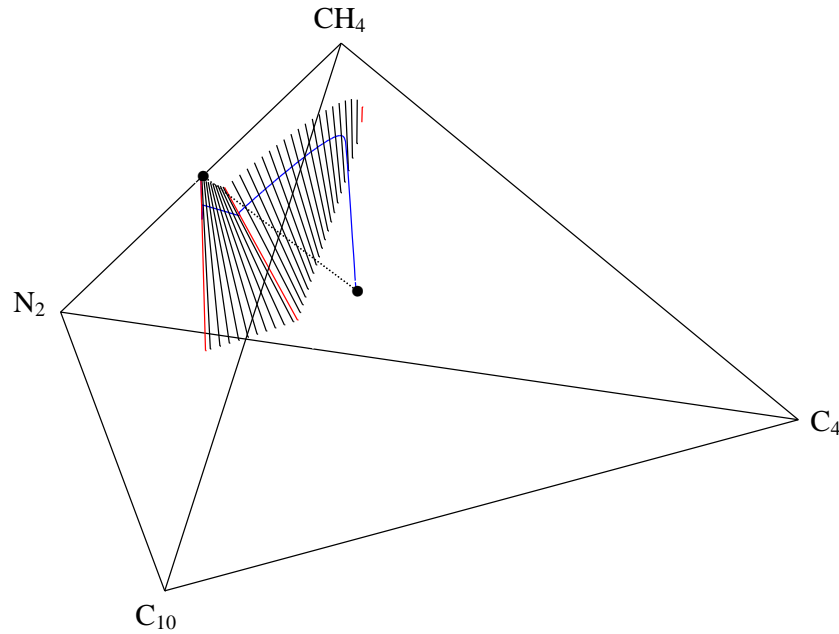


Figure 6.3: Displacement of Oil 5 by 50% N_2 and 50% CH_4 at 305 atm and 344 K. The red lines are the key tie lines predicted by the global approach. The blue line is the result of a 1000 grid FD simulation with $\Delta z/\Delta \tau = 10$.

The new injection gas composition does not alter the MMP of the displacement process as the initial tie line is fixed by the oil composition. However, the locations of the injection and the crossover tie lines are changed. Both tie lines are moved closer to the initial tie line. Consequently, the angle between the initial tie line and the dilution line is reduced. Two numerical simulations were made at 305 atm with the new injection gas: A coarse grid

simulation with 100 grid blocks and a fine grid simulation with 5000 grid blocks. The variation in the predicted recovery at 1.2 PVI for the two numerical experiments was 18% compared to 21% for the N_2 displacement process. Thus, the effects of numerical dispersion are still quite significant although the angle between the dilution line and the initial tie line is reduced. A third injection gas consisting of 10% N_2 and 90% CH_4 was injected into Oil 5. The structure of the displacement process is shown in Figure 6.4.

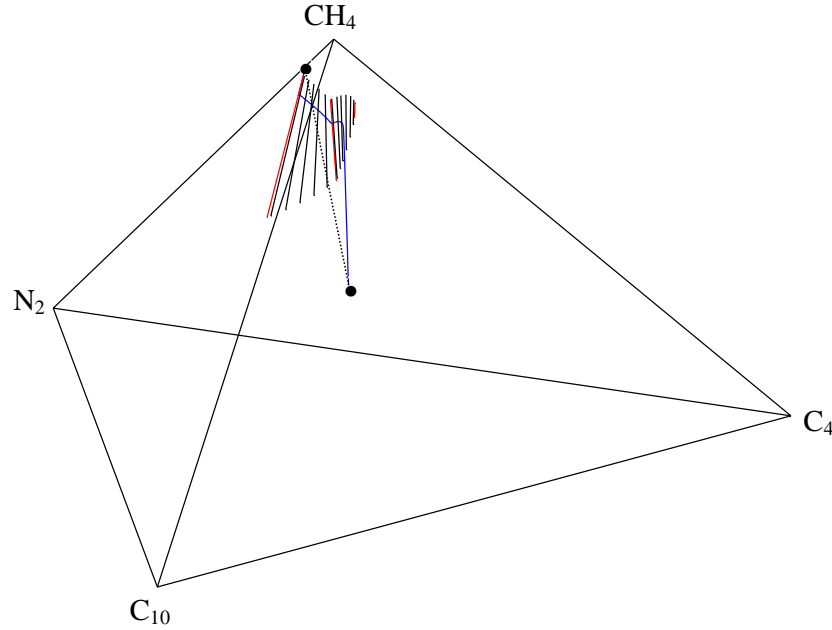


Figure 6.4: Displacement of Oil 5 by 10% N_2 and 90% CH_4 at 305 atm and 344 K. The red lines are the key tie lines predicted by the global approach. The blue line is the result of a 1000 grid FD simulation with $\Delta z/\Delta \tau = 10$.

Again, the injection of a CH_4 rich gas does not alter the location of the initial tie line and hence the MMP for the displacement process. The general structure of the analytical solution also remains the same. This experiment was performed to force the dilution line to be located similarly to the initial tie line. Recovery curves for this displacement process, based on analytical calculations and FD simulations, are compared in Figure 6.5. A very significant change is observed regarding the sensitivity of this displacement process. The numerical simulations converge rapidly towards the analytical recovery curve as the number of grid blocks is increased.

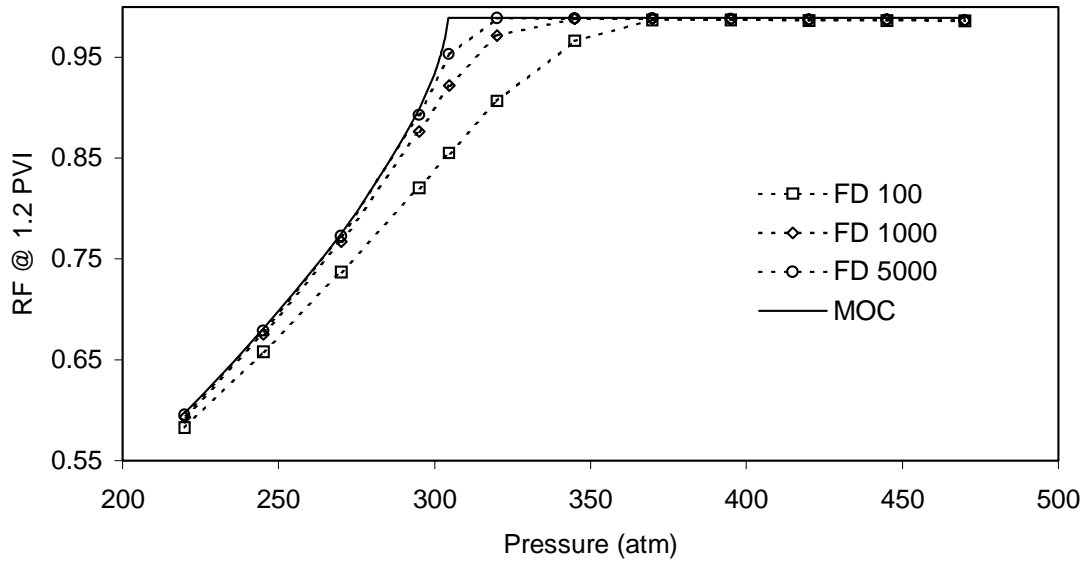


Figure 6.5: Comparison of recovery curves from analytical and FD simulations for the displacement of Oil 5 by 10% N_2 and 90% CH_4 at 344 K. The FD simulations were performed with 100, 1000 and 5000 grid blocks and $\Delta z/\Delta \tau = 10$.

A comparing the Figures 6.1 and 6.2 with 6.4 and 6.5 reveals that the relative orientation of the dilution line and the initial tie line (critical tie line) has a major impact on the significance of numerical dispersion in FD simulations of the investigated system.

For miscible/near-miscible multicomponent displacement processes, numerical dispersion has the effect of forcing the composition path away from the critical/near-critical key tie line and back into the two-phase region. Considerations similar to those applied to the investigation of the quaternary system can be applied to multicomponent systems. The results from the previous analysis suggest that the relative orientation of the dilution line and the lines connecting the critical tie line to the initial oil and the injection gas can be used as an indicator of the significance of sensitivity to numerical dispersion for a given system. The lines connecting the critical key tie line to the initial oil and the injection gas are referred to as critical lines.

To test this hypothesis the variations in recoveries predicted by coarse and fine grid (100/5000) FD simulations (from previously presented simulations) were compiled for the

near miscible displacement processes ($P \approx \text{MMP}$). The relative variations are plotted against the maximum angle between the critical lines and the dilution line in Figure 6.6.

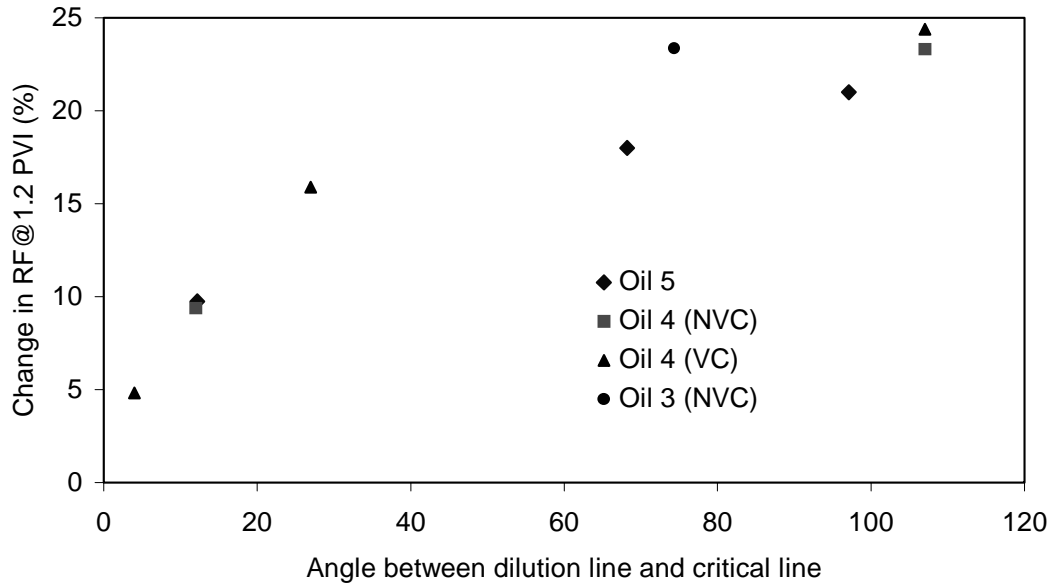


Figure 6.6: Sensitivity to numerical dispersion at the MMP vs. the maximum angle between the dilution line and the critical lines. The plot includes numerical simulations with and without volume change on mixing.

Some scatter is observed in Figure 6.6 but a general tendency is evident. As the orientation of the dilution line and the critical lines diverges the gas injection process becomes more sensitive to the presence of numerical dispersion. It is pointed out that the injection gases applied to displacement studies of this work range from pure injection gases (N_2 , CH_4 and CO_2) and artificial mixtures of these to realistic separator gases (Gas 3 and Gas 4).

Two methods can be used to obtain an indication of the sensitivity of a given system with respect to numerical dispersion. The sensitivity can be calculated directly by performing fine and coarse grid numerical simulations at the MMP and monitoring the variation of the predicted recovery. Alternatively, the orientation of the dilution line and the critical line can be determined from MMP calculations by the global approach where the approximated key tie lines are traced in the compositional space. This approach does not give a quantitative measurement of the dispersive effects but can be used to obtain a fast indication of the significance of numerical effects.

6.1 Results from Commercial Simulator E300

To investigate the potential of the new tool for prediction of dispersive effects on the calculation performed with commercial finite difference simulators, two numerical experiments were run for a 20 m slimtube on the compositional simulator Eclipse 300. The Oil 4 – Gas 6 and Oil 4 – N_2 systems were used in the numerical experiments since very different sensitivity to numerical dispersion is reported for the 1-D formulation of this work.

Numerical simulations with E300 involve a simultaneous solution of the mass conservation equations and the pressure equation. Different solution strategies can be used in E300. In this work the implicit pressure/explicit saturation (IMPES) approach for solving the flow problem was used. This selection is made because the full implicit approach is more dispersive than the IMPES approach. Details of the slimtube model are given in Appendix A.18. For the purpose of comparison, special care was taken to avoid a large build-up in pressure through the specification of a low injection velocity. The recovery curves for the model systems generated with E300 are given in Figure 6.7 and 6.8.

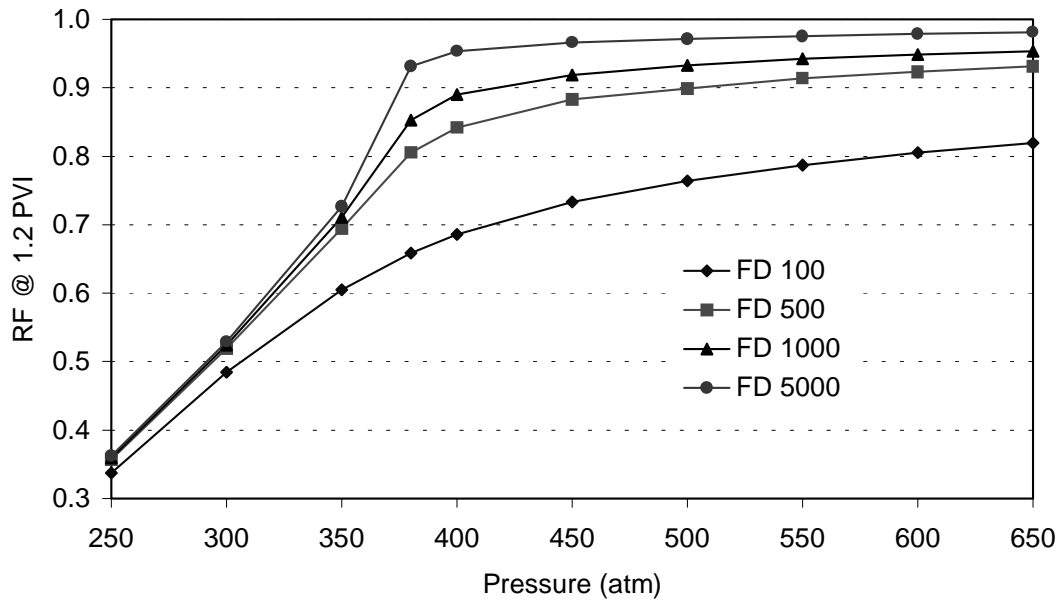


Figure 6.7: Comparison of recovery curves from E300 simulations for the displacement of Oil 4 by pure N_2 at 387.45 K. The E300 simulations were performed with 100, 500, 1000 and 5000 grid blocks and adaptive time step regulation.

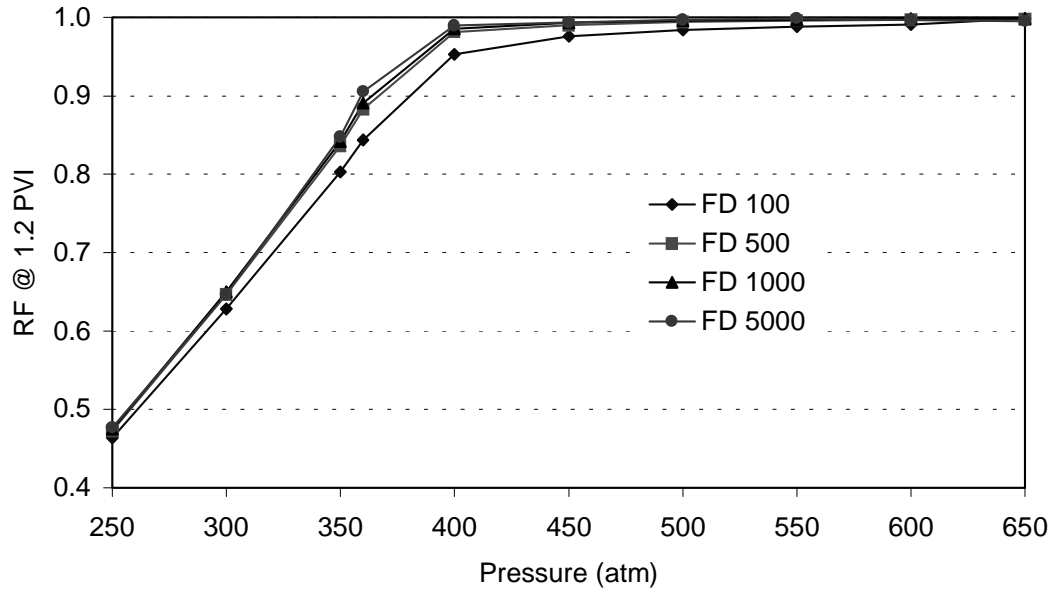


Figure 6.8: Comparison of recovery curves from E300 simulations for the displacement of Oil 4 by Gas 6 at 387.45 K. The E300 simulations were performed with 100, 500, 1000 and 5000 grid blocks and adaptive time step regulation.

It is seen from Figures 6.7 and 6.8 that the system specific sensitivity to numerical dispersion from E300 simulations is equivalent to the sensitivity reported in the preceding chapters. This result indicates that the new approach to prediction of system dependent sensitivity can be used as guidance for selection of a proper grid refinement, when E300 is used for simulation of 1-D displacements in a homogenous porous media. However, a more detailed analysis of the application is advised prior to further conclusions about this subject.

6.2 Summary

The analysis and examples given in this chapter verify the results presented by Walsh and Orr⁵¹. They demonstrated that the sensitivity of a given ternary system to the presence of numerical dispersion is related to the phase equilibrium of the specific system. The considerations of Walsh and Orr⁵¹ have been applied for systems with more than three components. Detailed analysis of the grid size effect on the recovery predictions for the displacement of a $\text{CH}_4 - \text{C}_4 - \text{C}_{10}$ system by pure N_2 and mixtures of N_2 and CH_4 is performed. The analysis, based on the geometrical structure of the true dispersion-free

solutions, shows that the sensitivity to the presence of numerical dispersion can be related to the relative orientation of the dilution line and the line connecting the initial oil to the critical tie line.

The predictive tool suggested from the analysis of the quaternary system is adopted for displacement processes where pure and multicomponent injection gases are used to displace real reservoir fluids. The quantitative variation in $RF_{1,2}$ predicted at the MMP by numerical simulations proves to correlate well with the maximum angle between the dilution line and the critical lines, connecting the initial oil and the injection gas to the critical tie line. Thus, the algorithm developed for prediction of the MMP can be used to indicate the grid size sensitivity of FD simulations for a given 1-D displacement process.

To compare the grid size effects observed from the FD simulations of the previous chapters and from a commercial simulator, two numerical slimtube experiments were made with Eclipse 300. The effect of the grid size used for the E300 simulations was found to be identical to what was observed for the FD simulators developed in the course of this work.

The similarity in grid size effects for the FD simulators of this work and E300 indicates that the new predictive tool can be used as guidance for selection of proper grid sizes when commercial simulators based on upstream weighting schemes are employed. However, it should be stressed that a more detailed comparison should be performed prior to further conclusions about the portability.

7. Conclusions and Suggestions for Future Work

The purpose of this work has been to develop efficient algorithms for the study of gas injection processes. The study and the development of such algorithms are qualified by time-consuming numerical simulators still being used worldwide in the design and development of miscible gas injection projects. Hence, there is room for improvements with respect to the computational expenses of such studies.

In this work, the analytical theory of 1-D gas injection processes has formed the basis of the study and the development of new efficient tools.

A new algorithm for prediction of the MMP has been developed. The algorithm is based on the intersecting tie line approach emanating from the 1-D analytical theory. The new approach allows prediction of the MMP for gas injection processes using any number of components for representing the phase equilibrium of the gas/oil system. The algorithm has been tested on a number of different gas/oil systems for which the corresponding finite difference simulations were available in the literature. Most of the reported systems are bubble-point systems but also a few gas condensates have been tested. Excellent agreement between reported values of the MMP and the values predicted by the global algorithm is found in all cases. For all the systems tested, where multicomponent separator gases are injected into a reservoir fluid, the mechanism controlling the development of miscibility is shown to be of a combined vaporizing/condensing nature. The application of simplified algorithms, like the single-cell approaches, to such systems must therefore be expected to overpredict the MMP.

Up to now systems with a maximum of 15 components in the oil description and 15 components in the injected gas have been investigated. The average time consumption for the MMP calculations is around a few seconds. Thus, the new algorithm is superior to any general approaches previously presented for prediction of the MMP, as regards the required CPU time.

Due to the modest CPU time consumption, the new algorithm is a powerful tool for reservoir engineers working with the design of gas injection projects. Two case studies are presented to indicate some fields of application.

The effects of tuning and lumping on the predicted MMP for a realistic reservoir fluid are investigated. The predicted MMP is found to be insensitive to the parameters used for tuning the fluid description of the given system to experimental swelling test data. The lumping study shows that the MMP predictions are also insensitive to the number of components in the fluid description as long as four or more components are used. This result agrees well with the fact that four or more components are needed in order to represent a combined vaporizing/condensing gas drive. In a second study, the algorithm was applied to determination of the optimal mixture of two available injection gases. In the first enrichment study the MMP was found to be a monotonous function of the enrichment factor. In a second study where a new solvent gas was considered a strongly non-monotonous behavior was found. The two cases show the need for more than a few points on the MMP vs. E curve and hence the need for an effective MMP algorithm.

Based on the global formulation of the intersecting tie line approach, developed in the course of Chapter 3, a new method for constructing approximate analytical solutions to the 1-D gas injection process has been developed and implemented. The basis of the new method is that the path in the compositional space defining a 1-D displacement process is bound to travel through a sequence of key tie lines. In general these key tie lines are approximated very accurately by the intersection approach.

The new method is initially developed for a simplified version of the conservation equations where components take up constant volumes during the displacement process (NVC). It is demonstrated how approximate solutions can be generated efficiently by assuming that all key tie lines are connected shocks. This is done by solving the shock balance equations for each adjacent pair of tie lines up- and downstream, starting at a primary key tie line. Proof is given that a primary tie line exists and that the primary tie line must be the shortest of the key tie lines. For oil/gas systems where all key tie lines are in fact connected by shocks (self-sharpening systems) the approximate solutions are rigorously correct. For systems with nontie

line rarefactions, a detailed comparison with fine and coarse grid finite difference (FD) simulations shows that the pure shock solution offers a far more refined approximation than a coarse grid FD simulation. The computation time required for construction of fully self-sharpening solutions is proved to be orders of magnitude lower than for the corresponding coarse grid numerical simulations.

A tool has been developed for prediction of nontie line rarefactions in 1-D analytical solutions. The tool, referred to as the fanning rule, utilizes the geometrical orientation of the key tie lines to predict the existence of nontie line rarefactions. The fanning rule allows construction of far more refined approximate solutions for systems with nontie line rarefactions. The refined approximations are obtained by combining the shock constructions with integration of predicted nontie line paths. It is shown that not all nontie line rarefactions predicted by the fanning rule are of significant importance to the quality of the approximate solutions, and a method for discarding insignificant rarefactions is presented.

Solution construction tools from the NVC algorithm have been used in the development of an algorithm taking volume change on mixing (VC) into account. The VC algorithm is used for construction of pure shock solutions to the general formulation of the 1-D displacement problem. The qualities of the approximations generated by the VC algorithm can be monitored by applying the fanning rule and subsequently checking for significant nontie line rarefactions. As for the NVC algorithm, the VC shock solutions prove to be far more accurate approximations than coarse grid FD simulations for oil/gas systems with significant nontie line rarefactions.

Both algorithms are used for generating recovery curves for the true dispersion-free displacement process. The recovery curves are compared with corresponding fine and coarse grid FD simulations. The comparison shows that the predicted recovery, for some oil/gas systems, is very sensitivity to the presence of numerical dispersion.

On the basis of this observation a method for obtaining a qualitative estimate of the system specific sensitivity to numerical dispersion has been proposed. The method is based on a

geometrical interpretation of the dispersion-free solution paths for quaternary systems, and it is shown to correlate the sensitivities of the gas/oil systems investigated in this work well.

The grid size effect observed for the FD simulators of this work has been compared with that of the commercial simulator Eclipse 300. Similarities in the observed grid size effects indicate that the proposed method can be used as guidance for selection of a proper grid size when commercial simulators with simple upstream weighting schemes are used. It is stressed that this analysis is based on displacements in homogeneous porous media. Thus, further investigation of this matter is needed prior to further conclusions on the portability.

Suggestions for future work:

An evident extension of the current work is to incorporate integration of nonline rarefactions in the VC algorithm in order to obtain more accurate approximations for systems with such rarefactions.

In equivalence with the lumping study performed with the MMP algorithm it could be interesting to investigate the sensitivity of predicted recovery factors with respect to the number of components used in a fluid description.

In this work the 1-D algorithms have been used for calculation of dispersion-free recovery of the OOIP. It is a well-known fact that some of the heavy ends, produced from an oil reservoir, can cause problems in the downstream processing facilities. Thus, it could be interesting to investigate the possibility of designing a component selective gas drive. This would include a study of the interactions between the injection gas composition and the composition of the produced fluids. Such a study can start at a low scale, e.g. by the use of 1-D modeling.

Finally, a study of 1-D gas injection problems with non-uniform initial data should be initiated.

8. Nomenclature

$\underline{\underline{A}}$	Coefficient matrix
$\underline{\underline{B}}$	Coefficient matrix
C_i	Overall molar concentration of component j
d	Length of a tie line
E	Enrichment factor
f	Fractional flow of vapor
f_j	Fractional flow of phase j
F_i	Overall flux of component i
G_i	Overall volume fraction of component i
g_{ij}	Volume fraction of component i in phase j
$\underline{\underline{I}}$	Unit matrix
$\underline{\underline{J}}$	Jacobian matrix
k_{ij}	Binary interaction parameter (EOS)
k_{rj}	Relative permeability of phase j
k_{rle}	Effective relative permeability of liquid
k_{rve}	Effective relative permeability of vapor
K_i	Equilibrium constant of component i
L	Length
M_w	Molecular weight
nc	Number of components
p	Pressure
P	Pressure
P_c	Critical pressure
P_{sat}	Saturation pressure
Q_i	Overall fractional flow of component i
S	Saturation of vapor
S_j	Saturation of phase j
S_{or}	Residual oil saturation
t	Time
T	Temperature
T_c	Critical temperature
v	Convective velocity
v_d	Dimensionless velocity
x	Distance
x_{ij}	Mole fraction of component i in phase j
x_i	Mole fraction of component i in liquid phase
y_i	Mole fraction of component i in vapor phase
$\underline{\underline{X}}$	Eigenvector (VC)
$\underline{\underline{Y}}$	Eigenvector (NVC)
z	Dimensionless distance
z_{eos}	Compressibility factor
z_i	Mole fraction of component i
Z_i	Mole fraction of component i

Greek letters:

β	Mole fraction of vapor
$\underline{\Delta}$	Correction vector
Δz	Size of grid block
Δt	Size of time step
ε	Step size in nontie line integration
ϕ	Porosity
η	Similarity variable (z/τ)
λ	Eigenvalue
Λ	Shock velocity
μ	Viscosity
μ_r	Viscosity ratio (vapor/liquid)
θ	Fictitious vapor saturation
ρ_j	Molar density of phase j
ρ_{ci}	Molar density of pure component i
ρ_j^{ideal}	Molar density of phase j (ideal mixing)
$\rho_{m,j}$	Mass density of phase j
τ	Dimensionless time (PVI)
ω	Acentric factor
φ	Fugacity coefficient
ψ	Parameter along envelope curve

Abbreviations:

CGD	Condensing gas drive
EOS	Equation of state
FD	Finite difference
MC	Multicell
MMP	Minimum miscibility pressure
MOC	Method of characteristics
NVC	No volume change
OOIP	Original oil in place
PR	Peng-Robinson
RF _{1.2}	Recovery factor at 1.2 PVI
PVI	Pore volumes injected
SRK	Soave-Redlich-Kwong
VC	Volume change
VGD	Vaporizing gas drive

9. Bibliography

1. Aris, R. and Amundson, N.R., "Some Remarks on Longitudinal Mixing or Diffusion in Fixed Beds", *AIChE J.*, 1975(3) p280.
2. Batycky, R.P., Thiele, M.R. and Blunt, M.J., "A Streamline Simulator to Model Field Scale 3-D Flow", *Proc. Fifth Euro. Conf. on the Mathematics of Oil Recovery*, Leoben, Austria, 1996.
3. Blunt, M.J., Liu, K. and Thiele, M.R., "A Generalized Streamline Method to Predict Reservoir Flow", *Proc. Eighth Euro. Symp. on Improved Oil Recovery*, Vienna, Austria, 1995.
4. Buckley, S.E. and Leverett, M.C., "Mechanism of Fluid Displacements in Sands", *Trans. AIME* (1941) 249, 107-116.
5. Clark, N.J., Schultz, W.P. and Shearin, H.M., "Condensing Gas Drive, Critical Displacement Process -- New Injection Method Affords Total Oil Recovery", *Pet. Eng.* (October 1958) 28, b-45.
6. Courant, R. And Hilbert, D., "Methods of Mathematical Physics", Vol. 2. Partial Differential Equations, Wiley-Interscience, New York, NY 1962.
7. Dindoruk, B., "Analytical Theory of Multiphase Multicomponent Displacement in Porous Media", Ph.D. Thesis, Department of Petroleum Engineering, University of Stanford, California 1992.
8. Dindoruk, B., Orr, F.M., Jr. and Johns, R.T., "Theory of Multicontact Miscible Displacement with Nitrogen", *SPEJ*, (1997) 2, No.3, 268-279.
9. Dumoré, J.M., Hagoort, J. and Risseuw, A.S., "An Analytical Model for One-Dimensional, Three-Component Condensing and Vaporizing Gas Drives" *SPE J.* April 1984, 24, p.169-179.
10. Eakin, E and Mitch, F.J., "Measurement and Correlation of Miscibility Pressures of Reservoir Oils", *SPE* 18065.
11. Firoozabadi, A. and Aziz, K., "Analysis and Correlation of Nitrogen and Lean-Gas Miscibility Pressure", *SPE* 13669.
12. Glasø, Ø., "Generalized Minimum Miscibility Pressure Correlation", *SPE* 12893
13. Harmon, R.A. and Grigg, R.B., "Vapor density Measurements for Estimating Minimum Miscibility Pressure", *SPE* 15403.
14. Helfferich, F.G., "Theory of Multicomponent, Multiphase Displacement in Porous Media", *SPEJ* (Feb. 1981) 51-62.

15. Helfferich, F.G., "Generalized Welge Construction for Two-Phase in Porous Media with Limited Miscibility", SPE 9730, Presented at 1982 ATCE, SPE, New Orleans, US.
16. Høier L., "Miscibility Variations in Compositionally Grading Petroleum Reservoirs", Ph.D. Thesis, NTNU, Trondheim, 1997.
17. Jensen, F. and Michelsen, M.L., "Calculation of First Contact and Multiple Contact Minimum Miscibility Pressures", *In Situ*, 14(1) 1-17, 1990.
18. Jessen, K., Michelsen M.L. and Stenby, E.H., "Global Approach for Calculation of Minimum Miscibility Pressure", *Fluid Phase Equilibria* (153) 1998, 251-263.
19. Jessen, K., Michelsen, M.L. and Stenby, E.H., "Effective Algorithm for Calculation of Minimum Miscibility Pressure", SPE 50632, Presented at 1998 SPE European Petroleum Conference, Hague, The Netherlands, 20–22 October 1998.
20. Jessen, K., Wang, Y., Ermakov, P., Zhu, J. and Orr, F.M. "Fast, Approximate Solutions for 1-D Multicomponent Gas Injection Problems", SPE 56608, Presented at 1999 ATCE, SPE, Houston, Texas.
21. Johansen, T., Dindoruk, B. and Orr, F.M., Jr. "Global Triangular Structure in Four-Component Conservation Laws", *Proc. Fourth Euro. Conf. on the Mathematics of Oil Recovery*, Roros, Norway, 1994.
22. Johns, R.T., Dindoruk, B. and Orr, F.M., Jr. "Analytical Theory of Combined Condensing/Vaporizing Gas Drives", *SPE Adv. Tech. Ser.* (1993) 2, No. 3, 7-16.
23. Johns, R.T. and Orr, F.M., Jr. "Miscible Gas Displacement of Multicomponent Oils", *SPEJ*, (1996) 1, No.1, 39-50.
24. Johns R.T., "Analytical Theory of Multicomponent Gas Drives with Two-Phase Mass Transfer", Ph.D. Thesis, Department of Petroleum Engineering, University of Stanford, California 1992.
25. Kovarik, F.S. "A Minimum Miscibility Pressure Study Using Impure CO₂ and West Texas Oil Systems; Data Base, Correlation's and Compositional Simulations", SPE 14689.
26. Lantz, R.B. "Quantitative Evaluation of Numerical Dispersion (Truncation Error)", *Soc. Pet. Eng. J.* 1971 (11) p.315.
27. Lax, P.D. "Hyperbolic Conservation Laws II", *Communications on Pure and Applied Mathematics*, 1957, 10, p.537-566.
28. Lax, P.D. "Contributions to Nonlinear Functional Analysis", Academic Press, New York (1971) 603-634.

-
29. Larson, R.G. and Hirasaki, G.J. "Analysis of the Physical Mechanisms in Surfactant Flooding", Soc. Pet. Eng. J. (Feb. 1978) p.42-58.
 30. Leibovici, C. F., "A Consistent Procedure for the Estimation of Properties Associated to Lumping Studies", Fluid Phase Equilibria, 87(2), 189-197, 1993.
 31. Lohrenz, J., Bray, B.G. and Clark, C.R. "Calculating Viscosities of Reservoir Fluids from Their Compositions", J. Pet. Technol., Oct. 1964, 1171-1176.
 32. Lim, T.M., Pope, G.A., Sepehrnoori, K. and Soni, Y., "Grid Refinement Study of a Hydrocarbon Miscible Gas Injection Reservoir", SPE 38060.
 33. Metcalfe R.S., Fussell, D.D. and Shelton, J.L., "A Multicell Equilibrium Separation Model for the Study on Multiple Contact Miscibility in Rich-Gas Drives", Soc. Pet. Eng. J. (June 1973) p. 147-155.
 34. Michelsen M.L., "Calculation of phase envelopes and critical points for multicomponent mixtures", Fluid Phase Equilibria, 4, 1-10, 1980.
 35. Michelsen M.L., "Speeding up the Two-Phase PT-Flash, with Application for Calculation of Miscible Displacements," Fluid Phase Equilibria 143 (1998), 1-12.
 36. Monroe, W.W., Silva, M.K., Larsen, L.L. and Orr, F.M., Jr.: "Composition Paths in Four-Component Systems: Effect of Dissolved Methane on 1 -D CO₂ Flood Performance", SPE Res. Eng., (1990) 5, 423-432.
 37. Montell, F. and Gouel, P.L., "A New Lumping Scheme of Analytical Data for Compositional Studies", SPE 13119 paper presented at the 56th Annual Technical Conference and Exhibition, Houston, TX, 1984.
 38. Orr, F.M., Jr., Dindoruk, B. and Johns, R.T., "Theory of Multicomponent Gas/Oil Displacement", Ind. Eng. Chem. Res. 1995 (34) 2661-2669.
 39. Pedersen, K.S., Fredenslund, A.A. and Thomassen P., "Properties of Oils and Natural Gases", Contributions in Petroleum Geology and Engineering, vol. 5, Gulf Publishing Company, Houston, Texas. 1989.
 40. Peng, D.Y. and Robinson, D.B., "A New Two-Constant Equation of State", Ind. Chem. Eng. Fundam., 15(1979), 59-64.
 41. Sebastian, H.M., Wegner, R.S. and Renner, T.A. "Correlation of Minimum Miscibility Pressure for Impure CO₂ Streams", SPE 12648.
 42. Slobod, R.L. and Koch, H.A. Jr., "Which to use -- I-Type or M-Type -- in High Pressure Gas Injection?", Oil and Gas J. (April 1953) 51, p.85-117.
 43. Soave, G., "Equilibrium Constants from a Modified Redlich-Kwong Equation of State", Chem. Eng. Sci., 27 (1972) 1197-1203.

-
44. Stalkup, F.I., "Displacement Behavior of the Condensing/Vaporizing Gas Drive Process", SPE 16715, 1987.
 45. Stalkup, F.I., "Effects of Gas Enrichment and Numerical Dispersion on Enriched-Gas-Drive Predictions", SPE 18060.
 46. Stalkup F.I., Lo, L.L. and Dean, R.H., "Sensitivity to Gridding of Miscible Flood Predictions Made With Upstream Differenced Simulators", SPE 20178.
 47. Stalkup, F.I., "Miscible Displacement", Monograph volume 8, Henry L. Doherty Series, Society of Petroleum Engineers of AIME, Dallas 1984.
 48. Thiele, M.R., Blunt, M.J. and Orr, F.M., Jr., "Predicting Multicomponent, Multiphase Flow in Heterogeneous Systems Using Streamtubes", Proc. Fourth Euro. Conf. on the Mathematics of Oil Recovery, Roros, Norway, 1994.
 49. Thiele, M.R., Blunt, M.J. and Orr, F.M., Jr. "A New Technique for Predicting Flow in Heterogeneous Systems Using Streamtubes", paper SPE/DOE 27834 presented at the 1994 SPE /DOE Symposium on Improved Oil Recovery, Tulsa, OK.
 50. Thiele, M.R., Batycky, R.P., and Blunt, M.J., "A Streamline-based 3-D Field-Scale Compositional Reservoir Simulator", SPE 38889, presented at the 1997 SPE Annual Conference and Exhibition, San Antonio, Oct. 5-8, 1997.
 51. Walsh, B.W. and Orr, F.M. Jr., "Prediction of Miscible Flood Performance: The Effect of Dispersion on Composition Paths in Ternary Systems", IN SITU (1990) 14, pp.19-47.
 52. Wang, Y. and Orr, F.M. Jr., "Analytical Calculation of Minimum Miscibility Pressure", Fluid Phase Equilibria, 139 (1997) 101-124.
 53. Wang, Y. and Orr, F.M. Jr., "Calculation of Minimum Miscibility Pressure", SPE, Stanford University, SPE 39683, 1998.
 54. Wang Y., "Analytical Calculation of Minimum Miscibility Pressure", Ph.D. Thesis, Department of Petroleum Engineering, University of Stanford, California 1998.
 55. Welge, H.J., "A simplified Method for Computation Oil Recovery by Gas or Water Drive", Trans. AIME (1952) 195, p.91-98.
 56. Whitson, C.H. and Michelsen, M.L., "The Negative Flash", Fluid Phase Equilibria (53), 1989, p51-72.
 57. Yelling, W.F. and Metcalfe, R.S., "Determination and Prediction of CO₂ Minimum Miscibility Pressures", J. Pet. Tech. (January 1980), p.160-168.
 58. Zick, A.A., "A combined Condensing/Vaporizing Mechanism in the displacement of Oil by Enriched Gases", SPE 15493, 1-11, 1986 .

10. Appendix

A.1 Critical Properties of Oil 3

-	$T_c(K)$	$P_c(atm)$	ω	$M_w (g/mol)$	$k_{CH_4,j}$	$K_{N_2,j}$	$k_{CO_2,j}$
CH ₄	190.6	45.44	0.0115	16.04	0	0.025	0.105
N ₂	126.3	33.55	0.045	28.01	0.025	0	0
CO ₂	304.2	72.84	0.231	44.01	0.105	0	0
C ₂	305.4	48.16	0.0908	30.07	0	0.01	0.13
C ₃	369.8	41.94	0.1454	44.1	0	0.09	0.125
i-C ₄	408.1	36.00	0.1756	58.12	0	0.095	0.12
n-C ₄	425.2	37.47	0.1928	58.12	0	0.095	0.115
i-C ₅	460.4	33.37	0.2273	72.15	0	0.1	0.115
n-C ₅	469.7	33.25	0.251	72.15	0	0.11	0.115
C ₆	507.4	29.73	0.2957	86.18	0	0.11	0.115
C ₇₊₍₁₎	563.2	31.36	0.2753	117.98	0.02	0.11	0.115
C ₇₊₍₂₎	638.3	25.84	0.3761	180.12	0.028	0.11	0.115
C ₇₊₍₃₎	736.5	19.38	0.5552	250.66	0.04	0.11	0.115
C ₇₊₍₄₎	837	14.33	0.8021	346.62	0.052	0.11	0.115
C ₇₊₍₅₎	936.9	10.92	1.108	547.83	0.064	0.11	0.115

Table A3.1: Critical properties and non-zero interaction parameters for Oil 3.

The data from Høier¹⁶ is for Peng-Robinson EOS.

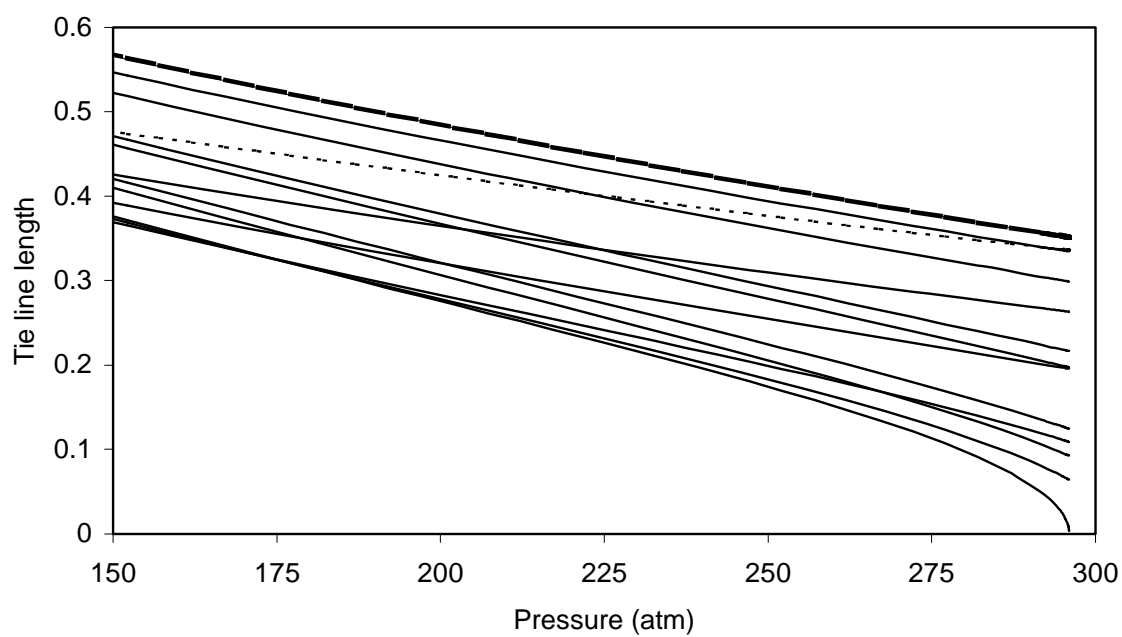
A.2 Calculation Results from Displacement of Oil 3 by Gas 5

Figure A3.2: Simulation results for Oil 3 displaced by Gas 5. The 8th crossover tie line becomes critical at 296 atm (MMP). Injection and initial tie lines are plotted as dotted and broken lines respectively.

A.3 Finite Difference (FD) Simulation

This appendix describes the finite difference formulation of the conservation equations used to verify the semi-analytical solutions presented in this work. Two different FD simulators have been employed to verify the NVC and the VC solutions generated by the MOC. Both are based on the fully explicit one-point upstream weighting approach. In a FD simulation a discretised version of the conservation equations is solved. The space and the time dimension are divided into N_g grid blocks and N_t time steps respectively. The conservation equations are rewritten in terms of difference quotients rather than true derivatives. Recalling that the NVC formulation of the conservation equations assume the form

$$\frac{\partial G_i}{\partial \tau} + \frac{\partial Q_i}{\partial z} = 0 \quad , \quad i = 1, \dots, nc - 1 \quad (\text{A4.1})$$

the corresponding FD formulation used in this work is given by

$$G_{i,n}^{t+1} = G_{i,n}^t - \frac{\Delta \tau}{\Delta z} (Q_{i,n}^t - Q_{i,n-1}^t) \quad , \quad i = 1, \dots, nc - 1 \quad (\text{A4.2})$$

where n is the grid block and t is the time step. In the NVC formulation Eq. A4.2 can be applied directly to generation of approximate solutions to the 1-D problem. This is due to the inherited volume conversion of the NVC formulation.

A more complex formulation must be used for the VC formulation of the conservation equations:

$$\frac{\partial C_i}{\partial \tau} + \frac{\partial F_i}{\partial z} = 0 \quad , \quad i = 1, \dots, nc \quad (\text{A4.3})$$

Special care must be taken to ensure that both mass and volume are conserved for each grid block. A discretised version of Eq. A4.3 can be written as

$$C_{i,n}^{t+1} = C_{i,n}^t - (v_{d,n}^t F_{i,n}^t - v_{d,n-1}^t F_{i,n-1}^t) \quad , \quad i = 1, \dots, nc \quad (\text{A4.4})$$

where

$$F_i = \sum_{j=1}^2 x_{ij} \rho_j f_j \quad (\text{A4.5})$$

The extra complexity entering the FD solution strategy is a result of letting the components change volume as they transfer between the flowing phases. This results in variable overall

convective velocity. The overall velocity in a given grid block n at time step t can be written as

$$v_{d,n}^t = \frac{\sum_{i=1}^{nc} G_{i,n}^t - \rho + v_{d,n-1}^t \frac{\Delta \tau}{\Delta z} \sum_{i=1}^{nc} F_{i,n-1}^t}{\frac{\Delta \tau}{\Delta z} \sum_{i=1}^{nc} F_{i,n}^t} \quad (\text{A4.6})$$

where

$$\rho = \left(\frac{\beta}{\rho_v} + \frac{1-\beta}{\rho_l} \right)^{-1} \quad (\text{A4.7})$$

β is the mole fraction of vapor in the grid block while ρ_v and ρ_l are the vapor and liquid phase densities respectively. Comparison of Eqs. A4.4 and A4.6 makes it clear that an inner iterative loop must be used. Dindoruk⁷ suggests an iterative scheme using the density as independent variable in the inner loop. The algorithm for solving and updating G in grid block n to time step $t+1$ is:

1. Evaluate $v_{d,n}^t$ from Eq. A4.6
2. Calculate $G_{i,n}^{t+1}$ by Eq. A4.4
3. Calculate the overall mole fractions by

$$Z_{i,n}^{t+1} = \frac{G_{i,n}^{t+1}}{\sum_{i=1}^{nc} G_{i,n}^{t+1}} \quad (\text{A4.8})$$

4. Calculate ρ based on $Z_{i,n}^{t+1}$ and evaluate the mass error by

$$\varepsilon = 1 - \frac{\sum_{i=1}^{nc} G_{i,n}^{t+1}}{\rho} \quad (\text{A4.9})$$

If the mass error ε is greater than a tolerance (10^{-2} - 10^{-4}), return to step 2 using the new density. Otherwise move to the next grid block and start with step 1.

When fully explicit formulations are used, in general, special care must be taken to ensure stability of the simulation. The simulation will be stable if sufficiently small time steps are applied in comparison with the space step. In this work a Courant number of 10 ($\Delta z / \Delta \tau$) was used and no instability was encountered.

A.4 Determination of Normal Vectors in Multidimensional Space

The problem of locating the normal vector to the plane spanned by two intersecting vectors \underline{a} and \underline{b} becomes an important issue, when the equal eigenvalue point is sought at which a solution path switches from a tie line path to a nontie line path. In the multidimensional space ($m > 3$) the normal vector \underline{n} to a given hyperplane may not be given uniquely. However, it is possible to locate a normal vector by posing an optimization problem. The normal vector \underline{n} must be perpendicular to the vectors \underline{a} and \underline{b} simultaneously. Hence, an objective function $F(\underline{n})$ can be defined by

$$F(\underline{n}) = (\underline{n} \bullet \underline{a})^2 + (\underline{n} \bullet \underline{b})^2 \quad \text{A.4.10}$$

$F(\underline{n})$ will be positive or zero for all values of \underline{n} . At the solution the derivatives of F with respect to the elements of \underline{n} must be zero. This requirement can be written as

$$\nabla F(\underline{n}_0) = \underline{0} \quad \text{A.4.11}$$

where \underline{n}_0 is the solution. The elements of the gradient vector are given by

$$\frac{\partial F}{\partial n_i} = 2(\underline{n} \bullet \underline{a})a_i + 2(\underline{n} \bullet \underline{b})b_i = 0, \quad i = 1, \dots, m \quad \text{A.4.12}$$

Given an initial estimate of the normal vector the solution to A.4.12 can be generated by using the steepest descent approach or a combination of the steepest descent approach and a Newton iteration. The Jacobian matrix required for the Newton iteration is given by

$$H_{ij} = \frac{\partial G_i}{\partial n_j} = 2(a_i a_j + b_i b_j) \quad \begin{cases} i = 1, \dots, m \\ j = 1, \dots, m \end{cases} \quad \text{A.4.13}$$

The steepest descent approach may exhibit slow convergence near the solution. In such cases a switch to a full Newton iteration will speed up the convergence.

A.5 Details of 1-D Shock Solution Given in Figure 4.8

Oil 4 displaced by pure N₂ at 275 atm and 387.45 K .

Tie line	μ_v/μ_l	ρ_v/ρ_l	$\ln(K_{nc})$	S	λ
Oil	-	-	-	0	1.9981- ∞
1*	1.252	0.1719	-5.8034	0.328	1.9981
1*	1.252	0.1719	-5.8034	0.394	1.3085
2	1.412	0.0565	-12.8906	0.706	1.3085-1.1639
3	1.412	0.0556	-13.0025	0.825	1.1639-1.0953
4	1.449	0.0492	-13.7463	0.826	1.0953-1.0245
5	1.510	0.0426	-14.4138	0.834	1.0245-0.9116
6	1.518	0.0418	-14.4895	0.845	0.9116-0.8189
7	1.558	0.0388	-14.7522	0.846	0.8189-0.7657
8	1.571	0.0378	-14.8221	0.852	0.7657-0.6486
9	1.596	0.0360	-14.9429	0.854	0.6486-0.6109
10	1.634	0.0336	-15.0917	0.858	0.6109-0.4610
11	1.899	0.0241	-15.3741	0.864	0.4610-0.1559
12	2.162	0.0181	-15.5495	0.900	0.1559-0.0643
13	2.468	0.0136	-15.6557	0.930	0.0643-0.0146
14	2.753	0.0109	-15.6793	0.951	0.0146-0.0073
14	2.753	0.0109	-15.6793	0.958	0.0073-0.0071
Gas	-	-	-	1	0.0071-0

*Primary tie line

A.6 Details of 1-D Shock Solution Given in Figure 4.9

Oil 4 displaced by 85 % CH₄ and 15 % N₂ at 275 atm and 387.45 K.

Tie line	μ_v/μ_l	ρ_v/ρ_l	$\ln(K_{nc})$	S	λ
Oil	-	-	-	0	1.998069- ∞
1*	1.2515	0.1719	-5.8035	0.3282	1.998069
1*	1.2515	0.1719	-5.8035	0.3802	1.435455
2	1.2886	0.1316	-7.1043	0.5366	1.435455-1.358416
2	1.2886	0.1316	-7.1043	0.6057	1.358416-1.19363
3	1.2912	0.1264	-7.2401	0.6116	1.19363-1.099905
4	1.3371	0.0961	-8.316	0.6585	1.099905-0.977401
5	1.3985	0.073	-9.3087	0.6983	0.977401-0.894986
6	1.4073	0.0705	-9.4277	0.7031	0.894986-0.844431
7	1.4429	0.062	-9.8311	0.7204	0.844431-0.752449
8	1.4552	0.0595	-9.9518	0.7263	0.752449-0.720468
9	1.4776	0.0553	-10.1517	0.7363	0.720468-0.606363
10	1.5126	0.0494	-10.4282	0.7528	0.606363-0.301007
11	1.7306	0.0306	-11.0763	0.8258	0.301007-0.173708
12	1.9685	0.02	-11.4886	0.8828	0.173708-0.052804
13	2.265	0.0132	-11.7138	0.9332	0.052804-0.008837
14	2.533	0.0099	-11.7649	0.9546	0.008837-0.006165
14	2.533	0.0099	-11.7649	1	0.006165-0
Gas	-	-	-	1	0

* Primary tie line

A.7 Details of 1-D Shock Solution Given in Figure 4.10

Oil 4 displaced by pure CH₄ at 275 atm and 387.45 K.

Tie line	μ_v/μ_l	ρ_v/ρ_l	$\ln(K_{nc})$	S	λ
Oil				0	1.997204- ∞
1*	1.2515	0.1719	-5.8035	0.320545	1.997204-1.451519
1*	1.2515	0.1719	-5.8035	0.38219	1.451519
1*	1.2515	0.1719	-5.8035	0.407213	1.221407
2	1.2463	0.1784	-5.6367	0.468295	1.221407-1.121263
3	1.2504	0.1695	-5.7932	0.592126	1.121263-0.998271
4	1.3052	0.1195	-7.0479	0.654817	0.998271-0.918956
5	1.371	0.0859	-8.168	0.66166	0.918956-0.869465
6	1.3801	0.0824	-8.3012	0.684889	0.869465-0.78352
7	1.4163	0.0711	-8.7493	0.692614	0.78352-0.752922
8	1.4289	0.0678	-8.887	0.705237	0.752922-0.647447
9	1.4513	0.0625	-9.1098	0.725571	0.647447-0.348221
10	1.4866	0.055	-9.4249	0.809849	0.348221-0.21444
11	1.6994	0.0326	-10.1983	0.872709	0.21444-0.072124
12	1.9324	0.0206	-10.6905	0.928577	0.072124-0.011485
13	2.2262	0.0132	-10.9592	0.955598	0.011485-0.006735
14	2.4913	0.0098	-11.0198	1	0.006735-0
Gas				1	0

*Primary tie line

A.8 Details of 1-D shock solution given in Figure 4.11

Oil 3 displaced by pure N₂ at 300 atm and 368.15 K

Tie line	μ_v/μ_l	ρ_v/ρ_l	$\ln(K_{nc})$	S	λ	
Oil	-	-	-	0	2.699345	∞
1*	1.5336	0.0345	-7.0682	0.188954	2.699345	
1*	1.5336	0.0345	-7.0682	0.236395	1.645552	
2	1.7956	0.0103	-13.9089	0.522951	1.645552	1.324804
3	1.7967	0.0103	-13.9354	0.52341	1.324804	1.112373
4	1.8607	0.009	-14.6603	0.540709	1.112373	0.804747
5	1.9319	0.0081	-15.1031	0.556146	0.804747	0.627263
6	1.9475	0.0079	-15.1771	0.559626	0.627263	0.5515
7	1.9944	0.0075	-15.3571	0.569135	0.5515	0.401119
8	2.0141	0.0073	-15.4145	0.573485	0.401119	0.357466
9	2.0476	0.007	-15.4991	0.580628	0.357466	0.22948
10	2.096	0.0066	-15.5861	0.592401	0.22948	0.124802
11	2.2367	0.0059	-15.7116	0.621861	0.124802	0.036671
12	2.5885	0.0047	-15.8099	0.698649	0.036671	0.004686
13	3.1524	0.0036	-15.8307	0.816858	0.004686	0.000269
14	3.8868	0.0027	-15.8322	0.86623	0.000269	0.000123
14	3.8868	0.0027	-15.8322	1	0.000123	0
Gas	-	-	-	1	0	

* Primary tie line

A.9 Details of 1-D shock solution given in Figure 4.14

Oil 4 displaced by pure CO₂ at 200 atm and 387.45 K

Tie line	μ_v/μ_l	ρ_v/ρ_l	$\ln(K_{nc})$	S	λ
Oil				0.162	3.82995- ∞
1	1.1876	0.0898	-8.8985	0.118505	3.82955-1.290996
2	1.1872	0.0911	-8.8073	0.1207	1.290996-1.160407
3*	1.1697	0.374	-3.4055	0.494162	1.160407
3*	1.1697	0.374	-3.4055	0.505332	1.075567
4	1.2443	0.2559	-4.7199	0.706924	1.075567-1.014097
5	1.3274	0.1732	-6.039	0.77145	1.014097-0.97409
6	1.3388	0.1648	-6.2032	0.777803	0.97409-0.948706
7	1.3817	0.138	-6.7605	0.798177	0.948706-0.903057
8	1.3971	0.1298	-6.9443	0.804838	0.903057-0.885855
9	1.423	0.1176	-7.2305	0.814958	0.885855-0.824143
10	1.4644	0.1008	-7.6499	0.830545	0.824143-0.596932
11	1.7002	0.0537	-8.7853	0.888074	0.596932-0.44394
12	1.9442	0.0324	-9.4503	0.925601	0.44394-0.204687
13	2.2434	0.0203	-9.8023	0.958171	0.204687-0.044935
14	2.5137	0.0147	-9.8805	0.975927	0.044935-0.025028
14	2.5137	0.0147	-9.8805	1	0.025028-0
Gas				1	0

* Primary tie line

A.10 Details of 1-D Shock Solution Given in Figure 4.21

Oil 3 displaced by Gas 3 at 300 atm and 368.15 K.

Tie line	μ_v/μ_l	ρ_v/ρ_l	$\ln(K_{nc})$	S	λ	
Oil	-	-	-	0	2.698707	∞
1	1.5336	0.0345	-7.0682	0.185131	2.698707	1.918674
2	1.5279	0.0356	-6.953	0.223645	1.918674	
2	1.5279	0.0356	-6.953	0.237154	1.397001	
3*	1.5269	0.0358	-6.9359	0.254620	1.397001	
3*	1.5269	0.0358	-6.9359	0.265874	1.243583	
4	1.5532	0.0318	-7.2519	0.344670	1.243583	1.045402
5	1.6134	0.0252	-7.833	0.411902	1.045402	0.931771
6	1.6162	0.025	-7.8571	0.414345	0.931771	0.866988
7	1.6543	0.022	-8.1502	0.443566	0.866988	0.756791
8	1.6656	0.0212	-8.2285	0.451864	0.756791	0.719709
9	1.6931	0.0195	-8.4042	0.470195	0.719709	0.597189
10	1.7264	0.0177	-8.5889	0.492049	0.597189	0.415781
11	1.8138	0.0144	-8.902	0.539645	0.415781	0.219434
12	2.0313	0.0097	-9.3232	0.637438	0.219434	0.070445
13	2.4347	0.0058	-9.5915	0.775269	0.070445	0.014252
14	2.9962	0.0036	-9.6892	0.902660	0.014252	0.002375
14	2.9962	0.0036	-9.6892	1	0.002375	0
Gas	-	-	-	1	0	

* Primary tie line

A.11 Details of 1-D Shock Solution Given in Figure 4.22

Oil 3 displaced by Gas 5 at 250 atm and 368.15 K .

Tie line	μ_v/μ_l	ρ_v/ρ_l	$\ln(K_{nc})$	S	λ	
Oil	-	-	-	0	3.171526	∞
1	1.5004	0.0228	-8.6599	0.067236	3.171526	1.514511
2	1.5004	0.0228	-8.6596	0.06724	1.514511	1.171592
3	1.494	0.0246	-8.4672	0.071099	1.171592	1.092878
4	1.4573	0.0303	-7.8781	0.083111	1.092878	1.006383
5	1.3433	0.0572	-6.3125	0.132232	1.006383	0.962889
6	1.3189	0.0665	-5.9654	0.147778	0.962889	0.938889
7	1.2314	0.1195	-4.674	0.232313	0.938889	0.899153
8	1.2039	0.1467	-4.234	0.276558	0.899153	0.88434
9*	1.1576	0.2126	-3.4385	0.47024	0.88434	
9*	1.1576	0.2126	-3.4385	0.477872	0.835109	
10	1.1678	0.1954	-3.6158	0.571843	0.835109	0.742035
11	1.1910	0.1642	-3.9496	0.646037	0.742035	0.611293
12	1.3124	0.0791	-5.083	0.79721	0.611293	0.405713
13	1.5149	0.0348	-5.87	0.891628	0.405713	0.201268
14	1.8152	0.0155	-6.2557	0.954836	0.201268	0.080245
14	1.8152	0.0155	-6.2557	1	0.080245	0
Gas	-	-	-	1	0	

* Primary tie line

A.12 Details of 1-D Shock Solution Given in Figure 4.23

Oil 3 displaced by pure CH₄ at 300 atm and 368.15 K.

Tie line	μ_v/μ_l	ρ_v/ρ_l	$\ln(K_{nc})$	S	λ	
Oil	-	-	-	0	2.68024	∞
1	1.5336	0.0345	-7.0682	0.168991	2.68024	1.894932
2*	1.5206	0.0370	-6.8056	0.227271	1.894932	
2*	1.5206	0.0370	-6.8056	0.257488	1.388917	
3	1.5220	0.0367	-6.829	0.278365	1.388917	1.237088
4	1.5943	0.0266	-7.6846	0.399307	1.237088	1.043549
5	1.6657	0.0206	-8.3431	0.450722	1.043549	0.929012
6	1.6815	0.0196	-8.4713	0.460331	0.929012	0.863911
7	1.7248	0.0172	-8.7794	0.483451	0.863911	0.751018
8	1.7439	0.0163	-8.8989	0.493318	0.751018	0.713224
9	1.7744	0.0150	-9.0747	0.507889	0.713224	0.586949
10	1.8207	0.0134	-9.3029	0.529999	0.586949	0.402147
11	1.9366	0.0106	-9.6547	0.575157	0.402147	0.205475
12	2.2221	0.0069	-10.0918	0.667391	0.205475	0.059015
13	2.6873	0.0044	-10.313	0.788512	0.059015	0.010241
14	3.3287	0.0028	-10.3872	0.907072	0.010241	0.001519
14	3.3287	0.0028	-10.3872	1	0.001519	0
Gas	-	-	-	1	0	

* Primary tie line

A.13 Details of 1-D Shock Solution Given in Figure 4.24

Oil 3 displaced by 75 % CO₂ and 25 % CH₄ at 275 atm and 368.15 K.

Tie line	μ_v/μ_l	ρ_v/ρ_l	$\ln(K_{nc})$	S	λ	
Oil	-	-	-	0	1.613431	∞
1	1.5237	0.0281	-7.8314	0.047601	1.613431	1.191951
2	1.5145	0.0298	-7.5947	0.050438	1.191951	1.109161
3*	1.1887	0.3572	-1.8766	0.495685	1.109161	
3*	1.1887	0.3572	-1.8766	0.502612	1.057492	
4	1.3206	0.1922	-3.0245	0.743313	1.057492	1.024916
5	1.4279	0.1233	-3.8685	0.795237	1.024916	1.005119
6	1.4508	0.1129	-4.0372	0.803228	1.005119	0.993493
7	1.5102	0.0908	-4.4516	0.820711	0.993493	0.96942
8	1.5363	0.0829	-4.6218	0.827459	0.96942	0.960334
9	1.5754	0.0728	-4.8639	0.836484	0.960334	0.92695
10	1.6339	0.0604	-5.1946	0.848695	0.92695	0.86471
11	1.7679	0.0419	-5.7752	0.870183	0.86471	0.744147
12	2.0703	0.0223	-6.5887	0.903674	0.744147	0.502959
13	2.5289	0.0117	-7.1188	0.938287	0.502959	0.226694
14	3.1568	0.0064	-7.3485	0.971455	0.226694	0.073111
14	3.1568	0.0064	-7.3485	1	0.073111	0
Gas	-	-	-	1	0	

* Primary tie line

A.14 Displacement (VC) of Oil 4 by Gas 6 at 275 atm and 387.45 K

Details of 1-D shock solution. Properties of the key tie lines are given in Table 4.3.

Tie line	S	v_d	λ	
Oil	0	0.951705	1.916983	∞
1	0.327694	0.971139	1.916983	1.365171
2	0.350849	0.971831	1.365171	1.137328
3	0.344404	0.971713	1.137328	1.050533
4*	0.429693	0.972047	1.050533	
4*	0.444027	0.972047	0.946128	
5	0.514057	0.972145	0.946128	0.880199
6	0.51702	0.972071	0.880199	0.83989
7	0.551699	0.972409	0.83989	0.774649
8	0.571168	0.972756	0.774649	0.750527
9	0.598427	0.973382	0.750527	0.67434
10	0.648088	0.975239	0.67434	0.43432
11	0.777113	0.984203	0.43432	0.312619
12	0.857434	0.992959	0.312619	0.141069
13	0.921774	0.998698	0.141069	0.029908
14	0.956542	0.999737	0.029908	0.014141
Gas	1	1	0.014141	0

* Primary tie line

A.15 Displacement (VC) of Oil 4 by pure N₂ at 275 atm and 387.45 K

Details of shock solution and a comparison of VC and NVC solutions. Key tie line properties are given in Appendix A.5.

Tie line	S	v_d	λ	
Oil	0	1.046255	2.107325	∞
1*	0.330314	1.067514	2.107325	
1*	0.399267	1.067514	1.343283	
2	0.68182	1.011644	1.343283	1.172547
3	0.683425	1.010776	1.172547	1.020871
4	0.697478	1.005166	1.020871	0.817946
5	0.714721	1.000906	0.817946	0.679143
6	0.717223	1.000546	0.679143	0.608584
7	0.727044	0.999274	0.608584	0.472118
8	0.730587	0.999062	0.472118	0.432961
9	0.737257	0.998727	0.432961	0.295701
10	0.74922	0.998652	0.295701	0.08366
11	0.816239	0.999376	0.08366	0.032045
12	0.869223	0.999874	0.032045	0.005822
13	0.905447	0.999995	0.005822	0.002108
14	0.915147	1	0.002108	0.002036
Gas	1	1	0.002036	0

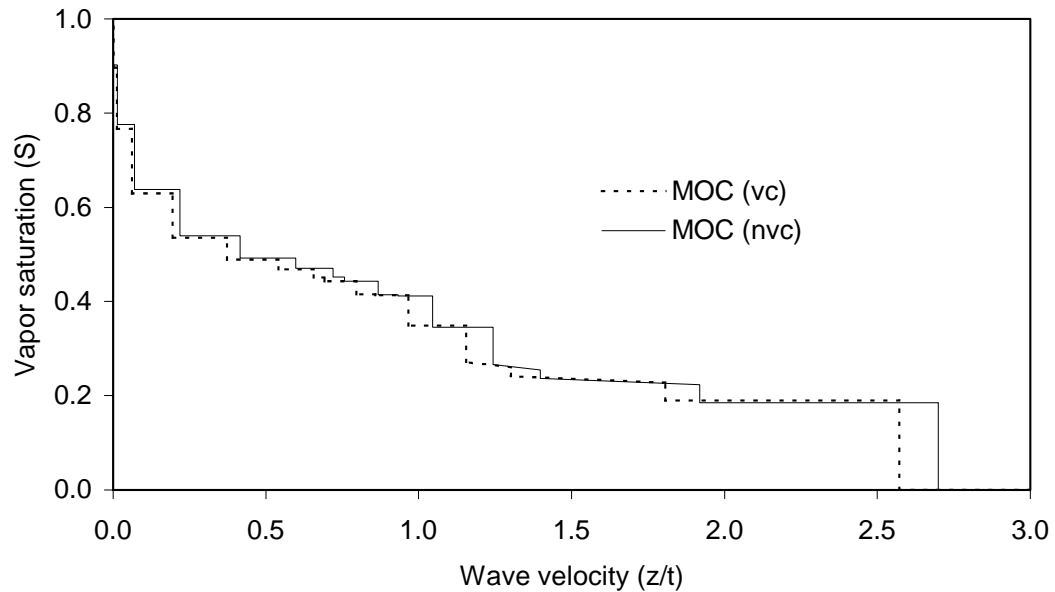
* primary tie line

A.16 Displacement (VC) of Oil 3 by Gas 3 at 300 atm and 368.15 K

Details of 1-D shock solution and a comparison of VC and NVC solutions. Key tie line properties are given in Appendix A.10.

Tie line	S	v_d	λ	
Oil	0	0.913949	2.571301	∞
1	0.190258	0.981463	2.571301	1.805965
2	0.227677	0.982876	1.805965	
2	0.241865	0.982876	1.302147	
3*	0.259621	0.983069	1.302147	
3*	0.271169	0.983069	1.155907	
4	0.348206	0.981703	1.155907	0.96635
5	0.4131	0.981445	0.96635	0.857445
6	0.415423	0.981493	0.857445	0.795753
7	0.443232	0.982223	0.795753	0.6911
8	0.451111	0.982588	0.6911	0.656061
9	0.468479	0.983494	0.656061	0.540972
10	0.489224	0.984894	0.540972	0.372948
11	0.534566	0.987936	0.372948	0.194591
12	0.629044	0.993934	0.194591	0.06189
13	0.766244	0.998576	0.06189	0.012457
14	0.896864	0.999849	0.012457	0.002062
14	1	1	0.002062	0
Gas	1	1	0	

* Primary tie line

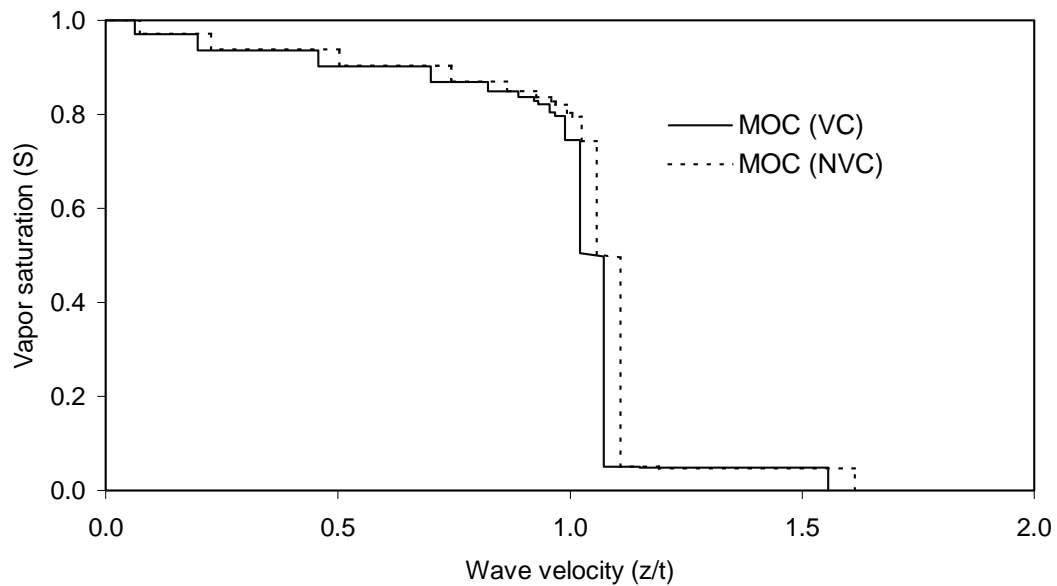


A.17 Displacement (VC) of Oil 3 by CO₂/CH₄ at 275 atm and 368.15 K

Shock solution and a comparison of VC and NVC solutions. Key tie line properties are given in Appendix A.13.

Tie line	S	v_d	λ	
Oil	0	0.962562	1.555963	∞
1	0.048489	0.979251	1.555963	1.149717
2	0.051257	0.979937	1.149717	1.07225
3*	0.497782	0.980686	1.07225	
3*	0.504797	0.980686	1.021393	
4	0.745113	0.978951	1.021393	0.988685
5	0.79647	0.978521	0.988685	0.968545
6	0.804318	0.978537	0.968545	0.956697
7	0.821405	0.978703	0.956697	0.931994
8	0.827974	0.978866	0.931994	0.922655
9	0.836736	0.979148	0.922655	0.88825
10	0.848561	0.979782	0.88825	0.82409
11	0.869229	0.98173	0.82409	0.700195
12	0.901557	0.987119	0.700195	0.458334
13	0.935773	0.994224	0.458334	0.198371
14	0.96974	0.998622	0.198371	0.062854
14	1	1	0.062854	0
Gas	1	1	0	

* Primary tie line



A.18 Input file for Eclipse (E300) Slimtube Simulation

```

-->Simulation of a 20 metre slimtube using lab units
-->Developed by Niels Lindeloff
-- PVT input and rock props supplied by K. Jessen
-----
RUNSPEC =====

OIL
GAS

IMPES

DIMENS
1000 1 1 /

-- Cartesian co-ord system

CART

-- Units: Lab

LAB

-- Number of components: implies compositional run
COMPS
15 /

MISCIBLE

GRID =====

DX
1000*2 /

--Cross section is 0.5 square cm

DY
1000*0.7071 /

DZ
1000*0.7071 /

-- Porosity and permeability

PORO
1000*0.3042 /

PERMX
1000*46000.0 /

PERMY
1000*46000.0 /

PERMZ
1000*46000.0 /

```

```

--Depth of cell centres

MIDS
1000*100.0 /

PROPS      =====

-- Properties section: PVT data from INCLUDE file

EOS
SRK  /

-- Names of Components
CNAMES
NITROGEN
CO2
METHANE
ETHANE
PROPANE
I-BUTANE
N-BUTANE
I-PENTANE
N-PENTANE
C6
C7
C11
C16
C23
C33
/

MISCEXP
0.000001 /

-- Component Critical Temperatures (K)
TCRIT
  126.20000   304.20000   190.60000   305.40000   369.80000
  408.10000   425.20000   460.40000   469.60000   507.40000
  632.80001   659.60533   703.64643   766.49716   892.98963
/

-- Component Critical Pressures (bar)
PCRIT
  34.04520    73.86592    46.00155    48.83865    42.45517
  36.47700    37.99687    33.84255    33.74122    29.68822
  30.70019    23.77062    19.54564    17.00758    15.33069
/

-- Component Critical Volumes (ccm)
-- set by user
VCRIT
  90.080000    93.950000    99.260000    147.950000    202.890000
  262.700000    254.710000    305.830000    304.020000    370.140000
  511.730000    737.840000    1079.190000    1612.480000    2758.530000
/

-- Critical Volumes for viscosity (ccm)
-- set by user
VCRITVIS
  90.080000    93.950000    99.260000    147.950000    202.890000

```

```

262.700000    254.710000    305.830000    304.020000    370.140000
511.730000    737.840000    1079.190000    1612.480000    2758.530000
/

-- Component acentric factor
ACF
0.04000 0.22800 0.00800 0.09800 0.15200
0.17600 0.19300 0.22700 0.25100 0.29600
0.18424 0.47731 0.81969 1.21141 1.37175
/

-- Components Parachors (dyn/cm)
-- (for IFT - Fanchi 1990)
PARACHOR
74.43680    111.22300    46.89890    79.15870    111.42080
239.61917    239.61917    280.57801    280.57801    321.53685
388.20114    581.85564    819.38791    1150.58805    1793.79357
/

-- Peneleux Correction (Shift parameters DM-less)
SSHIFT
0.03434    0.11197    0.02113    0.05829    0.08059
0.09050    0.09752    0.11156    0.12146    0.14005
0.17465    0.02796    -0.07706    -0.20962    -0.42467
/

-- Component Molecular Weight g/mol
MW
28.01600    44.01000    16.04300    30.06900    44.09600
58.12300    58.12300    72.15000    72.15000    86.17700
109.00723    175.32727    256.67393    370.09864    590.37450
/

-- Binary interaction parameters
BIC
0.000000
0.020000 0.120000
0.060000 0.150000 0.000000
0.080000 0.150000 0.000000 0.000000
0.080000 0.150000 0.000000 0.000000 0.000000
0.080000 0.150000 0.000000 0.000000 0.000000 0.000000
0.080000 0.150000 0.000000 0.000000 0.000000 0.000000 0.000000
0.080000 0.150000 0.000000 0.000000 0.000000 0.000000 0.000000 0.000000
0.000000
0.080000 0.150000 0.000000 0.000000 0.000000 0.000000 0.000000 0.000000
0.000000 0.000000
0.080000 0.150000 0.000000 0.000000 0.000000 0.000000 0.000000 0.000000
0.000000 0.000000 0.000000
0.080000 0.150000 0.000000 0.000000 0.000000 0.000000 0.000000 0.000000
0.000000 0.000000 0.000000 0.000000
0.080000 0.150000 0.000000 0.000000 0.000000 0.000000 0.000000 0.000000
0.000000 0.000000 0.000000 0.000000 0.000000
/

STCOND
15.0 1.0 /

```

```

GRAVITY
1* 1.01 1* /

-- Reservoir temperature: Deg C
RTEMP
114.3 /

-- Rock and properties

ROCK
250.0 0.00000 /

--Gas saturation functions
SGFN
--      Sg          Krg          Pcog
      0.000000      0.000000          0
      0.050000      0.003906          0
      0.100000      0.015625          0
      0.150000      0.035156          0
      0.200000      0.062500          0
      0.250000      0.097656          0
      0.300000      0.140625          0
      0.350000      0.191406          0
      0.400000      0.250000          0
      0.450000      0.316406          0
      0.500000      0.390625          0
      0.550000      0.472656          0
      0.600000      0.562500          0
      0.650000      0.660156          0
      0.700000      0.765625          0
      0.750000      0.878906          0
      0.800000      1.000000          0
      1.000000      1.000000          0
/

-- Oil saturation functions
SOF2
      0.000000      0.000000
      0.200000      0.000000
      0.250000      0.003906
      0.300000      0.015625
      0.350000      0.035156
      0.400000      0.062500
      0.450000      0.097656
      0.500000      0.140625
      0.550000      0.191406
      0.600000      0.250000
      0.650000      0.316406
      0.700000      0.390625
      0.750000      0.472656
      0.800000      0.562500
      0.850000      0.660156
      0.900000      0.765625
      0.950000      0.878906
      1.000000      1.000000
/

SOLUTION =====

```

```

-- Solution section: define explicitly

PRESSURE
1000*250.0 /

SGAS
1000*0.0 /

XMF
1000*0.0045 1000*0.0164 1000*0.4585 1000*0.0715 1000*0.0674 1000*0.00840
1000*0.03110 1000*0.01030 1000*0.01650 1000*0.02520
1000*0.12440 1000*0.06320 1000*0.05024 1000*0.03240 1000*0.01996 /

YMF
1000*0.0045 1000*0.0164 1000*0.4585 1000*0.0715 1000*0.0674 1000*0.00840
1000*0.03110 1000*0.01030 1000*0.01650 1000*0.02520
1000*0.12440 1000*0.06320 1000*0.05024 1000*0.03240 1000*0.01996 /

-- Calculate initial oil and gas in place at surface conditions

FIELDSEP
1 15.0 1.0 /
/

RPTSOL
PRES SOIL SGAS /

OUTSOL
PRES SOIL SGAS /

SUMMARY =====

WOPR
PRODUCER /

FOPR

WOPT
PRODUCER /

WGOR
PRODUCER /

RUNSUM

SCHEDULE =====

CVCRIT
-0.001 /

SEPSPEC
SEPP G2 1 15.0 1.0 /
/

WELLSPEC
INJECTOR G1 1 1 1* /
PRODUCER G2 1000 1 1* SEPP /
/

```

```

WELLCOMP
INJECTOR  1  1  1  1  1  1* 5000 /
PRODUCER 1000 1  1  1  1  1* 5000 /
/

WELLSTRE
LEANGAS  0.9999 0.0001 /
/

--Total pore volume is 304.2ccs, inject 1/10 PV per hour

WELLINJE
INJECTOR  STREAM  LEANGAS  RV  5* 30.42 /
/

WELLPROD
PRODUCER  BHP  4*  250.0  /
/

RPTPRINT
1 1 1 1 1  1 1 1 0 0 /

RPTSCHED
PRESSURE  SOIL  SGAS /

--Limit max step to get at least 500 timesteps per 10 hours = 1 PV injected
-- Her sat til mindst 1000 pr 10 hrs NL
TSCRIT
0.001 0.0001 0.01 /

--Run for 12 hours - ie 1.2 pore volumes injected

TIME
1 2 3 4 5 6 7 8 9 10 11 12 /

END

```